FU JEN STUDIES

SCIENCE AND ENGINEERING

NO. 30, DEC. 1996

CONTENTS

輔仁學誌—理工類

中華民國八十五年十二月　　第三十期

目　錄

在全球資訊網上之系務管理系統的研究與製作

梅　興　　黃貞瑛
輔仁大學資訊工程系

摘　　要

本文介紹在全球資訊網（World Wide Web）上建立之輔仁大學資訊工程系的系務管理實驗系統（Departmental Intranet）。本系統包括了佈告欄、課務、成績、財務與使用者管理等五個子系統。佈告欄子系統與系內 NetNews/BBS 結合以公告系所訊息。其特點在於行政佈告欄可在控制的環境下，提供教職員間交換資訊（如：會議記錄）。課務管理子系統包括課程查詢、選課、排課等部分。成績管理子系統配合課務系統，具有成績登錄、查詢等功能。財務管理子系統主要針對系所財產與帳號，協助行政及相關人員簡化繁覆的紙上作業與溝通。使用者管理子系統用以管理權限不同使用者的帳號與密碼（如：同學個人成績限於同學本人才可查詢，研究帳號查詢限由計畫主持人與秘書與才能使用）。本系統使用 HTML、C、Perl、Java 等語言；Common Gateway Interface（CGI）、Socket、等通訊機制做爲發展工具。系統發展者經由此系統之發展評估各種發展環境與工具，獲得了發展 WWW 應用的經驗。使用者可從任何裝置了瀏覽器的電腦上使用此系統。系上之行政人員、老師、助教、同學皆能因系所務之自動化與網路化而增加行政、學習、教學與研究的效率。

關鍵詞： 全球資訊網（WWW），Intranet。

一、簡　　介

全球資訊網（World Wide Web）在近兩年已成爲有史已來成長最快的資訊流通

方式。透過雙方的協定，可以存取網際網路上的超媒體文件，內容包括文字、聲音、以及各式各樣的圖片。然而目前 WWW 伺服器的建立多爲單純的資訊的儲存與瀏覽[1]。由於全球資訊網的跨平台特性與軟體技術的漸趨成熟，應用軟體系統已漸漸的從各種不同之平台發展到了全球資訊網的單一平台上。近來，網路電腦與企業網路（Intranet）的快速發展都著眼於利用全球資訊網的便捷特點[2－6]。

設計一個適用於學校科系的系務管理系統。可以使得系上的教授、行政人員、同學透過自動化以及網路化的系統，增加教學、研究、行政與學習的效率。輔仁大學資訊工程系的系務管理系統以 WWW 爲平台，使用者可以透過任何具備瀏覽器的電腦使用。基於 WWW 技術快速演進的特性，在此系統之發展同時，我們也試驗並評估了多種現存之 WWW 伺服器與發展工具，參與系統發展者獲得了發展 WWW 應用的經驗。經由輔大聖言會的支持，資訊工程系的系務管理系統，將於完成後，移轉至其它各系使用，若加以擴充，也適用於院務管理，並預期未來與校務資訊系統相結合。

除了一般系所首頁包括的系所簡介與各種鏈結（Link）外，本文介紹之輔大資工系務管理系統包括了佈告欄、課務、成績、財務與使用者管理等五個子系統。本系統之主畫面如圖 1。本文共分五節，第二節介紹 WWW 的起源與技術基礎，第三節介紹佈告欄、課務、成績、財務與使用者管理等子系統。第四節說明系統架構與發展環境，第五節爲結論並展望未來發展。

二、WWW 之起源與技術基礎

1. 起源與發展

全球資訊網是網際網路（Internet）上新近興起的一種技術，它的崛起，使得一般人更易於網際網路上取得欲於查詢的資訊，因此造成近年來網際網路風靡於全球的主因。

WWW 起源於 1989 年，由原任職於歐洲量子物理實驗室（CERN）的 Tim Berners－Lee 所提出，其構想主要是想建立一個更有效的方法以取得所有散佈在世界各地的某些相關資料，他所設計的瀏覽器（Browser）乃利用所謂的超本文（Hypertext）技術，在 Hypertext 中，有些文字或片語可連結到其它相關的文件，此技術即構成文件網的架構，而此架構不似傳統的資訊傳遞是具循序性的階層性架構，

因此使用者是依循固定的順序查詢資料。但在 Hypertext 中，文件與文件間形成鍊結，構成一類似蜘蛛網的架構，任何文件間，沒有明確的起點與終點，使用者在閱讀資訊時，可經由超鍊結（Hyperlink）的機制，即點選某些特殊文字，便會跳到連結的其它文件上，因此使用者可自已決定閱讀的順序，快速地查詢其所需的資料。

WWW 發展當初所設計的瀏覽器，僅侷限於文字，直至 1993 年才由國家超級電算應用中心（NCSA）發展出第一個圖形瀏覽器，此瀏覽器稱爲馬賽克（Mosaic），除了可以顯示文字外，還可以顯示圖形、影像、聲音等其它資料型態，這種不但可連結文字資訊，且可連結圖形、影像、聲音等資訊的技術，便稱之爲超媒體（Hypermedia），馬賽克圖形瀏覽器的誕生，造成全球的風靡，並引起各界的震撼，也因其架構於網際網路上的技術優勢，使其具有無遠弗屆的傳播效力，而其具備豐富的多媒體展現能力，及其親切友善的視窗圖形介面，使它迅速普及於群衆，又因其超鍊結的特性，使其成爲網際網路上成長最快的資訊服務系統。

2. WWW 之技術基礎

WWW 主要是建立在主從式系統架構（Client－Server Model）上，顧名思義，此架構可分爲兩部份，即用戶端（Client）與伺服器（Server），通常伺服器是一台功能較佳的電腦，它一般負責文件檔案的存取管理，可提供用戶端不同的服務，而用戶端一般則負責文件內容的展示，WWW 經由網際網路作爲橋樑，使得伺服器與用戶端建立主從關係，並且伺服端需有已建立之超媒體文件（Hypermedia documents）的存在，經由超本文傳輸協定（Hypertext Transfer Protocol；HTTP），伺服器與客戶端可以互相傳達訊息，以便資料可在網路上正確的傳輸，而客戶端需使用統一資源定址器（Uniform Resource Locator；URL）指定資源的所在位址，以便網際網路上正確的找到伺服器及檔案的所在位置。

如前所述，WWW 是利用一廣域網路主從架構的方式，擷取超媒體文件。而目前 WWW 所認定的標準語言以顯示多媒體資訊文件，則爲超本文標籤語言（Hypertext Markup Language；HTML）。HTML 利用一般普通文字格式，撰寫一超媒體文件資訊，藉由 HTML 的指令，首頁（Homepage）的作者可以標示標題及各項目的位置，並決定要如何安置圖片及文字，甚至要連結至其它的頁面等。

HTML 文件的設計以單向的資訊提供爲主，並不具備資訊雙向交流的功能，而共同閘道介面（Common Gateway Interface；CGI）的通訊機制，可使得 CGI 程式經由 CGI 介面執行某些應用服務，例如線上電子訂購服務、問卷調查、資料庫查詢服

務等。因此 CGI 提供了互動式的服務功能，使得 WWW 更富有內容，充滿生機。但要使用 CGI，必須以伺服器上的程式語言撰寫，而目前較受歡迎的 CGI 程式語言有 C，Shell，Perl，Visual BASIC，Java 等。

因此，設計一雙向互動的 WWW 系務管理系統，除了撰寫 HTML 程式外，必須撰寫 CGI 應用程式，並且對系統整体架構的相關技術需有所瞭解。如 WWW 伺服器、主從式架構、網路等技術層次，另外必須善用發展工具，才有可能設計出一生動且具內涵的 WWW 系統。

三、系所管理系統

輔大資工系所管理系統共包含了佈告欄、課務、成績、財務與使用者管理等五個子系統。

1. 佈告欄子系統

佈告欄子系統與系上 NetNews Server / BBS 結合並擴充以公告系所訊息。其主要特點在行政佈告欄部分，可在安全的環境下供教職員間交換資訊（如：會議通知，會議記錄）。使用者各依其權限可發佈與查看系所之最新消息。

如圖 2，佈告欄子系統目前分成最新報導，新聞放送二部分。最新報導部分爲針對秘書、助教或教師欲發布全系事宜的狀況。公布大抵爲全系事務，且具廣發性、時效性及重要性，例如：調課通知、繳交期限通知，選課、註冊時間表，學生事務注意事項等。秘書、助教或教師有權編輯及上載，以公布日期及標題讓使用者選擇欲閱讀的公告。

新聞放送部分爲最新報導之資料發報處。提供使用者能於線上發布公告上載於最新報導。如圖 3，輸入如新聞標題、新聞種類、內容及發佈單位、發佈對象等資料後傳送。至於各班與學會之公告，目前的規劃是與 NetNews Server / BBS 結合之。

2. 課務管理子系統

課務管理子系統包括課程查詢、選課、排課等部分。課程查詢系統部分，教師可線上輸入所開課程介紹，以供同學參考。學生可自由查詢各教師所開之課程簡介。選課系統（如圖 4）以資工系所開之課程爲主，資工系所同學進入系統，輸入學號、密碼後，即可看見開課課表，選定課程後送出，傳回已選課表。排課系統則提供秘

書排課與安排教室用。

本計畫對課程教材內容與輔助教學部份目前僅有簡單界面供老師使用。另外本系尚有有一 Java Based 教材管理與 CAI 工具系統計畫正在發展中。該計畫發展出之工具將與本計畫課務管理子系統之課程部分結合使用。

3. 成績管理子系統

系所成績管理的主要目的在讓師生在學期中課程進行時方便的了解成績狀況。成績管理子系統具有各課程成績登錄、查詢等功能。依使用情況分爲老師使用與同學生查詢使用二部分。各科老師或助教可線上設定各項成績比例，公佈作業、程式、段考與學期成績，並可查看任一學生成績。試算表的功能不但方便計算成績，也方便調整成績。學生則可依其學號及密碼查詢自己各科成績狀況。如圖 5 顯示同學進入成績系統畫面。

成績系統所包含的課程範圍，目前僅限於本系之課程，共同必修、通識、與外系選修課程並未在內。因此，本系統無法提供各學期修業總成績與排名等訊息。所幸輔大資訊中心也正在發展一全校性之 WWW Based 成績查詢系統，可彌補本系統之不足。

4. 財務管理子系統

財務管理子系統主要針對系所財產與帳號，協助行政及相關人員簡化繁覆的紙上作業與溝通。財務管理系統主要將財務業務分爲兩部份，一是經費帳號部份，爲各老師們的經費帳號，及系上所有的經費之登錄查詢，二爲處理系上各種軟硬體登錄查詢之器材部份 (如圖 6)。

帳號管理的資料包括帳號負責人經費來源 (例如: 聖言會，教育部，國科會等)，經費金額，經費填報日期等。各帳號負責人隨時可了解該帳號下各類經費的使用狀況。系上器材管理的資料包括器材管理人，器材種類，財產編號，器材存置地點等。

最後，使用者管理子系統是整個系統的核心部分。各種不同使用者的權限與密碼都經由此子系統設定與維護。譬如: 同學個人成績限於同學本人才可查詢，個人研究帳號查詢限由計畫主持人與秘書才能使用。使用者管理子系統也是維護管理系統的一部分。配合上佈告欄，課務，成績，與財務等維護系統才可確保系統的長久運作。

四、系統架構與發展環境

本系統之各子系統統首頁關係如圖 7 所示，各首頁以 HTML 建立。在發展的過程中，各子系統分別建立了 html、data、及 graphic 三個子目錄，CGI 程式置於 cgi－bin 目錄。未來上線使用時將重新配置重要資料檔與共享資源檔於適當的位置。現階段尚未考慮與全校性課務、成績資料庫的結合。

基於本計畫的實驗性質，應用程式發展使用了 C、Perl 及 Java 等語言。Client/Server 間用了 Common Gateway Interface (CGI)、Socket、等通訊機制來連絡。目前本系統是在輔大資工系統實驗室之 ie4. csie. fju. edu. tw 伺服器上發展，未來上線後，將由系上之各主要 WWW Server/Homepage 直接提供鏈結 icon。

五、結　　論

本文介紹一個建立在全球資訊網上的系務管理系統。系統發展者經由此系統之發展評估了各種發展環境與工具，獲得了發展 WWW 應用的經驗。使用者可從任何裝置了 WWW 瀏覽器的電腦上使用此系統。系所之教職員與同學透過此系統的使用，可曾加彼此間的溝通與互動，減少系務行政的負荷。

在本系統發展至今一年的過程中曾面對一些困難，謹提出此類系統發展之三特性供未來發展類似系統時參考：

1. WWW 相關技術快速發展。

不論是軟硬體伺服器系統，還是發展環境與工具，在一年來都有相當的演進。這影響到了發展人員的訓練，對應用的專注性，發展時程的控制，以及未來的擴充。

2. 相關單位與使用者的配合。

除了發展單位的支持外，相關同級與上級單位的配合會影響到行政管理系統適用程度。使用者（尤其是要負責到部分管理功能的使用者）的配合更關係到系統是否能眞正上線服務。

3. 安全性的考量。

應用系統的安全考量是曾從應用使用者與管理者的觀點來設計的。然而在

WWW 上的應用必須將 WWW 伺服器、作業系統、與網路的安全性一併考量。

本計畫的發展分爲四個階段。第一階段是需求分析及架構設計，第二階段是細部設計，第三階段爲程式設計，第四階段爲測試以及驗收。基於 WWW 相關技術的快速演進，本系已規劃常態的維護與發展此系統。未來新版本將應用 Remote Method Invocation (RMI) 與分散式物件環境 (譬如: Joe from Sun) 來開發。本系統現在程式設計與測試階段，預計在完成後，將整理成爲易於安裝之套裝軟體，移轉至其它各系所使用。

六、銘　　謝

本系統屬於輔仁大學聖言會專題研究計畫的成果。作者感謝輔大聖言會的經費支援，與輔仁大學資訊工系第六屆同學陳貽浚、陳志榮、李依峻、李俊緯、鐘運光、王志彥 、鍾俊傑等的程式製作。

參 考 文 獻

(1) T.J. Berners-Lee, R. Cailliau, J-F. Groff, and B. Pollermann, "World-Wide Web: The Information Universe", *Electronic Networking Research*, Application and Policy, Vol. 2, No. 1, Spring 1992, pp. 55-58.

(2) http://hoohoo.ncsa.uiuc.edu/cgi/

(3) http://java.sun.com/

(4) http://www.gamelan.com/

(5) 王秋鳳, 林泰旭, "WWW 學術研討會籌辦系統", *Proceedings of First Workshop on Real-time and Media Systems*, July 1995, pp. 159-164.

(6) http://www.w3.org/pub/Conferences/WWW5/

85年10月 8日　收稿
85年11月 1日　修正
85年11月10日　接受

Building a Departmental Administrative System on World Wide Web

HSING MEI AND JEN-ING GRACE HWANG
Department of Computer Science and Information Engineering
Fu-Jen University
Taipei, Taiwan 242, R.O.C.

ABSTRACT

This paper describes the departmental administrative system we have designed and implemented on the World Wide Web (WWW) for the Department of Information Engineering and Computer Science at Fu Jen University. This departmental intranet includes five subsystems: the Bulletin Board System (BBS) Sub-system; the Curricula Affairs Sub-system; the Student Grade Reports Sub-system; the Financial Affairs Sub-system and the Maintenance Sub-system. The newly-developed BBS Sub-system is integrated with our original department NetNews/BBS system to provide departmental information. An extension of the original system is the administrative BBS, which facilitates communication among individuals in the department. The faculty and staff are allowed to access the information in the sub-system with proper authorization (e.g., reading meeting records). The Curricula Affairs Sub-system provides information about curriculum queries, selection of courses, and scheduling of courses. The Student Grade Reports Sub-system can be used for recording and querying grades. The Financial Affairs Sub-system saves time and simplifies the processing of paperwork. The Maintenance Sub-system ensures the security of all data accessions; it specifies the particular privileges that each account holds. For example, a student is allowed to query his own grades through his account; in addition, the project investigator and secretary are permitted to access information from a certain research account. This system is implemented not only by the use of HTML (hypertext markup language), C, Perl and Java computer languages but also by the use of communication mechanisms such as Common Gateway Interface (CGI), Socket, and Remote Method

Invocation (RMI). As a result of the implementation of this project, the designers have gained experience in the implementation of a system on WWW. All users will be able to access departmental information by means of a Web browser. Moreover, all students, teaching assistants, faculty and staff will benefit from this system, with respect to learning, teaching, research and administrative affairs.

Key Words: WWW, Intranet。

圖 1 輔大資工系所管理系統主畫面 (main.htm)

圖 2 佈告欄子系統主畫面 (board.htm)

圖 3 發送新聞畫面 (catv.htm)

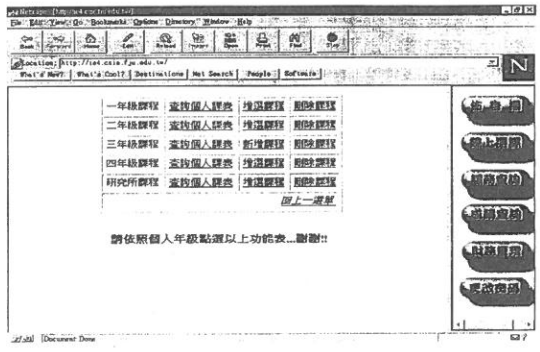

圖 4 選課系統畫面 (SelectCourse.htm)

圖 5 進入成績系統畫面（Report.htm）

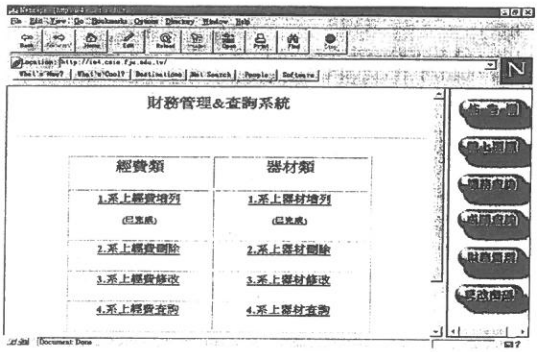

圖 6 財務系統主畫面（mon.htm）

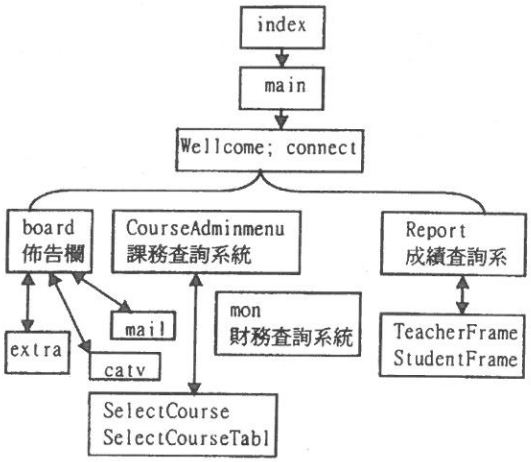

圖 7 系統架構圖

Tunable Gain Voltage-Mode Precision Rectifier using two CCII+s

YUNG-CHANG YIN
Department of Electronic Engineering
Fu-Jen Catholic University
Taipei, Taiwan 242, R.O.C.

ABSTRACT

In this paper, a voltage-mode full-wave rectifier circuit with tunable voltage gain is presented. This rectifier circuit contains only two Current Conveyors (CCII). Finally, the proposed circuit has been confirmed experimentally and two experimental results are included.

Key Words: Rectifier, Current Conveyors (CCII).

INTRODUCTION

It is well known that CCII has wide bandwidth and high accuracy. Current Conveyor has many applications in nonlinear circuits such as multipliers, dividers and rectifiers[(1)~(3)]. However, it is complicated to design a voltage-mode fixed gain full-wave rectifier circuit using the combination of a CCII+ and a CCII−. Here two CCII+s were used to implement the voltage-mode gain-adjusted full-wave rectifier circuit. The feature of rectifier constructed in this way is a simple structure.

CIRCUIT DESCRIPTION

Basically, a CCII is a three port network having terminal characteristic described by the matrix equation

$$\begin{bmatrix} i_y \\ V_x \\ i_z \end{bmatrix} = \begin{bmatrix} 0 & 0 & 0 \\ 1 & 0 & 0 \\ 0 & \pm 1 & 0 \end{bmatrix} \begin{bmatrix} V_y \\ i_x \\ V_z \end{bmatrix}$$

where the plus and minus signs indicate that whether the conveyor is formulated as an inverting or an noninverting circuit, termed CCII− or CCII+ . By convention, positive is taken to mean that i_x and i_z are both flowing simultaneously towards or away from the conveyor. The circuit symbol of a CCII+ is shown in Fig. 1.

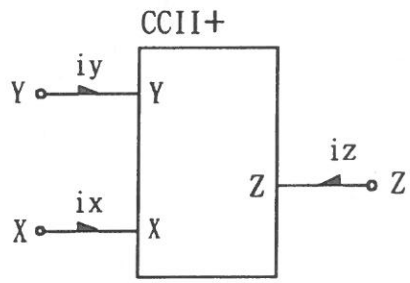

Fig. 1. Circuit symbol of CCII+

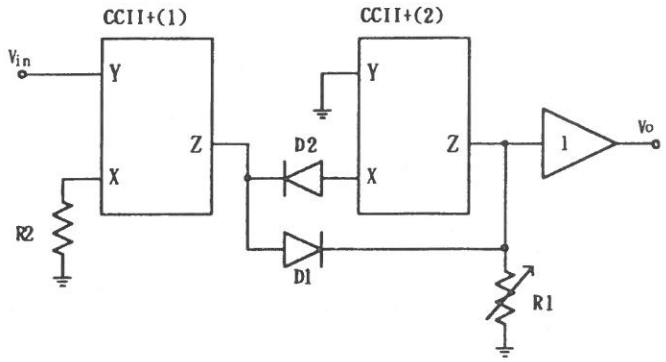

Fig. 2. Voltage-mode full-wave rectifier with tunable voltage gain.

The proposed tunable gain voltage-mode full-wave rectifier circuit, shown in Fig. 2, consists of two CCII+s, two Schottky diodes and two resistors. Assume that all the

components are ideal. Since V_{in} is in the positive half-period, D_1 is on, D_2 is off, the current flows through D_1 and R_1. The voltage-mode rectifier response is obtained by:

$$V_o = (\frac{R_1}{R_2}) V_{in} \tag{1}$$

Similarly, if V_{in} is in the negative half-period, D_1 is off, D_2 is on, the current flows through D_2, CCII+(2) and R_1. The voltage-mode rectifier response is characterised by:

$$V_o = -(\frac{R_1}{R_2}) V_{in} \tag{2}$$

From the above equations, the full-wave rectifier circuit is implemented using two CCII+s. No matter whether V_{in} is in a positive or negative half-period, V_o is always positive and the amplitude of the output signal can be adjusted by using potentiometer R_1.

EXPERIMENTAL RESULTS

In order to verify the theoretical analysis, the proposed circuit is experimentally demonstrated. The ISS97 is chosen as the Schottky diode. The CCII+ has been implemented using op-amp.(LF351) together with BJT(CA3096AE)[4]. The used oscilloscope is Tektronix 7623A. They are briefly described in the following:

(1) Fig.3(a) shows V_{in} = 500mv, R_1 = 1K ohms, R_2 = 1K ohms and f = 10 KHz

(2) Fig.3(b) shows V_{in} = 500mv, R_1 = 2K ohms, R_2 = 1K ohms and f = 10 KHz

The experimental results are agree with the theoretical analysis.

CONCLUSION

A new voltage-mode full-wave rectifier circuit with tunable voltage gain is presented. The use of only two plus-type CCIIs greatly simplifies the configuration. The experimental results are agree with the theoretical analysis. The purpose of the experimental investigation is illustrative of the simplification of the tunable rectifier using only two CCII+s.

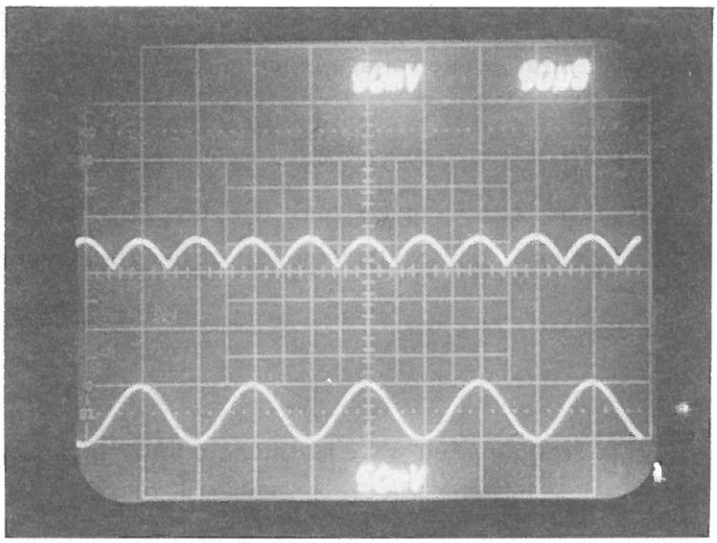

Fig. 3 (a). The transfer curve of V_{in} = 500mv, at f = 10 KHz and $R_1 = R_2$ = IKΩ

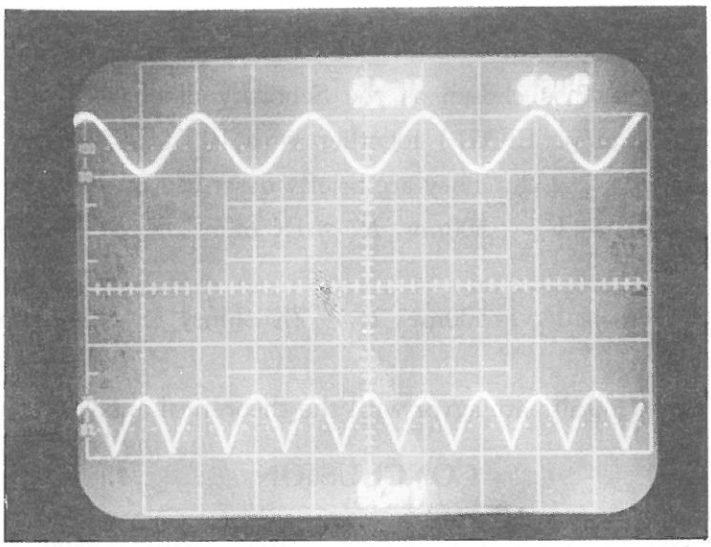

Fig. 3 (b). The input and rectified waveforms of V_{in} = 500mv, at f = 10 KHz and $R_1 = 2R_2$ = IKΩ

ACKNOWLEDGMENT

The author acknowledges the constructive suggestions from Dr. Chun-Li Hou and financial support from Societas Verbi Divini.

REFERENCES

(1) S. I. Liu, D. S. Wu, H. W. Tsao, J. Wu and J. H. Tsay, "Nonlinear circuit applications with current conveyors", *Proceedings of the Institutions of Electrical Engineers*, Pt. G, **140**, 1-6 (1993).

(2) C. Toumazou and F. J. Lidgey, "Wide-band precision rectification", *Proceedings of the Institution of Electrical Engineers*, Pt. G **134**, 7-15 (1987).

(3) D. C. Wadsworth, C. Toumazou, F. J. Lidgey and D. G. Haigh, Analogue IC design: the current mode approach (London: Peter Peregrinus Ltd.), (1990).

(4) B. Wilson, "High performance current conveyor implement", Electronics Letters, **20**, 990-991 (1984).

85年 9月30日 收稿
85年10月23日 修正
85年11月19日 接受

使用兩個正型電流傳輸器合成可調增益之電壓式精密整流器

鄞 永 昌
輔仁大學電子工程系

摘　　要

一種可調電壓增益之全波整流器電路在本文中被提出。此種可調增益之整流器僅使用了二個第二代電流傳輸器，最後並以兩個實驗證明之。

關鍵詞： 整流器、電流傳輸器。

Refractive Indices of Single-Crystal $KTiOAsO_4$

YU-LUNG YEH AND CHI-SHUN TU

Department of Physics

Fu-Jen Catholic University

Taipei, Taiwan 242, R.O.C.

ABSTRACT

We report here the refractive indices (n_x, n_y, n_z) of single crystal $KTiOAsO_4$ (KTA) measured by the ellipsometer for wavelength range 400-1700 nm. The various parameters of the Cauchy's equation, $n(\lambda) = A + B/\lambda^2 + C/\lambda^4$, for different refractive indices were obtained by fitting the experimental data. The phase-matching angle of frequency doubling for the 1.32 μm Nd: YAG laser line was calculated and is consistent with the earlier experimental result.

Key Words: Refractive Indices, $KTiOAsO_4$ and Cauchy's equation

INTRODUCTION

Potassium titanyl arsenate, $KTiOAsO_4$, belongs to the family of nonlinear optical crystals with the general formula $M^{1+}TiOX^{5+}O_4$, where M = {K, Rb, Tl, Cs} and X = {P, As}.[1-2] The high damage threshold and broad angular acceptance have made this type of crystals attractive materials for frequency doubling of Nd-based laser and for optical parametric oscillators (OPO). In addition, the ion exchange properties also make them one of the best candidates for waveguide applications. Potassium titanyl phosphate, $KTiOPO_4$ (KTP), is the most famous among such materials and has been used successfully in different applications.[1-2]

At room temperature, KTP-type crystals have an orthorhombic structure with non- centrosymmetric point group C_{2V} (mm2) and space group P_{na2} (Z = 8). The

crystal framework is a three-dimensional structure made from corner-linked TiO_6 octahedra and AsO_4 tetrahedra. Four oxygen ions of the TiO_6 belong to AsO_4 tetrahedral groups which link the TiO_6 groups. For crystal with an orthorhombic structure, three principal refractive indices (n_x, n_y, n_z) are different. Here, we report for the first time these refractive indices obtained by using an ellipsometer as a function of wavelength from 400 to 1700 nm.

EXPERIMENTAL PROCEDURE

Single crystal, $KTiOAsO_4$, was grown using the tungstate flux method. [1] The crystal was oriented by x-ray diffraction and was cut into rectangular shape having (100), (010) and (001) faces. The dimensions of crystal is $3.0 \times 2.86 \times 2.11$ mm^3. The surfaces for measurements were polished to be optically smooth. A J.A. Woollam Co. Variable Angle Spectroscopy Ellipsometer Model VB-200 was used with a WVASE32™ software (version 2.38). A Xe gas lamp was used for the detected light source. The fundamental theory and operating process of ellipsometry can be found in Ref. 3.

In order to determine refractive indices for various wavelength continuously, the Cauchy's Equation was used to fit the experimental data, [3] i.e.

$$n(\lambda) = A + B/\lambda^2 + C/\lambda^4 \tag{1}$$

Here, A, B and C are parameters whose values depend on optical properties of materials.

RESULTS AND DISCUSSION

Fig. 1 shows the refractive indices for three principal axes. The solid lines are the fits of Cauchy's equations with parameters listed below[3]

$$\begin{aligned} n_z(\lambda) &= 1.8453 + 0.02486/\lambda^2 - 0.0005/\lambda^4 \\ n_y(\lambda) &= 1.7654 + 0.02318/\lambda^2 - 0.0007/\lambda^4 \\ n_x(\lambda) &= 1.7612 + 0.02248/\lambda^2 - 0.00120/\lambda^4 \end{aligned} \tag{2}$$

Here the unit of wavelength (λ) is μm. Table 1 summarizes the refractive indices for four various wavelengths (λ =633, 660, 1060 and 1320 nm) that can be used for the

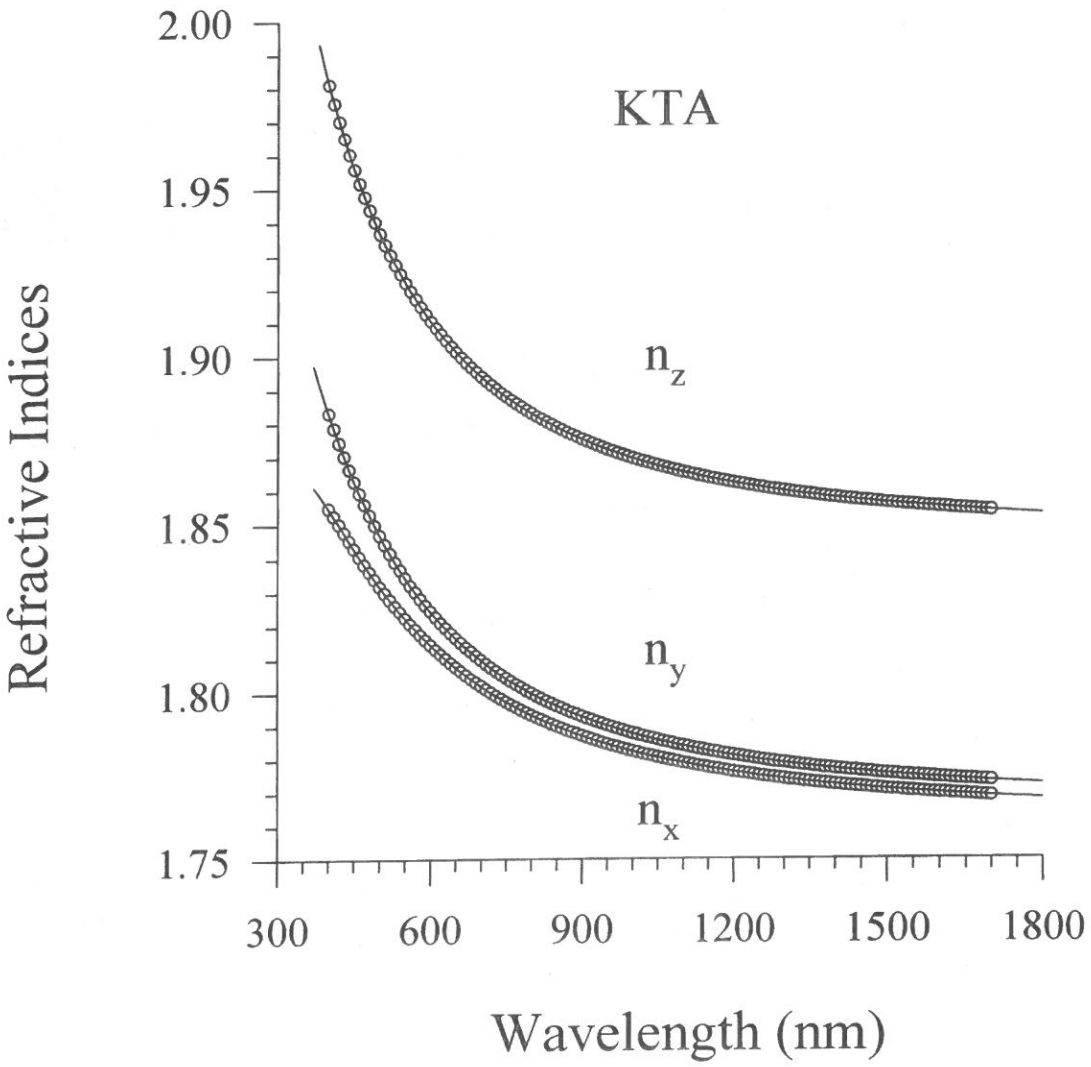

Fig. 1. Refractive indices (n_x, n_y, n_z) of KTA. Solid lines are fits of the Cauchy's equation with parameters listed in Eq. (2).

application of frequency doubling. One can note that the intrinsic optical birefringence of KTA crystal decreases as increasing wavelength. Our results, refractive indices and birefringence (n_z-n_x) are consistent well with the earlier results obtained by L.T. Cheng et al. [4]

Table 1. Refractive indices, birefringences (n_z-n_x) for four different wavelengths. The data also were compared with the earlier Cheng's results (Ref. 4).

	n_x	n_y	n_z	n_z-n_x	
λ =633 nm	1.8098	1.8189	1.9042	0.0944	present work
	1.8083	1.8142	1.9048	0.0965	Cheng (Ref. 4)
λ =660 nm	1.8065	1.8149	1.8997	0.0932	present work
	1.8042	1.8104	1.8997	0.0955	Cheng (Ref. 4)
λ =1060 nm	1.7803	1.7855	1.8683	0.0880	present work
	1.7813	1.7867	1.8677	0.0864	Cheng (Ref. 4)
λ =1320 nm	1.7737	1.7785	1.8594	0.0857	present work
	1.7751	1.7798	1.8589	0.0838	Cheng (Ref. 4)

According to the calculation of phase-matching angle for the biaxial crystal, [5] we predict that both types I and II phase matching are allowed in the y-z plane of KTA single crystal. The phase-matching angles θ_{pm} for the 1.32 μm Nd: YAG laser line in the y-z plane are θ_{pm} =59.2° (type II) and θ_{pm} =35.2° (type I). Our calculated value agrees quite well with the earlier experimental result θ_{pm} =55.9° (type II) observed by Cheng et. al. [4]

CONCLUSIONS

A main feature of the refractive indices in KTA is that a strong wavelength dependent character has been observed in the measured wavelength range (400-1700 nm). Our results (refractive indices, birefringences and calculated phase-matching angles agree consistently well with the earlier experimental results obtained by L.T. Cheng et al. [4]

ACKNOWLEDGMENTS

The authors express sincere thanks to Profs. Ruyan Guo, A.S. Bhalla and R.S. Katiyar for the providence of KTA single crystal. This work was supported by NSC86-2112-M-030-002 (R.O.C).

REFERENCES

(1) C.-S. Tu, A.R. Guo, Ruiwu Tao, R.S. Katiyar, Ruyan Guo, and A.S. Bhalla, J. Appl. Phys. **79**, 3235 (1996).

(2) A.R. Guo, M.S. thesis, University of Puerto Rico, 1996; A.R. Guo, C.S. Tu, Ruiwu Tao, R.S. Katiyar, Ruyan Guo, and A.S. Bhalla, Ferroelectric Lett. **21**, 71 (1996).

(3) User guide for the J.A. Woollam Co. Variable Angle Spectroscopy Ellipsometer Model VB-200 with a WVASE32™ software (version 2.38).

(4) L.K. Cheng, L.-T. Cheng, J.D. Bierlein and F.C. Zumsteg, Appl. Phys. Lett. **62**, 346 (1993).

(5) J.Q. Yao and T.S. Fahlen, J. Appl. Phys. **55**, 65 (1984).

85年10月13日 收稿
85年11月 4日 修正
85年11月24日 接受

$KTiOAsO_4$ 單晶的折射率

葉玉隆　杜繼舜
輔仁大學物理系

摘　要

我們在這裡要報告一個具有雙光軸的非線性光學晶體材料，$KTiOAsO_4$（KTA），的光學性質（折射率及 phase-matching angle（雷射光源倍頻時，相對於 z 軸及 x 軸的低頻入射角度（θ, ϕ））. 在這個實驗，我們顯示橢圓儀（Variable Angle Spectroscopy Ellipsometer）不僅對於等向性材料的折射率，是一個相當可靠的量測方法，對於非等向性材料也是一個相當精確的方法. 我們同時使用 Cauchy's equation，$n(\lambda) = A + B/\lambda^2 + C/\lambda^4$，去得到連續波長範圍（400-1700 nm）的折射率.

關鍵詞： 折射率，$KTiOAsO_4$ 和 Cauchy's 方程式

A Simulation Study on Vännman-Type Indices

SY-MIEN CHEN AND AI-YEN WU
Institute of Mathematics
Fu-Jen University
Taipei, Taiwan 242, R.O.C.

ABSTRACT

Vännman (1995) proposed a family of process capability indices $C_p(u, v)$ under normality. In this paper, we study the performance of estimators of $C_p(u, v)$ under various distributions. It is found from the simulation that the traditional estimators obtained by substituing sample mean and sample variance for the process mean and process variance, respectively, give the best results. Estimators derived by using median as estimator of the process mean underestimate the true indices under chi-square distribution.

Key Words: Process Capability Index

INTRODUCTION

Process capability analysis has received a substantial attention in the applications of statistical process control to the continuous improvement of quality and productivity since Burr's (1976) piorneering work. Process capability index, a unitless measurement, is designed to compute the capability of producing conforming items for processes. It is a function of the variance of the process, and it allows one to compare the capabilities of different processes even when they are in different measurement scales.

Lots of research have been done about the well known indices C_p, C_{pk}, C_{pm} and C_{pmk}. For instance, Sullivan (1984), Kane (1986), Chan et al. (1988), Clements (1989), Chou and Owen (1989), Zhang et al. (1990), Bissell (1990), Boyles (1991),

Spiring (1991), Kushler and Hurley (1992), Franklin and Wasserman (1992), Pearn et al. (1992), Kotz and Johnson (1993), Bolyes (1994), and Chen and Hsu (1995).

For processes with symmetric tolerances (i.e. when Target value = Midpoint of the specification limits), Vännman (1995) proposed a superstructure of indices involving two auxiliary parameters, defined for the case of two-sided specificaton intervals. Such family of indices generalizes the four basic indices, C_p, C_{pk}, C_{pm} and C_{pmk}. She suggested estimators of the proposed indices. In addition, analytical derivations of the expected value, the mean square error, and the variance of the estimators are given. Under the assumption of normality, Vännman and Kotz (1995a) derived the distribution of the estimated indices $\hat{C}_p(a,b)$ of the Vännman family of indices $C_p(a,b)$. Also, Vännman and Kotz (1995b) discussed the estimators' asymptotic expected value and asymptotic mean square error. Chen (1996) examines some asymptotic properties related to the natural estimator proposed by Vännman provided that the fourth moment exists. The assumption of normality is relaxed in such article.

The main result of the present paper is about the performance of several estimators of the indices under various distributions. In section two, the definition and estimators of the Vännman - type indices are given. In section 3, the simulation study is conducted. And finally it comes to the conclutions and suggestions.

DEFINITION AND ESTIMATORS

Let $X_1,\ldots,X_n$ be a sample of measurement from a process which has distribution G with mean μ and variance δ^2 under stationary controlled conditions.

Let L, U be the lower and the upper specification limit of the measurement of the characteristic which we are interested in, respectively. Denote $d = (U - L)/2$, half the length of the specification interval $[L, U]$; $M = (U + L)/2$, the midpoint of the specfication interval; and T is the target value which is predetermined by customers.

The Vännman family of process capability indices $C_p(u,v)$, which depend on two non-negative parameters, u and v, is defined as follows:

$$C_p(u,v) = \frac{d - u|\mu - M|}{3\sqrt{\sigma^2 + v(\mu - T)^2}},$$

where $u, v \geq 0$

It is clear that $C_p(0,0) = C_p$, $C_p(0,1) = C_{pm}$, $C_p(1,0) = C_{pk}$, and $C_p(1,1) = C_{pmk}$. Pearn et al. (1992) pointed out some undesirable properties of C_{pm} when T lies in the specification limits but not equal to the midpoint M. Hence in this paper, we consider only the processes with symmetric tolerance like Vännman (1995) did. Therefore,

$$C_p(u,v) = \frac{d - u|\mu - T|}{3\sqrt{\sigma^2 + v(\mu - T)^2}},$$

When both the process mean μ and the proces variance σ^2 are unknown, an estimator

$$\hat{C}_p(u,v) = \frac{d - u|\hat{\mu} - T|}{3\sqrt{\hat{\sigma}^2 + v(\hat{\mu} - T)^2}},$$

is considered, where $\hat{\mu}$ and $\hat{\sigma}^2$ are esitmator of μ and σ^2 respectively.

Vännman (1995) proposed two estimators of $C_p(u,v)$ when $G = N(\mu, \sigma^2)$,

$$\hat{\mu} = \overline{X} \quad \hat{\sigma}^2 = \begin{cases} S_n^2 = \sum_{i=1}^{n}(X_i - \overline{X})^2/n \\ S_{n-1}^2 = \sum_{i=1}^{n}(X_i - \overline{X})^2/(n-1) \end{cases}$$

In their research, Vännman and Kotz (1995b) suggested that the estimators of the three indices $C_p(0,3)$, $C_p(0,4)$ and $C_p(1,2)$ have better statistical properties based on some rules. In general, a good index should be able to reveal the truth. e. g. provide a larger (smaller) value of $C_p(u,v)$ when the process is capable (incapable) of producing products which meet the specification limits. Without loss of generality, in this paper we assume $C_p(u,v) \geq 1$.

Let $U = 65$, $L = 25$, $d = (U - L)/2 = 20$, $T = 45$, $\sigma = 1(1)6$. Then, for a given σ,

$$C_p(u,v) \geq 1 \Longleftrightarrow T - \frac{-2du + 6\sqrt{vd^2 + \sigma^2(u^2 - 9v)}}{2(9v - u^2)} \leq \mu \leq T + \frac{-2du + 6\sqrt{vd^2 + \sigma^2(u^2 - 9v)}}{2(9v - u^2)}.$$

$$C_p(0,v) \geq 1 \Longleftrightarrow T - \sqrt{\frac{\frac{d^2}{9} - \sigma^2}{v}} \leq \mu \leq T + \sqrt{\frac{\frac{d^2}{9} - \sigma^2}{v}}, \text{ for any non-negative } v.$$

$$C_p(u,0) \geq 1 \Longleftrightarrow T - \frac{d - 3\sigma}{u} \leq \mu \leq \frac{d - 3\sigma}{u}, \text{ for any non-negative } u.$$

In particular,

$$C_p(0,3) \geq 1 \Longleftrightarrow 45 - \sqrt{\frac{44.\overline{4} - \sigma^2}{3}} \leq \mu \leq 45 + \sqrt{\frac{44.\overline{4} - \sigma^2}{3}}.$$

$$C_p(0,4) \geq 1 \Longleftrightarrow 45 - \sqrt{\frac{44.\overline{4} - \sigma^2}{3}} \leq \mu \leq 45 + \sqrt{\frac{44.\overline{4} - \sigma^2}{3}}.$$

$$C_p(1,2) \geq 1 \Longleftrightarrow 45 - \frac{-40 + \sqrt{1600 - 68(9\sigma^2 - 400)}}{34} \leq \mu \leq 45 + \frac{-40 + \sqrt{1600 - 68(9\sigma^2 - 400)}}{34}.$$

The range of μ for different σ when $C_p(0,3)$, $C_p(0,4)$ and $C_p(1,2) \geq 1$ are given in Table 1.

Table 1. The range of μ when indices are greater than 1.

σ	$C_p(0,3) \geq 1$	$C_p(0,4) \geq 1$	$C_p(1,2) \geq 1$
1	$41.19 \leq \mu \leq 48.81$	$41.70 \leq \mu \leq 48.30$	$41.24 \leq \mu \leq 48.76$
2	$41.33 \leq \mu \leq 48.67$	$41.82 \leq \mu \leq 48.18$	$41.40 \leq \mu \leq 48.60$
3	$41.56 \leq \mu \leq 48.44$	$42.02 \leq \mu \leq 47.98$	$41.69 \leq \mu \leq 48.31$
4	$41.92 \leq \mu \leq 48.08$	$42.33 \leq \mu \leq 47.67$	$42.12 \leq \mu \leq 47.88$
5	$42.45 \leq \mu \leq 47.55$	$42.80 \leq \mu \leq 47.20$	$42.76 \leq \mu \leq 47.24$
6	$43.32 \leq \mu \leq 46.68$	$43.55 \leq \mu \leq 46.45$	$43.76 \leq \mu \leq 46.24$

In addition to the parameters given above, let $\mu = 25(5)65$, u, $v = 0(0.5)6$. Then it is found that

1. For $\forall \sigma$, when $\mu = 25, 65$,
   (1) and $u = 0, 0.5$, $C_p(u,v)$ is decreased as the value of v is increased.
   (2) $C_p(1,v) = 0$.
   (3) all the values of $C_p(u,v)$ discussed here are negative when $u = 1.5(0.5)6$. And the value of $C_p(u,v)$ is increased as v is increased.
2. For $\forall \sigma$, when $\mu = 30, 60$, and
   (1) when $u = 0, 0.5, 1$, the value of $C_p(u,v)$ is decreased

(2) all the value of $C_p(u,v)$ are negative when $u = 1.5(0.5)6$. The value of $C_p(u,v)$ is increased when the value of v is increased.

3. For $\forall\sigma$, when $\mu = 35, 55$, and
   (1) $u = 0(0.5)1.5$, the value of $C_p(u,v)$ is decreased as the value of v is increased.
   (2) $C_p(2,v) = 0$
   (3) when $u = 2.5(0.5)6$, the value of $C_p(u,v)$ are all negative. The value of $C_p(u,v)$ isincreased as v is increased.
4. For $\forall\sigma$, when $\mu = 40, 50$, and
   (1) $u = 0(0.5)3.5$, the value of $C_p(u,v)$ is decreased as the value of v is increased.
   (2) $C_p(4,v) = 0$
   (3) when $u = 4.5(0.5)6$, the value of $C_p(u,v)$ are all negative. The value of $C_p(u,v)$ isincreased as v is increased.
5. When the process is on target, i.e. $\mu = 45 = T$, $C_p(u,v) = C_p$. Therefore, the value of $C_p(u,v)$ remains the same when the value of v is increased. If the process standard deviation σ is small, it is good enough to use the index C_p. But if the standard deviation σ is large, the proportion of out of specification limits will be large, hence a better index should be used instead.

From table 2, we know that when $\mu \neq T$ (i.e. when $\mu \neq 45$), the value of u, v should not be too large. Because if u and v are too large, the value of $C_p(u,v)$ may be underestimated. In the simulationwe consider only the situation when $0 \leq u \leq 3$, $0 \leq v \leq 1.5$.

Table 2. Indices which are greater than 1 under different combination of μ and σ.

(a) $\mu = 25, 65$

σ	1	2	3	4	5	6
$C_p(0,0)$	6.6667	3.3333	2.2222	1.6667	1.3333	1.1111
$C_p(0.5,0)$	3.3333	1.6667	1.1111			

(b) $\mu = 30, 60$

σ	1	2	3	4	5	6
$C_p(0,0)$	6.6667	3.3333	2.2222	1.6667	1.3333	1.1111
$C_p(0.5,0)$	4.1667	2.0833	1.3889	1.0417		
$C_p(1,0)$	1.6667					

(c) $\mu = 35, 55$

σ	1	2	3	4	5	6
$C_p(0,0)$	6.6667	3.3333	2.2222	1.6667	1.3333	1.1111
$C_p(0.5,0)$	5.0000	2.5000	1.6667			
$C_p(1,0)$	3.3333	1.6667				
$C_p(1.5,0)$	1.6667					

(d) $\mu = 40, 50$

σ	1	2	3	4	5	6
$C_p(0,0)$	6.6667	3.3333	2.2222	1.6667	1.3333	1.1111
$C_p(0,0.5)$	1.8144	1.6412	1.4378	1.2488	1.0887	
$C_p(0,1)$	1.3074	1.2380	1.1433	1.0412		
$C_p(0,1.5)$	1.0744	1.0349				
$C_p(0.5,0)$	5.8333	2.9167	1.9444	1.4583	1.1667	
$C_p(0.5,0.5)$	1.5876	1.4361	1.2580	1.0927		
$C_p(0.5,1)$	1.1440	1.0832	1.0004			
$C_p(1,0)$	5.0000	2.5000	1.6667	1.2500	1.0000	
$C_p(1,0.5)$	1.3608	1.2309	1.0783			
$C_p(1.5,0)$	4.1667	2.0833	1.3889	1.0417		
$C_p(1.5,0.5)$	1.1340	1.0258				
$C_p(2,0)$	3.3333	1.6667	1.1111			
$C_p(2.5,0)$	2.5000	1.2500				
$C_p(3,0)$	1.6667					

(e) $\mu = 45$, u, $v = 0$ (0.5) 6

σ	1	2	3	4	5	6
$C_p(u,v)$	6.6667	3.3333	2.2222	1.6667	1.3333	1.1111

Remark: Empty cell means under such combination of (μ, σ), $C_p(u, v) \leq 1$.

SIMULATION STUDY

1. Parameters

Distributions G considered here are $N(\mu, \sigma^2)$, $\sigma(\chi^2_{4.5} - 4.5)/3 + \mu$ and $\sqrt{(3/4)}\sigma t_8$

$+\mu$. All of them have the same mean and the same standard deviation.

Consider the following estimators of $C_p(u,v)$:

$$\hat{C}_1(u,v) = \frac{d - u|\overline{X} - T|}{3\sqrt{S_n^2 + v(\overline{X} - T)^2}}$$

$$\hat{C}_2(u,v) = \frac{d - u|\overline{X} - T|}{3\sqrt{S_{n-1}^2 + v(\overline{X} - T)^2}}$$

$$\hat{C}_4(u,v) = \frac{d - u|m - T|}{3\sqrt{S_n^2 + v(m - T)^2}}$$

$$\hat{C}_5(u,v) = \frac{d - u|m - T|}{3\sqrt{S_{n-1}^2 + v(m - T)^2}}$$

where

$$\overline{X} = \sum_{i=1}^{n} X_i/n$$

$$S_n^2 = \sum_{i=1}^{n} (X_i - \overline{X})^2/n$$

$$S_{n-1}^2 = \sum_{i=1}^{n} (X_i - \overline{X})^2/(n-1)$$

$$m = Median\{X_1, \ldots, X_n\}.$$

Remark: $\hat{C}_1(u,v)$ and $\hat{C}_2(u,v)$ are proposed by Vännman (1995).

From the analysis in Vännman (1995, 1995a) and the result in Table 2, we choose five indices to discuss, namely $C_p(2,0)$, $C_p(3,0)$, $C_p(0,3)$, $C_p(0,4)$ and $C_p(1,2)$. We study the performance of these estimators under three different distributions for different sample sizes. The study will be conducted from the following two points of view:

(I) for $n = 10\ (20)\ 90$, study the frequency that the value of estimators $\hat{C}_i(u,v)$ of each index is larger than c under three distributions, where c locates near the true value of the related indices. The advantage of this approach is that we have fixed rule to compare. In this study, we choose $c = C_p(u,v) \pm h \cdot 0.25$, where $h = 0, 1, 2$. (See Table 3-1-Table 3-5).

Table 3-1. Frequency of each estimator which is greater than c under different distribution in 1000 experiments where $C_i = \hat{C}_i$ (2, 0).

$u=2$ $v=0$		C_1			C_2			C_4			C_5		
n	c	N	t	χ^2	N	t	χ^2	N	t	χ^2	N	t	χ^2
10	2.8333	1000	1000	1000	1000	1000	1000	1000	1000	1000	1000	1000	1000
	3.0833	955	975	952	968	984	985	953	975	922	964	984	965
	3.3333*	555	594	644	546	599	630	551	587	580	534	589	570
	3.5833	185	208	224	191	212	201	193	209	206	194	202	193
	3.8333	47	44	55	50	55	48	43	42	49	51	54	48
30	2.8333	999	999	996	999	999	998	999	999	989	1000	999	991
	3.0833	903	928	910	904	933	920	913	930	849	909	930	870
	3.3333*	556	567	611	553	569	594	557	555	496	556	563	493
	3.5833	202	200	216	200	202	213	202	201	164	196	204	163
	3.8333	45	58	42	43	49	47	43	55	35	45	51	34
90	2.8333	993	991	988	992	990	993	990	992	976	990	992	977
	3.0833	885	868	878	885	872	875	884	873	770	886	873	769
	3.3333*	540	538	547	538	540	539	535	541	388	536	546	384
	3.5833	189	184	187	188	188	192	192	194	99	189	189	105
	3.8333	41	44	36	42	43	38	40	46	16	40	45	17

Remark: * means the value of C_p (2, 0), where $c = C_p$ (2, 0) $\pm h \cdot$ (0.25), $h = 0, 1, 2$.

Table 3-2. Frequency of each estimator which is greater than c under different distribution in 1000 experiments where $C_i = \hat{C}_i$ (3, 0).

$u=3$ $v=0$		C_1			C_2			C_4			C_5		
n	c	N	t	χ^2	N	t	χ^2	N	t	χ^2	N	t	χ^2
10	1.1667	998	1000	1000	1000	1000	1000	998	1000	996	1000	1000	999
	1.4167	907	947	956	931	972	975	905	944	862	925	969	896
	1.6667*	565	604	608	543	581	631	554	596	453	530	577	476
	1.9167	192	209	217	195	203	198	191	218	157	182	202	145
	2.1667	44	47	52	52	58	51	40	43	39	51	54	41
30	1.1667	991	998	996	997	1000	996	993	997	972	997	999	972
	1.4167	883	909	914	889	924	913	891	920	739	902	929	749
	1.6667*	570	560	585	563	548	593	567	554	320	550	541	323
	1.9167	192	209	219	196	205	217	206	219	78	200	215	84
	2.1667	39	45	40	41	48	46	39	43	13	43	45	12
90	1.1667	985	991	987	992	994	987	985	990	977	987	992	976
	1.4167	877	865	875	876	866	877	857	875	643	862	874	645
	1.6667*	527	546	527	512	538	533	528	528	155	522	529	155
	1.9167	194	180	192	194	186	192	194	195	10	193	193	12
	2.1667	37	36	33	35	42	34	27	34	0	31	33	0

Remark: * means the value of C_p (3, 0), where $c = C_p$ (3, 0) $\pm h \cdot$ (0.25), $h = 0, 1, 2$.

Table 3-3. Frequency of each estimator which is greater than c under different distribution in 1000 experiments where $C_i = \hat{C}_i$ (0, 3).

$u=0$ $v=3$		C_1			C_2			C_4			C_5		
n	c	N	t	χ^2	N	t	χ^2	N	t	χ^2	N	t	χ^2
10	0.5851	989	995	1000	995	997	1000	993	996	992	993	997	993
	0.8351	851	886	881	853	895	887	865	884	732	868	891	738
	1.0851*	499	513	493	493	508	490	503	518	285	499	513	283
	1.3351	170	180	171	169	177	164	167	178	83	166	174	81
	1.5851	29	40	45	30	42	47	45	38	19	45	38	19
30	0.5851	983	990	993	986	992	994	996	989	982	997	989	982
	0.8351	864	871	859	863	875	862	883	878	645	886	880	643
	1.0851*	521	523	497	518	520	495	519	522	162	518	519	163
	1.3351	170	174	162	167	174	162	178	158	23	174	156	23
	1.5851	34	35	39	35	36	41	45	41	4	46	41	4
90	0.5851	983	976	992	984	976	992	989	984	995	989	985	995
	0.8351	856	847	846	856	848	847	848	857	578	849	857	577
	1.0851*	520	499	503	518	497	501	514	501	41	513	501	42
	1.3351	178	151	165	178	151	162	168	162	0	167	162	1
	1.5851	33	31	32	34	32	32	34	28	0	34	28	0

Remark: * means the value of C_p (0, 3), where $c = C_p$ (0, 3) $\pm h \cdot$ (0.25), $h = 0, 1, 2$.

Table 3-4. Frequency of each estimator which is greater than c under different distribution in 1000 experiments where $C_i = \hat{C}_i$ (0, 4).

$u=0$ $v=4$		C_1			C_2			C_4			C_5		
n	c	N	t	χ^2	N	t	χ^2	N	t	χ^2	N	t	χ^2
10	0.5960	995	998	1000	997	999	1000	995	998	996	995	998	997
	0.8460	860	899	888	863	907	897	875	897	738	876	900	745
	1.0960*	498	511	492	493	506	490	498	514	285	496	512	283
	1.3460	172	181	168	170	179	163	169	178	84	166	174	84
	1.5960	31	45	48	32	47	48	48	39	20	48	39	21
30	0.5960	986	992	994	987	992	994	997	989	983	997	989	983
	0.8460	866	875	863	866	877	864	890	880	644	890	882	643
	1.0960*	520	525	496	515	522	496	519	521	163	518	518	164
	1.3460	170	173	164	168	172	163	179	159	23	178	155	24
	1.5960	36	38	41	37	39	41	47	42	4	47	43	4
90	0.5960	984	976	992	985	977	992	991	987	995	991	989	995
	0.8460	858	851	849	858	851	850	851	857	578	852	858	576
	1.0960*	518	499	503	515	499	501	513	502	42	513	500	42
	1.3460	177	153	165	177	152	164	170	167	1	170	166	1
	1.5960	34	33	33	36	33	33	35	28	0	35	28	0

Remark: * means the value of C_p (0, 4), where $c = C_p$ (0, 4) $\pm h \cdot$ (0.25), $h = 0, 1, 2$.

Table 3-5. Frequency of each estimator which is greater than c under different distribution in 1000 experiments where $C_i = \hat{C}_i$ (1, 2).

$u=1$ $v=2$		C_1			C_2			C_4			C_5		
n	c	N	t	χ^2	N	t	χ^2	N	t	χ^2	N	t	χ^2
10	0.5892	988	995	999	995	997	1000	993	996	991	993	997	992
	0.8392	851	884	880	855	895	884	862	883	732	868	894	738
	1.0892*	503	518	497	491	504	486	503	519	288	499	517	285
	1.3392	172	178	171	169	176	167	166	180	80	161	175	81
	1.5892	28	39	47	32	40	47	45	38	19	41	39	19
30	0.5892	983	988	993	986	992	993	996	989	982	996	989	982
	0.8392	860	870	859	860	873	860	884	879	643	886	883	644
	1.0892*	519	525	499	518	521	493	518	522	164	516	517	162
	1.3392	168	172	161	165	171	160	178	161	21	177	160	22
	1.5892	31	35	39	32	36	41	44	41	3	45	43	4
90	0.5892	983	975	990	984	976	992	989	983	995	989	983	995
	0.8392	855	850	846	858	851	846	846	855	577	848	858	576
	1.0892*	518	502	506	516	501	501	515	500	39	514	498	40
	1.3392	179	155	163	179	155	163	170	163	0	170	163	0
	1.5892	32	32	30	36	32	31	33	28	0	34	28	0

Remark: * means the value of C_p (1, 2), where $c = C_p$ (1, 2) $\pm h \cdot$ (0.25), $h = 0, 1, 2$.

Table 3-6. Estimated indices which the frequency of underestimation is larger than the frequency of overestimation where $C_i = \hat{C}_i$ (u, v).

(a)

C_p (2, 0)	n / k	10	30	50
N	1	C_2, C_5		C_5
	0.5	C_2, C_5		
t	1	C_4, C_5	C_4, C_5	
	0.5	C_2, C_4, C_5	C_1, C_2, C_4, C_5	
χ^2	1	C_5	C_4, C_5	C_4, C_5
	0.5	C_4, C_5	C_4, C_5	C_4, C_5

(b)

C_p (3, 0)	n / k	10	30	50
N	1	C_2, C_5	C_5	C_2, C_5
	0.5	C_2, C_5		
t	1	C_2, C_5	C_2, C_4, C_5	C_2
	0.5	C_2, C_4, C_5	C_1, C_2, C_4, C_5	C_1, C_2
χ^2	1	C_4, C_5	C_4, C_5	C_4, C_5
	0.5	C_1, C_4, C_5	C_4, C_5	C_4, C_5

(c)

C_p (0, 3)	n / k	10	30	50
N	1	C_1, C_2, C_4, C_5	C_4, C_5	C_1, C_2
	0.5	C_2		
t	1	C_1, C_2, C_4, C_5	C_2	C_1, C_2
	0.5	C_2	C_1, C_2, C_5	
χ^2	1	C_1, C_2, C_4, C_5	, C_2, C_4, C_5	, C_2, C_4, C_5
	0.5	C_1, C_2, C_4, C_5	C_4, C_5	C_4, C_5

(d)

C_p (0, 4)	n / k	10	30	50
N	1	C_1, C_2, C_4, C_5	, C_2, C_4, C_5	C_1, C_2
	0.5	C_2	C_2	
t	1	C_1, C_2, C_4, C_5	C_2, C_5	C_1, C_2, C_4, C_5
	0.5	C_1, C_2, C_4, C_5	C_1, C_2, C_4, C_5	
χ^2	1	C_1, C_2, C_4, C_5	C_1, C_2, C_4, C_5	C_1, C_2, C_4, C_5
	0.5	C_1, C_2, C_4, C_5	C_4, C_5	C_4, C_5

(e)

C_p (0, 3)	n / k	10	30	50
N	1	C_1, C_2, C_4, C_5	C_4, C_5	C_1, C_2
	0.5	C_2		
t	1	C_2, C_4, C_5	C_2, C_5	C_1, C_2
	0.5	C_2	C_1, C_2, C_5	
χ^2	1	C_1, C_2, C_4, C_5	, C_2, C_4, C_5	, C_2, C_4, C_5
	0.5	C_1, C_2, C_4, C_5	C_4, C_5	C_4, C_5

Table 3-7. The probability that $\hat{C}_i$ (0, 3) -C_p (0, 3) lie in $[-k\cdot\sigma_{\hat{C}_i(0,3)},\ k\cdot\sigma_{\hat{C}_i(0,3)}]$ for $n=30$ where $C_i=\hat{C}_i$ (0, 3).

$u=0$	$v=3$		C_1			C_2			C_4			C_5		
μ	σ	κ	N	t	χ^2	N	t	χ^2	N	t	χ^2	N	t	χ^2
41.5	1	1	0.694	0.697	0.697	0.696	0.701	0.700	0.705	0.720	0.622	0.712	0.724	0.620
		2	0.949	0.955	0.954	0.951	0.956	0.953	0.951	0.948	0.978	0.951	0.948	0.978
		3	0.996	0.993	0.994	0.994	0.992	0.993	0.995	0.994	1.000	0.995	0.993	1.000
41.5	2	1	0.699	0.712	0.698	0.703	0.718	0.713	0.727	0.733	0.615	0.736	0.740	0.617
		2	0.955	0.952	0.958	0.955	0.954	0.955	0.948	0.947	0.983	0.947	0.947	0.985
		3	0.992	0.989	0.994	0.990	0.987	0.993	0.993	0.990	0.999	0.988	0.990	0.998
42	3	1	0.698	0.717	0.683	0.720	0.741	0.694	0.725	0.736	0.605	0.745	0.752	0.607
		2	0.955	0.950	0.959	0.955	0.952	0.956	0.943	0.952	0.990	0.943	0.951	0.991
		3	0.993	0.991	0.995	0.986	0.988	0.993	0.991	0.990	0.999	0.986	0.988	0.997
42	4	1	0.686	0.705	0.683	0.724	0.740	0.699	0.710	0.716	0.604	0.735	0.738	0.603
		2	0.955	0.951	0.962	0.954	0.950	0.957	0.946	0.953	0.991	0.941	0.951	0.990
		3	0.995	0.996	0.996	0.988	0.988	0.994	0.995	0.993	1.000	0.989	0.987	0.999
42.5	5	1	0.694	0.690	0.690	0.704	0.713	0.695	0.693	0.703	0.606	0.711	0.719	0.602
		2	0.956	0.959	0.960	0.957	0.950	0.957	0.955	0.954	0.991	0.958	0.955	0.992
		3	0.997	0.992	0.998	0.993	0.990	0.996	0.997	0.990	1.000	0.993	0.992	1.000
43.5	6	1	0.687	0.689	0.676	0.687	0.707	0.670	0.689	0.700	0.626	0.693	0.703	0.620
		2	0.954	0.962	0.961	0.955	0.962	0.965	0.956	0.951	0.986	0.963	0.950	0.986
		3	0.997	0.992	0.998	0.995	0.989	0.998	0.998	0.993	1.000	0.999	0.990	1.000

Table 3-8. The probability that $\hat{C}_i$ (0, 4) -C_p (0, 4) lie in $[-k\cdot\sigma_{\hat{C}_i(0,4)},\ k\cdot\sigma_{\hat{C}_i(0,4)}]$ for $n=30$ where $C_i=\hat{C}_i$ (0, 4).

$u=0$	$v=4$		C_1			C_2			C_4			C_5		
μ	σ	κ	N	t	χ^2	N	t	χ^2	N	t	χ^2	N	t	χ^2
42	1	1	0.696	0.702	0.699	0.698	0.705	0.701	0.711	0.721	0.621	0.712	0.727	0.619
		2	0.950	0.954	0.953	0.950	0.953	0.953	0.950	0.947	0.979	0.950	0.946	0.979
		3	0.994	0.992	0.993	0.993	0.989	0.993	0.994	0.993	1.000	0.993	0.993	1.000
42	2	1	0.700	0.715	0.706	0.707	0.725	0.717	0.734	0.739	0.617	0.741	0.746	0.616
		2	0.955	0.953	0.955	0.955	0.953	0.957	0.947	0.950	0.986	0.946	0.951	0.989
		3	0.990	0.988	0.994	0.989	0.987	0.992	0.990	0.990	0.998	0.988	0.988	0.998
42.5	3	1	0.703	0.725	0.684	0.730	0.755	0.700	0.731	0.740	0.603	0.749	0.761	0.609
		2	0.954	0.947	0.959	0.956	0.949	0.956	0.940	0.949	0.992	0.942	0.950	0.993
		3	0.990	0.991	0.995	0.986	0.986	0.993	0.989	0.989	0.999	0.983	0.986	0.997
42.5	4	1	0.686	0.707	0.680	0.720	0.741	0.694	0.702	0.715	0.596	0.731	0.738	0.595
		2	0.958	0.951	0.962	0.954	0.950	0.958	0.949	0.951	0.993	0.944	0.952	0.992
		3	0.994	0.993	0.996	0.989	0.988	0.993	0.995	0.990	1.000	0.989	0.986	0.999
43	5	1	0.693	0.688	0.688	0.699	0.711	0.690	0.686	0.696	0.603	0.699	0.707	0.597
		2	0.959	0.959	0.961	0.959	0.953	0.964	0.959	0.958	0.994	0.956	0.954	0.994
		3	0.998	0.994	0.998	0.993	0.989	0.998	0.998	0.992	1.000	0.995	0.992	1.000
44	6	1	0.681	0.683	0.672	0.676	0.691	0.674	0.686	0.690	0.619	0.684	0.691	0.617
		2	0.954	0.956	0.963	0.958	0.959	0.966	0.951	0.953	0.987	0.957	0.949	0.987
		3	0.997	0.996	0.997	0.997	0.993	0.997	0.997	0.996	1.000	0.998	0.995	1.000

Table 3-9. The probability that $\hat{C}_i$ (1, 2) -C_p (1, 2) lie in $[-k\cdot\sigma_{\hat{C}_i(1,2)},\ k\cdot\sigma_{\hat{C}_i(1,2)}]$ for $n=30$ where $C_i=\hat{C}_i$ (1, 2).

$u=1$	$v=2$		C_1			C_2			C_4			C_5		
μ	σ	κ	N	t	χ^2	N	t	χ^2	N	t	χ^2	N	t	χ^2
		1	0.692	0.698	0.698	0.695	0.702	0.700	0.706	0.718	0.622	0.709	0.723	0.622
41.5	1	2	0.952	0.953	0.954	0.954	0.956	0.952	0.952	0.948	0.979	0.951	0.946	0.978
		3	0.996	0.994	0.994	0.995	0.991	0.994	0.996	0.994	1.000	0.995	0.993	1.000
		1	0.694	0.715	0.693	0.702	0.722	0.707	0.726	0.726	0.618	0.731	0.742	0.617
41.5	2	2	0.955	0.952	0.957	0.955	0.953	0.958	0.950	0.946	0.982	0.947	0.946	0.983
		3	0.994	0.991	0.995	0.991	0.988	0.993	0.994	0.992	0.999	0.988	0.990	0.999
		1	0.689	0.704	0.680	0.714	0.733	0.689	0.715	0.722	0.608	0.737	0.736	0.613
42	3	2	0.950	0.951	0.960	0.957	0.949	0.959	0.945	0.953	0.986	0.943	0.953	0.989
		3	0.995	0.994	0.997	0.989	0.987	0.993	0.995	0.993	0.999	0.989	0.990	0.999
		1	0.686	0.690	0.688	0.711	0.725	0.698	0.686	0.706	0.613	0.710	0.731	0.613
42.5	4	2	0.958	0.954	0.954	0.956	0.949	0.959	0.953	0.953	0.988	0.948	0.952	0.989
		3	0.996	0.992	0.997	0.991	0.988	0.994	0.997	0.992	1.000	0.990	0.987	1.000
		1	0.689	0.691	0.679	0.706	0.706	0.689	0.688	0.699	0.609	0.697	0.708	0.610
43	5	2	0.953	0.957	0.956	0.960	0.957	0.959	0.959	0.955	0.984	0.954	0.951	0.988
		3	0.998	0.992	0.996	0.993	0.988	0.997	0.998	0.993	1.000	0.996	0.992	1.000
		1	0.688	0.686	0.676	0.679	0.698	0.673	0.690	0.693	0.630	0.684	0.698	0.630
44	6	2	0.954	0.957	0.958	0.958	0.955	0.957	0.952	0.953	0.976	0.955	0.948	0.973
		3	0.997	0.996	0.997	0.997	0.993	0.997	0.997	0.994	1.000	0.998	0.993	1.000

Table 3-10. The probability that $\hat{C}_i$ (2, 0) -C_p (2, 0) lie in $[-k\cdot\sigma_{\hat{C}_i(2,0)},\ k\cdot\sigma_{\hat{C}_i(2,0)}]$ for $n=30$ where $C_i=\hat{C}_i$ (2, 0).

$u=2$	$v=0$		C_1			C_2		
μ	σ	κ	N	t	χ^2	N	t	χ^2
		1	0.701	0.728	0.694	0.704	0.731	0.707
40	1	2	0.954	0.941	0.954	0.956	0.950	0.951
		3	0.994	0.993	0.993	0.993	0.988	0.989
		1	0.694	0.720	0.693	0.701	0.719	0.704
40	2	2	0.955	0.949	0.954	0.953	0.949	0.957
		3	0.995	0.990	0.994	0.993	0.988	0.989
		1	0.691	0.700	0.695	0.693	0.719	0.696
40	3	2	0.952	0.953	0.956	0.956	0.952	0.950
		3	0.996	0.992	0.994	0.994	0.988	0.994
$u=2$	$v=0$		C_4			C_5		
μ	σ	k	N	t	χ^2	N	t	χ^2
		1	0.711	0.729	0.685	0.713	0.726	0.707
40	1	2	0.956	0.944	0.954	0.955	0.948	0.957
		3	0.994	0.992	0.995	0.994	0.987	0.991
		1	0.696	0.722	0.695	0.704	0.726	0.687
40	2	2	0.948	0.949	0.955	0.953	0.949	0.954
		3	0.996	0.989	0.998	0.994	0.986	0.996
		1	0.685	0.701	0.661	0.702	0.714	0.665
40	3	2	0.954	0.954	0.959	0.954	0.954	0.960
		3	0.999	0.991	0.999	0.996	0.987	0.999

Table 3-11. The probability that $\hat{C}_i$ (3, 0) -C_p (3, 0) lie in $[-k\cdot\sigma_{\hat{C}_i(3,0)},\ k\cdot\sigma_{\hat{C}_i(3,0)}]$ for $n=30$ where $C_i=\hat{C}_i$ (3, 0).

$u=2$	$v=0$		C_1			C_2		
μ	σ	k	N	t	χ^2	N	t	χ^2
		1	0.691	0.700	0.695	0.693	0.719	0.696
40	1	2	0.952	0.953	0.956	0.956	0.952	0.950
		3	0.996	0.992	0.994	0.994	0.988	0.994
$u=2$	$v=0$		C_4			C_5		
μ	σ	k	N	t	χ^2	N	t	χ^2
		1	0.685	0.701	0.661	0.702	0.714	0.665
40	1	2	0.954	0.954	0.959	0.954	0.954	0.960
		3	0.999	0.991	0.999	0.996	0.987	0.999

(II) for n = 10 (20) 50, study the frequency that the errors $\hat{C}_i(u,v) - C_p(u,v)$ which porduced from five estimators lie in $[-k\cdot\sigma_{\hat{C}_i(u,v)},\ 0]$, $[0,\ k\cdot\sigma_{\hat{C}_i(u,v)}]$ (see Table 3-6) and lie in $[-k\cdot\sigma_{\hat{C}_i(u,v)},\ k\cdot\sigma_{\hat{C}_i(u,v)}]$ (see Table 3-7 – 3-11). The advantage of this approach is that we can see if estimators underestimate or overestimate the true indices. Also we can see the skewness of the distribution of estimators.

In this study, we concern only those processes with higher capability, i.e. when $C_p(u,v)\geq 1$. Proper values of the process mean μ and process standard deviation σ for each index are given as following:

(Ⅰ) $C_p(2,0)$: $\sigma = 1(1)3$, $\mu = 40$;

(Ⅱ) $C_p(3,0)$: $\sigma = 1$, $\mu = 40$;

(Ⅲ) $C_p(0,3)$:

(1) $\sigma = 1$, $\mu = 41.5\ (0.5)\ 44.5$

(2) $\sigma = 2$, $\mu = 41.5\ (0.5)\ 44.5$

(3) $\sigma = 3$, $\mu = 42\ (0.5)\ 44.5$

(4) $\sigma = 4$, $\mu = 42\ (0.5)\ 44.5$

(5) $\sigma = 5$, $\mu = 42.5\ (0.5)\ 44.5$

(6) $\sigma = 6$, $\mu = 43.5\ (0.5)\ 44.5$;

(Ⅳ) $C_p(0,4)$:

(1) $\sigma = 1$, $\mu = 42\ (0.5)\ 44.5$ (2) $\sigma = 2$, $\mu = 42\ (0.5)\ 44.5$ (3) $\sigma = 3$, $\mu = 42.5\ (0.5)\ 44.5$ (4) $\sigma = 4$, $\mu = 42.5\ (0.5)\ 44.5$ (5) $\sigma = 5$, $\mu = 43\ (0.5)\ 44.5$ (6) $\sigma = 6$, $\mu = 44\ (0.5)\ 44.5$;

(V) $C_p(1,2)$:

(1) $\sigma = 1$, $\mu = 41.5\ (0.5)\ 44.5$ (2) $\sigma = 2$, $\mu = 41.5\ (0.5)\ 44.5$ (3) $\sigma = 3$, $\mu = 42\ (0.5)\ 44.5$ (4) $\sigma = 4$, $\mu = 42.5\ (0.5)\ 44.5$ (5) $\sigma = 5$, $\mu = 43\ (0.5)\ 44.5$ (6) $\sigma = 6$, $\mu = 44\ (0.5)\ 44.5$.

2. Simulation Results

One thing we can see from Table 3-3, 3-4, and 3-5 is that for $(u,v) = (0,3)$, $(0,4)$ and $(1,2)$, the number of $\hat{C}_3(u,v)$ which makes $\hat{C}_i(u,v) \geq C_i(u,v)$ is quite different for small sample (i.e. $n = 10$) from that for large samples (i.e. $n \geq 30$). Same result holds for $\hat{C}_6(u,v)$. But such result is not shown in the case when $(u,v) = (2,0)$ and $(3,\ 0)$. See Table 3-1 and 3-2.

For chi-square distribution, when we compare $\hat{C}_1(u,v)$ with $\hat{C}_4(u,v)$, and compare $\hat{C}_2(u,v)$ with $\hat{C}_5(u,v)$, we see that use $\hat{\mu} = \overline{X}$ and $\hat{\mu} = m$ will lead to very different result even when $\hat{\sigma}$ are kept the same in those estimators. Especially, when the value of n and c are increased, the difference among those estimators become more and more significant.

When we compare estimators under three different distributions, we found out that the chances estimators $\hat{C}_4(u,v)$ and $\hat{C}_5(u,v)$ greater than the true value of correspoding indices under chi-square distribution are quite smaller than the chances when under the other two symmetric distributions regardless the sample size. See Table 3-3, 3-4 and 3-5. This result consists of the result gotten by Kotz and Johnson (1993).

From Table 3-6(c)(d), when the sample is small (i.e. $n = 10$), all the estimators underestimate the true value within one standard deviation. The underestimation is within 0.5 standard deviation for chi-square distribution.

Based on the simulation under normal distribution and t distribution, the number that $\hat{C}_1(u,v) - C_p(u,v)$ and $\hat{C}_4(u,v) - C_p(u,v)$ lying in $[-k \cdot \sigma_{|\hat{C}_i(u,v)}, 0]$ and $[0, \cdot\ \sigma_{C_i(u,v)}]$ are close to each other. And the number that $\hat{C}(u,v) - C_p(u,v)$ and $\hat{C}_5(u, v) - C_p(u,v)$ lying in $[-k \cdot \sigma_{\hat{C}_i(u,v)}, 0]$ and $[0, k \cdot \sigma_{C_i(u,v)}]$ are similar too. i.e. For symetric type distribution, use $\overline{X}$ and median to estimate μ will lead to similar results. But, for χ^2 distribution, use median to estimate μ will underestimate the true value of

indices.

Based on those parameters given in section 3.1, the probability that $\hat{C}_i(u,v) - C_p(u,v)$ lying in $[-k \cdot \sigma_{\hat{C}_i(u,v)}, k \cdot \sigma_{\hat{C}_i(u,v)}]$ for five indices $C_p(2,0)$, $C_p(3,0)$, $C_p(0,3)$, $C_p(0,4)$ and $C_p(1,2)$ are listed in Table 3-7, 3-8, 3-9, 3-10, 3-11, respectively. Due to the restriction of pages, we only list the results for sample size 30. The results for other sample sizes can be gotten from the authors.

From table 3-7, 3-8, 3-9, 3-10 and 3-11, the simulation results under normality coincide with the result derived by Vännman. For the other two distributions, since the fourth moment μ_4 of t-distribution and chi-square distribution exist, our simulation results are reasonable compare with Chen's (1996) theoretical results for non-normal processes.

Table 3-12.

(a) The frequency of $\hat{C}_i(3,0) - C_p(3,0)$ lie in $[-k \cdot \sigma_{\hat{C}_i(3,0)}, 0]$ for $n = 100$ under chi-square distributionwhere $C_i = \hat{C}_i(3,0)$.

μ	σ	κ	C_1	C_2	C_4	C_5
40	1	1	330	328	494	507
		2	432	432	832	838
		3	449	447	857	862

(b) The frequency of $\hat{C}_i(3,0) - C_p(3,0)$ lie in $[0, k \cdot \sigma_{\hat{C}_i(3,0)}, 0]$ for $n = 100$ under chi-square distributionwhere $C_i = \hat{C}_i(3,0)$.

μ	σ	κ	C_1	C_2	C_4	C_5
40	1	1	368	368	136	129
		2	513	512	143	138
		3	548	550	143	138

Table 3-12 (a) (b) give us an idea how do the estimator perform under chi-square distribution for $n = 100$. As we can see from the table, the frequency of $C_1(u,v)$ and $C_2(u,v)$ to lie in the upper 1, 2, 3 standard deviation of the true value are about the same. But for $C_4(u,v)$ and $C_5(u,v)$ the chance that estimators underestimate the true value in all 1, 2, 3 standard deviation are quite different. And when we look at

$C_3(u,v)$ and $C_6(u,v)$, both estimators underestimate the true value of indices but in two standard deviation. So in order to use these two estimators properly, we have to do some transformation before studying the capability of processes.

Table 3-13 (a) (b) give us similar results. But it also looks like there is a tendency of overestimating the true value for $C_1(u,v)$ and $C_2(u,v)$, but reverse results for $C_4(u,v)$ and $C_5(u,v)$.

Table 3-13.

(a) The frequency of $\hat{C}_i(2,0) - C_p(2,0)$ lie in $[-k\cdot\sigma_{\hat{C}_i(2,0)}, 0]$ for $n=100$ under chi-square distributionwhere $C_i=\hat{C}_i(2,0)$.

μ	σ	κ	C_1	C_2	C_4	C_5
		1	346	353	417	427
40	1	2	449	456	604	614
		3	461	468	635	639
		1	336	340	454	450
40	2	2	444	444	741	735
		3	459	458	776	771
		1	330	329	494	507
40	3	2	432	432	832	838
		3	449	447	857	862

(b) The frequency of $\hat{C}_i(2,0) - C_p(2,0)$ lie in $[0, k\cdot\sigma_{\hat{C}_i(2,0)}, 0]$ for $n=100$ under chi-square distributionwhere $C_i=\hat{C}_i(2,0)$.

μ	σ	κ	C_1	C_2	C_4	C_5
		1	346	338	270	265
40	1	2	503	496	347	342
		3	537	527	364	360
		1	359	357	187	190
40	2	2	503	504	222	227
		3	538	539	223	228
		1	368	368	136	129
40	3	2	513	512	143	138
		3	548	550	143	138

CONCLUSIONS AND SUGGESTIONS

The four basic process capability indices C_p, C_{pk}, C_{pm} and C_{pmk} have been well studied. This article concentrate on the differences among six estimators under three distributions.

From the simulation, we found that all estimators for indices $C_p(2,0)$, $C_p(3,0)$, $C_p(0,3)$, $C_p(0,4)$ and $C_p(1,2)$ which derived by setting $\hat{\sigma} = R$ perform poorly. For chi-square distribution, estimators derived by setting $\hat{\mu} = median$ always underestimate the true value of the corresponding indes.

For symmetric type distributions, $\hat{C}_1(u,v)$, $\hat{C}_2(u,v)$, $\hat{C}_4(u,v)$ and $\hat{C}_5(u,v)$ have about the same effect. For asymmetric distributions, $\hat{C}_1(u,v)$ and $\hat{C}_2(u,v)$ lead to better results. Therefore, we suggest that if we don't know the true distribution for a process, use $\overline{X}$ to estimatae μ, and use S_n or S_{n-1} to estimate σ. But if the true distribution is known to be symmetric, then use median to estimate μ will give similar good results.

Another way to deal with asymmetric distributions is do some transformation on the measurement before study the process capability of such process.

BIBLIOGRAPHY

(1) Bissell, A. F. "How Reliable is Your Capability Index?", *Applied Statistics*, **39**, 331-340 (1990).

(2) Boyles, R. A. "The Taguchi Capability Index", *Journal of Quality Technology*, **23** (1), 17-26 (1991).

(3) Boyles, R. A. "Process Capability with Asymmetric Tolerances," *Communication in Statistics-Simulation*, **23** (3), 615-643 (1994).

(4) Chan, L. K., Cheng, S. W., and Spiring, F. A. "A new measure of process capability: C_{pm}". *Journal of Quality Technology*, **20**, 162-175 (1988).

(5) Chen, S. M., and Hsu, N. F. "The asymptotic distribution of the estimated process capability index $\hat{C}_{pmk}$". *Communications in Statistics: Theory and Methods*, **24**, 1279-1291 (1995).

(6) Chen, S. M. " Asymptotic distribution of the Vännman type indices for non-normal Process". Submitted to Scandinavian Journal of Statistics (1996).

(7) Chou, Y. M. and Owen, D. B. "On The Distributions of the Estimated Process Capability Indices", *Communication in Statistics-Theory and Methods*, **18** (12), 4549-4560 (1989).

(8) Clements. "Process Capability Calculations for Non-NormalDistributions", *Quality Progress*, Sep, 95-100 (1989).

(9) Gunter, B. "The use and abuse of C_{pk}: Parts 2". *Quality Progress*, p. 108-109 (1989).

(10) Juran, J. M. Jurans Quality Control Handbook, Third Edition. McGraw-Hill, New York (1974).

(11) Kane, V. E. "Process capability indices". *Journal of Quality Technology*, **18**, 41-52 (1986).

(12) Kotz, S., and Johnson, N. L., Process Capability Indices. Chapman Hall, London (1993).

(13) Kushler, R. and Hurley, P. "Confidence Bounds of Capability Indices", *Journal of Quality Technology*, **24**, 188-195 (1992).

(14) Pearn, W. L., Kotz, S., and Johnson, N. L. , "Distributional and inferential properties of process capability indices". *Journal of Quality Technology*, **24**, 216-231 (1992).

(15) Pearn, W., Kotz, S. and Johnson, N. "Some Process Capability Indices are More Reliable than One Might Think", *Applied Statistics*, **42** (1), 55-62 (1993).

(16) Spiring, F. A. "The $C- {pm} $ Index", *Quality Progress*, **24** (2), 57-61 (1991).

(17) Sullivan L. P. "Letters: C_p and C_{pk}", *Quality Progress*, **18**, 4, 7-8 (1985).

(18) Vännman, K. "Aunified approach to capability indices". *Statistica Sinica*, **5**, 805-820 (1995).

(19) Vännman, K., and Kotz, S. "A superstructure of capability indices-distributional properties and implications". *Scandinavian Journal of Statistics*, **22**, 477-491 (1995a).

(20) Vännman, K., and Kotz, S. "A superstructure of capability indices-asymptotics and its implications". *International Journal of Reliability, Quality and Safety Engineering*, **2**, 343-360 (1995b).

(21) Zhang, N. F., Stenback, G. A. and Wardrop, D. P. "Interval Estimation of Process Capability Index C_{pk}", *Communications in Statistics: Theory and Methods*, **19**, 4455-4471 (1990).

85年10月13日 收稿
85年11月 3日 修正
85年11月28日 接受

范氏製程能力指標之研究

陳思勉　　巫靈燕
輔仁大學數學系

摘　要

1995 年 Vännman 針對常態品質特性之製程，提出一個新的製程能力指標族 $C_p(u, v)$。

本論文主要觀察該指標族在常態與非常態的製程中，幾種不同估計式的敏感度。由模擬的結果吾人發現當製程特性屬卡方分佈時，用中位數估計期望值會產生低估的現象。而且在所有模擬之分佈中用樣本平均數估計母體平均數及用樣本標準差 S_n 或 S_{n-1} 來估計母體標準差最適當。

關鍵詞： 製程能力指標

同時測量光纖中法拉第旋轉與雙折射的一種新方法

王光宙　蔡政男　柯頓　蕭光志
輔仁大學物理研究所

摘　要

本研究提出一種測量光纖中法拉第旋轉及雙折射的新方法，利用加壓調動系統雙折射的方式，在調動前後，分別測量光偏振態在系統中的改變，再由量得的兩組數據聯立解出雙折射及法拉第旋轉角。作電流檢測時，這個方法不受雙折射的限制，也間接降低了環境變動所引起的干擾。實驗結果顯示，法拉第旋轉角與電流約成線性關係，Verdet 常數爲 4.88×10^{-6}rad/A，雙折射則近於定值 133 $\pm0.9^0$。由數據可以看出，這是測量雙折射及法拉第效應的一個有效可靠的方法。

關鍵詞： 光纖、法拉第效應、雙折射

一、簡　介

法拉第效應（Faraday Effect）常被用在電流及磁場的測量［1］。特別是在大電流、高電壓或有電磁干擾的情況下，在同時考慮響應速度及穩定性時，最能凸顯它的安全、快速及不受干擾等優點。近年來在技術上已有相當進步，尤其應用在極大脈波電流的測量上，有許多成功的例子［2-5］。

另一方面，法拉第效應感測器仍存有許多問題。首先要瞭解法拉第旋轉及線性雙折射兩種效應［6-8］。在光纖中，法拉第旋轉及雙折射無法從光纖末端所讀取的信號中分開來，有時法拉第旋轉角數值不大，於是感測器的靈敏度取決於線性雙折射的大小［9］，雙折射愈小，靈敏度愈高。爲了壓制線性雙折射效應，有下列幾種方法：

1.使用超低雙折射光纖，可消除大部分的本質（Intrinsic）雙折射［10］。但是在纏繞固定時，無法避免由彎曲、張力及壓力所產生的雙折射［11-14］。
2.扭轉（Twist）光纖可以抑制雙折射效應［7、8、15、16］，但是所需的扭轉率往往太高，使光纖不能承受。此外，扭轉產生的圓雙折射略隨溫度改變［17］，使系統不穩定。
3.使用一種特殊的維持圓偏振的光纖［18-20］。此種光纖必須特別製作，取得不易。
4.用特殊的纏繞方式［21-23］，使彎曲產生的雙折射大部分自相抵消。
5.加溫退火［24］以消減光纖內的應力，降低雙折射。

以上諸多方法都有一定的成效，但也各有其限制，主要困難在於雙折射極易發生，對環境亦甚敏感，因而使其效果及實用性大打折扣。

另一種解決雙折射問題的途徑，即是，在量測法拉第旋轉的同時，也量測雙折射。理論上當雙折射的影響爲已知時，從量測的數據可以算出正確的法拉第旋轉角。此一理念首見於 Ren 及 Robert［25］的實驗中，他們用線偏光及圓偏光先後輸入光纖，量得二信號後，計算法拉第旋轉角及雙折射值。

本文採行同樣的概念，以兩次量測求解兩個未知數。對光纖施力，使系統雙折射值作定量的微小改變，用改變前後的兩個信號計算法拉第旋轉及雙折射值。這個方法突破傳統量測單一信號所受的限制，不因雙折射而影響法拉第旋轉的測量結果，也較不受溫度、壓力等環境因素干擾，可以精確量出法拉第旋轉及電流。

二、光纖系統的偏振特性

1. 法拉第效應

在磁場的作用下，線偏光的偏振面會旋轉，旋轉的角度可表示爲

$$\phi = \int VH \cdot dL \tag{1}$$

這個現象稱爲法拉第磁光效應。式中的 V 爲 Verdet 常數，定義爲光行進方向上，單位磁場強度下單位距離的偏振面旋轉角，與光的波長，環境溫度，及材料性質有關。熔矽光纖的 Verdet 常數參考值爲 4.68×10^{-6} rad/A。實驗上常使用較小電流，爲使法拉第效應容易檢測，故而將電流導線及光纖分別纏繞 N_c 及 N_f 圈，對封閉之迴路，利用安培定律（1）式可化成

$$\phi = V\oint H.dL = VN_cN_fI \tag{2}$$

式中 I 爲電流。

2. 雙折射與磁場的綜合效應

低雙折射光纖的折射率分佈及構造近圓對稱，因此本質雙折射低，而外界的干擾，如彎曲、壓力、溫差等等，均能產生感應雙折射。不論使用何種光纖，系統中的雙折射不能忽略。

法拉第效應與雙折射並存時，對偏振光的作用可以用下式表示［6］

$$\text{Eout} = \begin{bmatrix} A & -B \\ B & A^* \end{bmatrix} \text{Ein} \tag{3}$$

式中 Ein 及 Eout 分別爲輸入光及輸出光的 Jones 向量，星號（＊）表示共軛複數，A 及 B 與雙折射 δ 及法拉第旋轉 ϕ 的關係爲

$$\begin{aligned} A &= \cos(\alpha/2) + i\cos x \sin(\alpha/2) \\ B &= \sin x \sin(\alpha/2) \\ \alpha &= (4\phi^2 + \delta^2)^{1/2} \\ \tan x &= 2\phi/\delta \end{aligned} \tag{4}$$

爲了簡化分析，假設入射偏振光爲

$$\text{Ein} = \begin{bmatrix} E_0 \\ O \end{bmatrix} \tag{5}$$

在輸出端檢測與 Ein 成 45°的二偏振分量

$$\text{Eout} = E_1 + E_2 \tag{6}$$

$$\begin{aligned} E_1 &= (\sqrt{2}/2)E_0(A - B) \\ E_2 &= (\sqrt{2}/2)E_0(A + B) \end{aligned} \tag{7}$$

$$\begin{aligned} I_1 &= |E_1|^2 = (1/2)E_0^2|A - B|^2 \\ I_2 &= |E_2|^2 = (1/2)E_0^2|A + B|^2 \end{aligned} \tag{8}$$

定義信號

$$S = \frac{I_2 - I_1}{I_2 + I_1} \tag{9}$$

$$S = (2\phi/\alpha)\sin\alpha \tag{10}$$

當 $\delta \gg 2\phi$ 時

$$S = (2\phi/\delta)\sin\delta \tag{11}$$

信號與法拉第效應成正比，但因雙折而衰減，當雙折射接近 π 的整數倍（0 除外）時，信號極小，不易測量法拉第效應，實驗中應避免這種情況發生。

3. 不均勻磁場的誤差

前節的結果，尤其（4）式，乃基於雙折射及法拉第旋轉沿光纖均勻分佈的假設，亦即，單位長度光纖的雙折射及法拉第旋轉爲定值。若分佈不均勻，則應沿光纖積分，結果無法表示成（3）及（4）的簡單形式［24］。以下以簡單模型探討此一問題。

將光纖分成等長的 $2N$ 段，設法拉第旋轉均分於第 1、3、5…$(2N-1)$ 段，而雙折射則分佈於全長，這種情形相當於磁場僅覆蓋 N 圈光纖環的半圓，而另半圓不在磁場內，令

$$M = \begin{bmatrix} \exp(i\delta/4N) & 0 \\ 0 & \exp(-i\delta/4N) \end{bmatrix} \begin{bmatrix} a & -b \\ b & a^* \end{bmatrix} \tag{12}$$

$$a = \cos(\alpha'/2) + i\cos x'\sin(\alpha'/2)$$

$$b = \sin x'\sin(\alpha'/2)$$

$$\alpha' = [(2\phi/N)^2 + (\phi/2N)^2]^{1/2}$$

$$\tan x' = 4\phi/\delta \tag{13}$$

M 爲一圈的等效 Jones 矩陣，對光纖環

$$\mathrm{Eout} = M^N \mathrm{Ein} \tag{14}$$

由此出射 Jones 向量可以計算信號 S_N。以典型的數值 $\phi = 0.1$ rad，$\delta = 1$ rad，代入計算，結果如表一，當 $N = 10$ 時，信號誤差爲 1.4%，已可接受。在實驗中（詳見下章），光纖環爲 11 圈，電流導線靠近光纖環的一定點繞過。假設法拉第效應集中但均勻分佈於每圈 1/20，則類似的計算得到信號誤差爲 1.2%，實際上磁場分佈應較假設情況均勻，誤差應小於此值。

表一 磁場分佈不均勻的影響，$\phi = 0.1\text{rad}$ $\delta = 1\text{rad}$，$S = 0.1671$。

N	S_N	$(\Delta S/S) \times 100\%$
1	0.1438	13.9
2	0.1559	6.9
5	0.1625	2.7
10	0.1648	1.4
20	0.1659	0.7

4. 雙折射的調動

爲了解出雙折射與法拉第旋轉角，需要量測兩個信號，實驗中用加壓的方式改變雙折射。假設系統原有雙折射 δ_0，在與慢軸夾角爲 θ 的方向加壓力，產生雙折射 δ_1，則合成的雙折射爲［27］

$$\delta = (\delta_0^2 + \delta_1^2 - 2\delta_0\delta_i \cos\theta)^{1/2} \tag{15}$$

當 $\theta = 0$ 時

$$\delta = |\delta_0 - \delta_1| \tag{16}$$

改變壓力可以得到不同的雙折射值。

令雙折射爲 δ_1 及 δ_2 時，信號分別爲 S_1 及 S_2，

$$S_i = (2\phi/\alpha_i)\sin\alpha_i \tag{17}$$

$$\alpha_i = (4\alpha^2 + \delta_i^2)^{1/2}, i = 1,2 \tag{18}$$

若雙折射改變量 $\Delta = \delta_2 - \delta_1$ 已知，則由（2. 17）式可以解出 δ_1, δ_2 及 ϕ。當 $\Delta \to 0$

$$\frac{\partial S}{\partial \delta} = (2\phi\delta/\alpha^2)\cos\alpha - (2\phi\delta/\alpha^3)\sin\alpha \tag{19}$$

上述方法相當於量測信號 S 及其導函數 $\partial S/\partial\delta$，聯立解出雙折射 δ 及法拉第旋轉 ϕ。

前曾提及實驗中應避免使雙折射接近 π 的整數倍，另一方面，當 δ 近於 $\pi/2$ 的奇數倍時，雖然 S 爲極值，容易測量，但 $\partial S/\partial\delta \sim 0$，測量誤差大，也是應該避開的狀況。

三、實　　驗

1. 實驗裝置

實驗系統如圖 1，光源使用波長 632.8nm 的氦氖雷射，輸出 5mW 的線偏光，爲提高入射光的偏振比（$\leq 10^{-5}$），使用 Glan-Thompson 偏振器，偏振方向則用半波片控制。

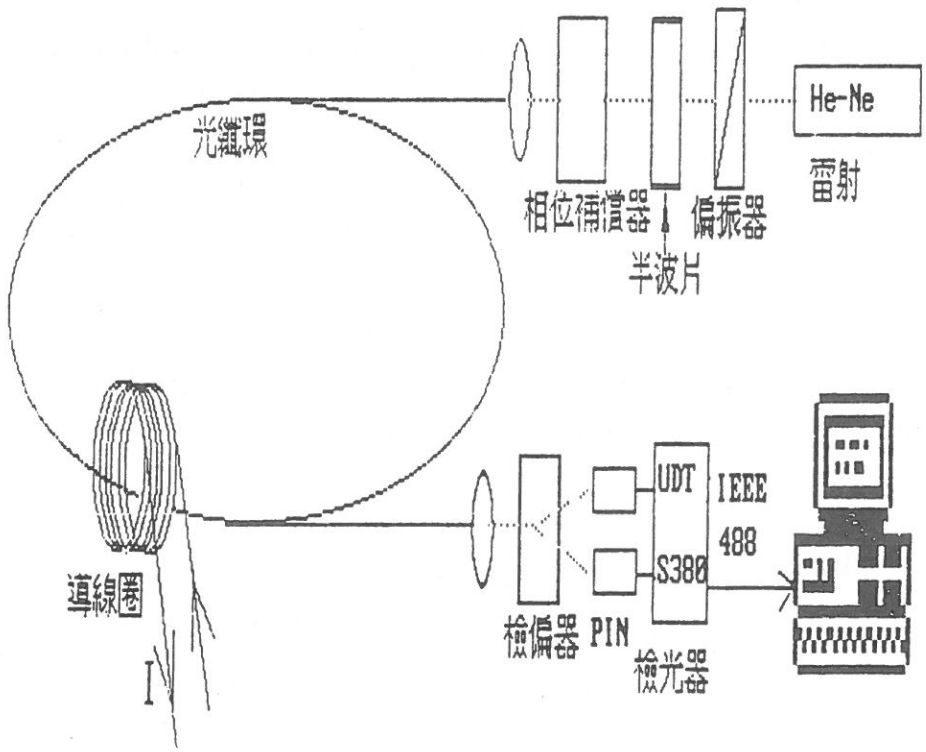

圖 1　實驗系統，詳見本文。相位補償器爲測量光纖系統雙折射所用，電流量測實驗時，自系統中移去。

導光用低雙折射單模光纖，纖心及纖衣的折射率分別爲 1.4627 及 1.4587，直徑分別爲 5 及 125μm，數值孔徑 0.11，繞成直徑 0.7m 的環形，共 11 圈。

在雷射—光纖及光纖—檢光器間，光耦合使用顯微物鏡，爲了匹配光纖的數值孔徑，選用 10X 的物鏡。

檢光器爲 PIN-60 矽光二極體（United Detector Technology，型號 S380），有兩個波道，可以同時測量 Wollaston 檢偏器所分出的二束光。經由 IEE488 界面，連接電腦操控檢測過程。

提供磁場的電流爲 0-18A 的直流電流，導線繞成 123 圈，直徑約 2m。

2. 方法與步驟

首先將偏振面對準光纖系統的雙折射主軸，用半波片控制偏振方向，經由 Wollaston 稜鏡檢偏，當出射光仍爲線偏振時，偏振面與主軸之一（快軸或慢軸）重合。放入相位補償器，旋轉其方向，以同樣的方法，將補償器的主軸對準光纖系統的主軸。

測量光纖系統的雙折射時，將入射偏振面轉離主軸方向，此時出射光成橢圓偏振。調整補償器使出射光變成線偏振，則光纖的雙折射可由補償器的相位延遲量推算出來。

調動雙折射的方法是以小塊平板置於光纖上，板上再放砝碼，以重量加壓，改變系統的雙折射。實驗結果如圖 2，曲線顯示雙折射與壓力並非如理論［13］所預測的線性關係，原因可能是纖被（Jacket）極有彈性，將所受的力分散到各方向，減弱了壓力的作用。

測量電流或法拉第旋轉角時，先將入射光偏振面調回雙折射主軸的方向，移走相位補償器，並旋轉 Wollaston 稜鏡，使受檢的二束光偏振面與入射偏振面成 45°，如此在小電流時，信號對電流的敏感度最高，線性區域最寬。對每一電流，在不同壓力下分別量測信號，再用（17）式計算法拉第效應及雙折射。

3. 實驗結果

在各種砝碼重量加壓之下，測得的信號與電流關係如圖 3，圖中明白顯示出 (11) 式的線性近似。將加壓重量換算出雙折射的變化（圖 2），再代入（17）式計算，得到的雙折射及法拉第旋轉及雙折射如圖 4、圖 5 及表 2，以最小平方差擬合 (least square fit) 的線性近似爲

$$\phi = 0.378I \pm 0.1 \tag{20}$$

$$\delta = 133 \pm 0.9 \tag{21}$$

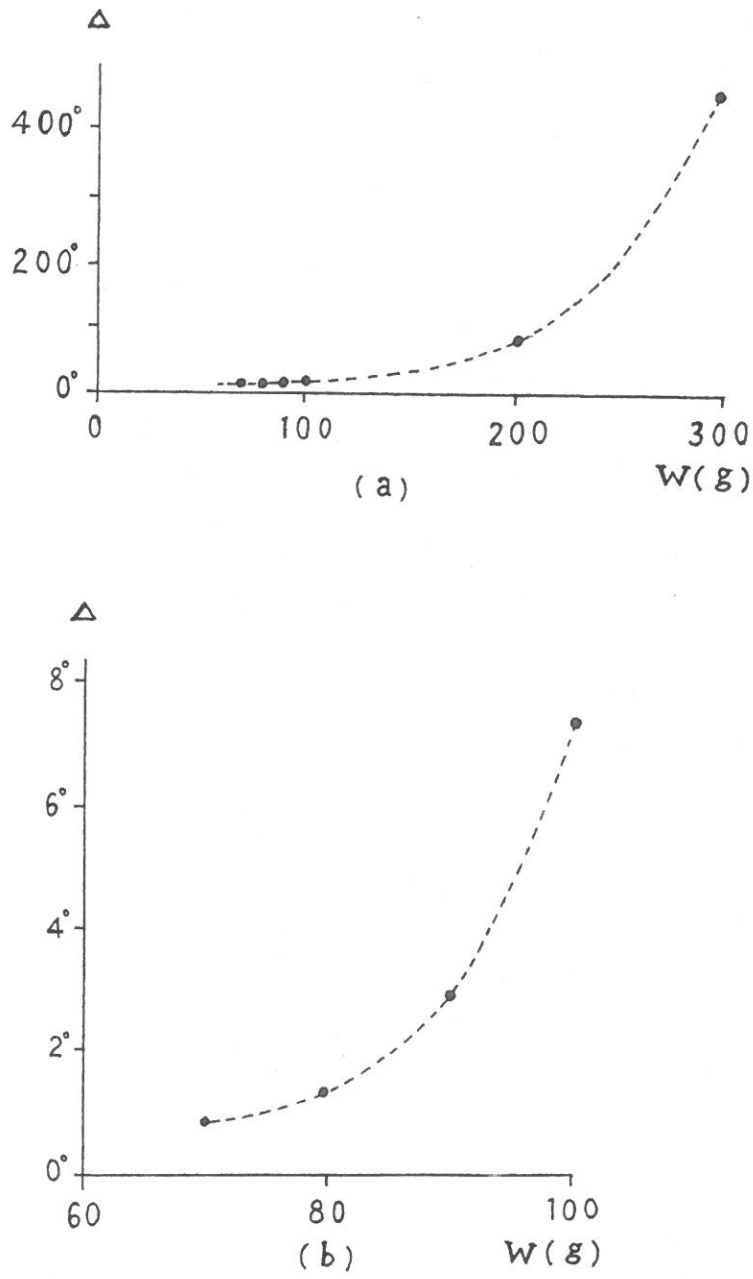

圖 2　雙折射改變量與加壓法碼重量的關係。(b) 圖爲 (a) 的局部放大。虛線僅供視覺參考。

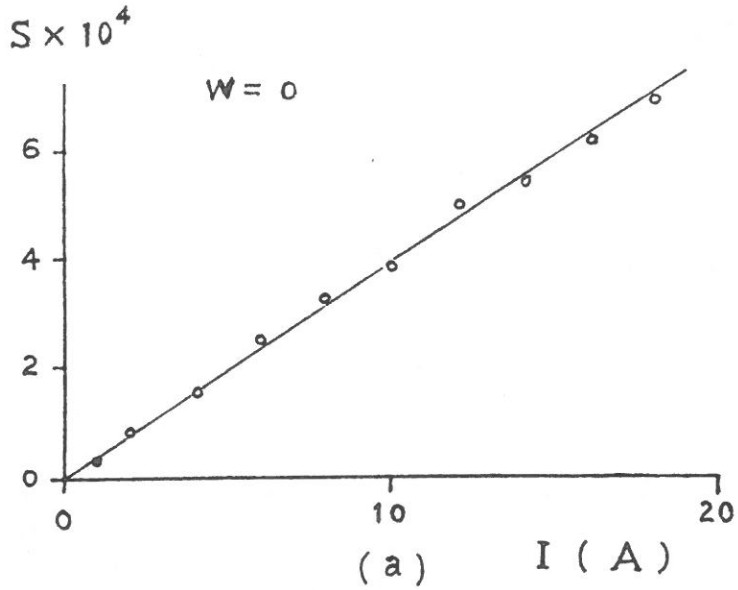
S × 10⁴
W = 0
6
4
2
0
0
10
20
(a) I (A)

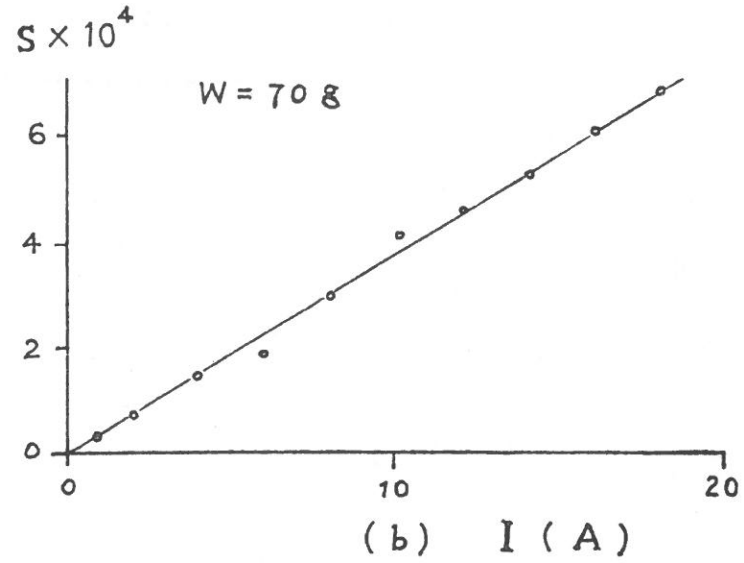
S × 10⁴
W = 70 g
6
4
2
0
0
10
20
(b) I (A)

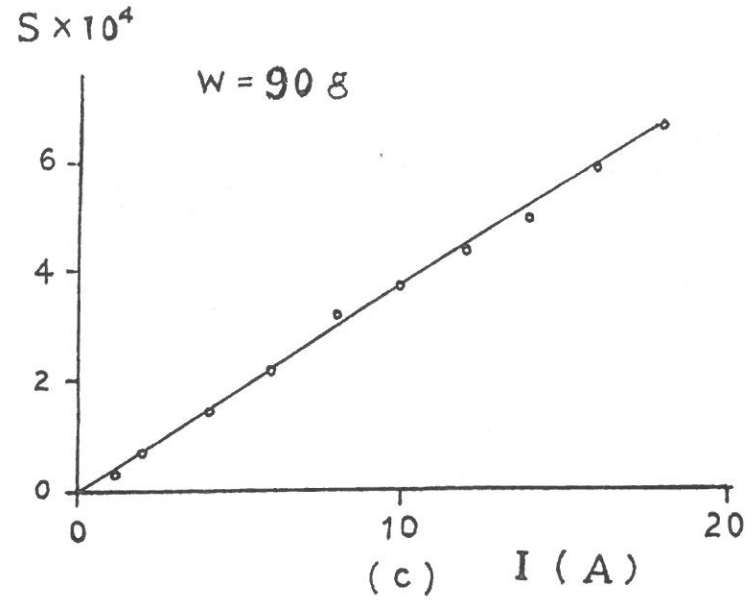

(c)

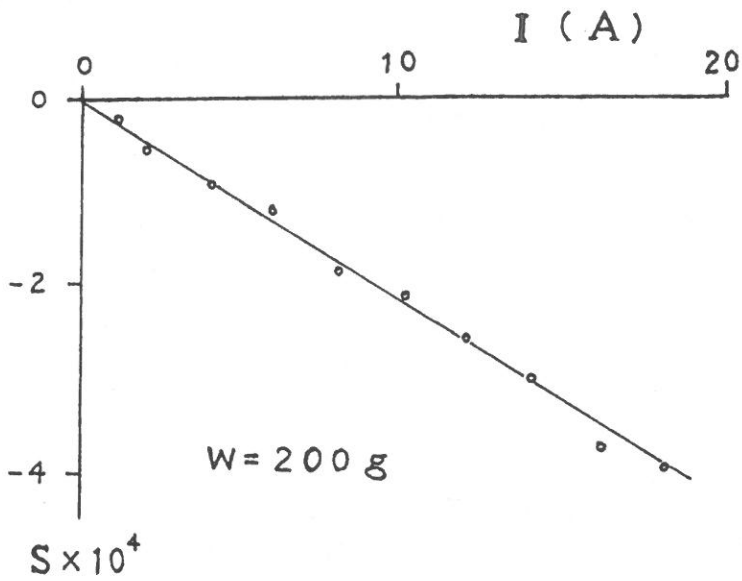

(d)

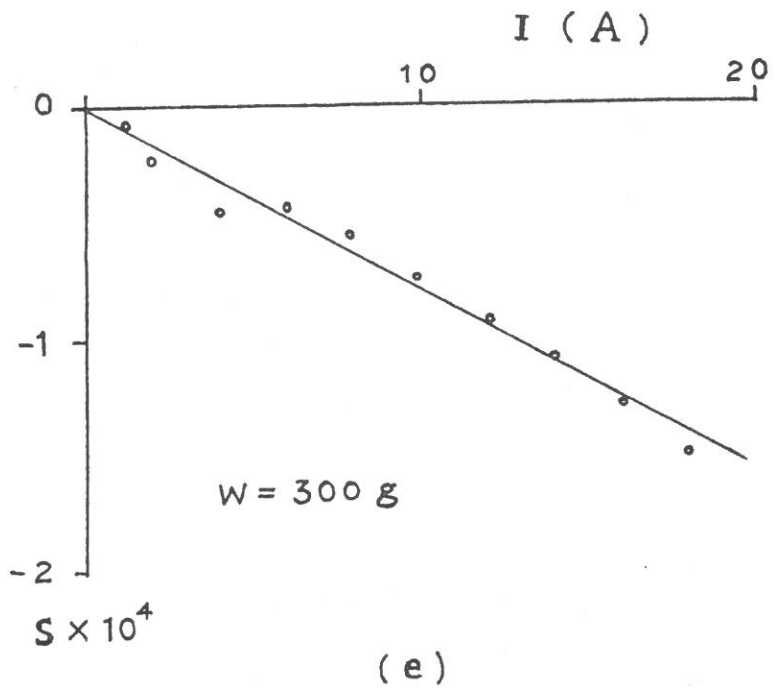

圖 3　不同重量加壓之下，信號與電流的關係。直線爲各組實驗數據的線性近似。

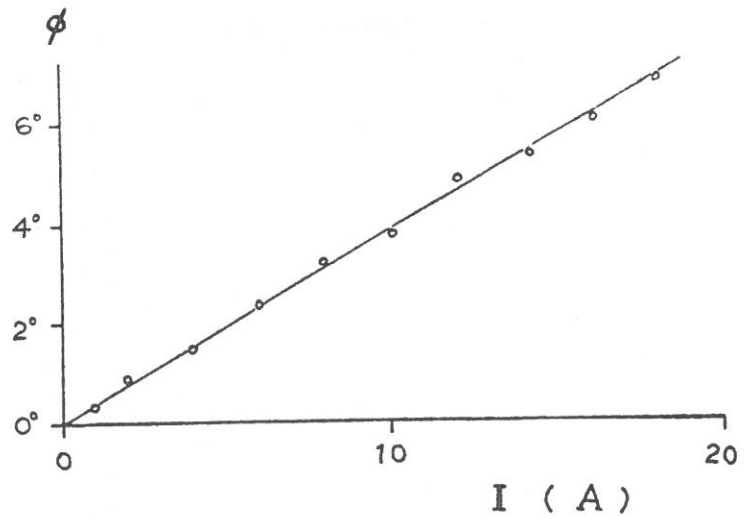

圖 4　法拉第旋轉角與電流的關係，實驗數據可近似爲 $\phi = VN_cN_fI$，$V = 2.79 \times 10^{-4}$deg/A。

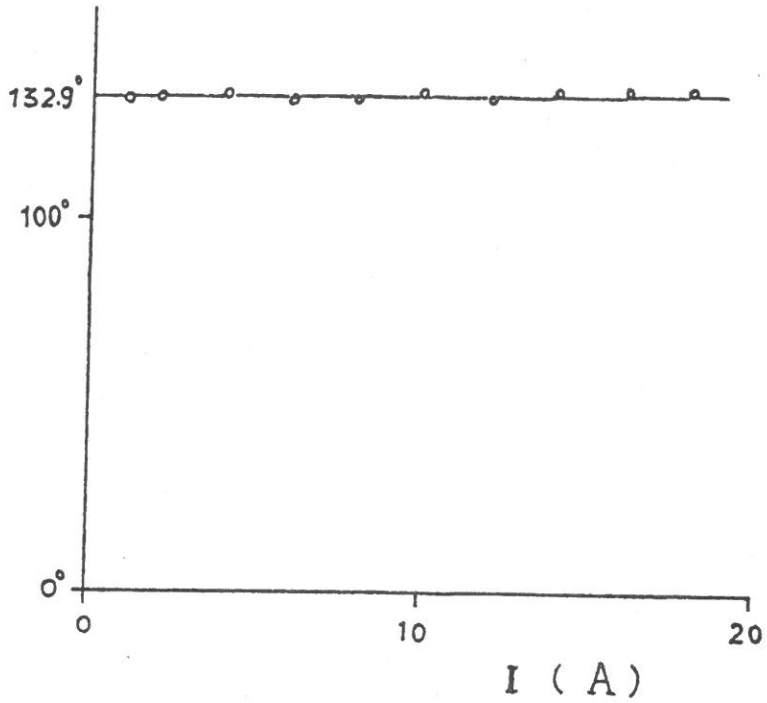

圖 5　雙折射與電流的關係。雙折射約爲定值 133°。

表二　法拉第旋轉角與雙折的實驗值。

$I(A)$	ϕ (deg)	δ (deg)
1	0.384	132.58
2	0.842	132.83
4	1.534	133.43
6	2.450	131.66
8	3.188	131.96
10	3.799	133.98
12	4.861	131.65
14	5.312	134.02
16	6.052	134.20
18	6.776	134.41

式中 ϕ 及 δ 的單位爲度，I 的單位爲安培，式末的誤差爲標準偏差（standard deviation）。由（20）式推算的 Verdet 常數爲

$$V = 2.79 \times 10^{-4}\text{deg/A} = 4.88 \times 10^{-6}\text{rad/A} \tag{22}$$

與文獻［9，16］中的參考值 4.68×10^{-6}rad/A 相當接近。

雙折射值可用補償器直接測量，或配合法拉第效應，由（17）式計算。補償器晶體位移的誤差約 ±0.01mm，相當於 $\pm1.5°$的相位誤差；計算的雙折射標準偏差爲 0.9°，最大誤差爲 1.5°後者恰與補償器測量的誤差相符，顯示調動雙折射的方法對測量雙折射的準確度相當高。

由於系統中雙折線效應較強（$\delta \gg \phi$），實驗誤差較小（0.67%），而較弱的法拉第效應，相對的誤差就稍高，以 18A 電流爲例，ϕ 的誤差爲 1.47%，約爲 δ 誤差的二倍。由此可見，雙折射存在之下，測量法拉第效應雖已可行，但基於準確性及敏感度的考慮，仍應盡量壓低雙折射。

四、結　　論

我們用調動雙折射的方式，測量光纖系統的雙折射及法拉第效應，量得的 Verdet 常數爲 4.88×10^{-6}rad/A，與文獻中的數值極爲接近，實驗數據顯示，雙折射約爲定值，標準偏差爲 0.9°，法拉第旋轉角與電流近於線性關係，誤差爲 0.1°，相當於 0.26A 或 350 安培圈。

所用的方法是以兩個信號聯立解出雙折射及法拉第效應，因此適用於一般狀況，不因雙折射太大而無法測量法拉第效應，此點突破以往多數研究［1］的限制。另一項特點是對環境干擾的敏感度降低。光纖電流檢測器不受電磁輻射干擾是衆所熟知的優點，其他因素，特別是溫度、壓力及振動，都會改變系統的雙折射，但本文所提的方法不受雙折射的限制，自然也相對的降低了環境變動引起的影響。

基於同時測量法拉第效應及雙折射的理念，我們必須在不同狀況下取得二組數據。在此初步的實驗中，我們選擇加壓調動雙折射的方式，因爲其簡便易行，但基本上祇能測量直流電流或頻率振幅固定的交流電流，在未來的實驗中可以試行高頻調變的方式，以推廣於非直流電流的測量。

參考文獻

(1) 見G. A. Day and A. H. Rose, SPIE, **985**, 138 (1988) 及其中參考文獻。
(2) L. R. Veeser, G. I. Chandler, and G. W. Day, SPIE, **648**, (1987)。
(3) B. T. Neyer, J. Chang, and L. E. Ruggles, Proc. SPIE, **566**, 201 (1985)。
(4) H. S. Lassing, A. A. M Ooments, R. Woltier, and P. C. T. van der Laan, Rev. Sci. Imstrum., **57**, 851 (1986)。
(5) H. S. Lassing, W. J. Mastop, A. F. G. van der Meer, and A. A. M. Oomens, Appl. Opt., **26**, 2456 (1987)。
(6) W. J. Tabor and F. S. Chen, J. Appl. Phys., **40**, 2760 (1969)。
(7) A. M. Smith, Appl. Pot., **17**, 52 (1978)。
(8) R. Ulrich and A. Simon, Appl. Opt., **18**, 2241 (1979)。
(9) P. R. Formen and F. C. Jahoda, Appl. Opt., **27**, 3088 (1988)。
(10) S. R. Norman, D. N. Payne, M. J. Adams, and A. M. Smith, Elect. Lett., **15**, 309 (1979)。
(11) R. Ulrich, S. C. Rashleigh, and W. Eickhoff, Opt. Lett., **5**, 273 (1980)。
(12) S. C. Rashleigh and R. Ulrich, Opt. Lett., **5**, 345 (1980)。
(13) A. M. Smith, Elect. Lett., **16**, 733 (1980)。
(14) A. Kumar and R. Ulrich, Opt. Lett., **6**, 644 (1981)。
(15) S. C. Rashleigh and R. Ulrich, Appl. Phys. Lett., **34**, 768 (1979)。
(16) G. I. Chandler and F. C. Jahoda, Rev. Sci. Imstrum, **56**, 852 (1985)。
(17) Z. B. Ren, Ph. Robert, and P. A. Parattd. Opt. Lett., **13**, 62 (1988)。
(18) M. P. Varnham, R. D. Birch, and D. N. Payne, Technical Digest, 5th Int. Conf. Integrated Optics and Optical Fiber Commun. and 11th Eur. Conf. Optical Commun., Venice (1985)。
(19) Y. Fujii and C. D. Hussey, Proc. Iee. **133J**, 249 (1986)。
(20) I. M. Bassett, Opt. Lett., **13**, 844 (1988)。
(21) H. Aulich, W. Beck, N. Douklias, H. Harms, A. Papp, and M. Schneider, Appl. Opt., **19**, 3735 (1980)。
(22) R. A. Bergh, H. C. Lefevre, and H. J. Show, in Fiber-Optic Rotation

Sensors and Related Technologies', S. Ezekiel and H. J. Arditty, eds., Springer Verlag (1982)。

(23) G. W. Day, D. N. Payne, A. H. Barlow, and J. J. Ramskov Hansen, Opt. Lett., **7**, 238 (1982)。

(24) G. W. Day and S. M. Etzel, Tecnnical Digest, 5th Int. Conf. Integrated Optics and Optical Fiber Commun. and 11th Eur. Conf. Optical Commun., Venice (1985)。

(25) Z. B. Ren and Ph. Robert, Opt. Lett., **14**, 1228 (1989)。

(26) R. M. A. Azzam and N. M. Bashara, Ellipsometry and Polarized Light, North-Holland Publishing, Amsterdam (1977)。

(27) S. L. A. Carrara, B. Y. Kim, and H. J. Shaw, Opt. Lett., **11**, 470 (1986)。

85年10月30日 收稿
85年11月22日 修正
85年11月30日 接受

A New Method for Simultaneous Measurement of Faraday Rotation and Linear Birefringence in Optical Fibers

KUNG-CHOE WANG, CHENG-NAN TSAI, TON KO, AND KUNGCHI SHAO
Graduate Institute of Physics
Fu-Jen University
Taipei, Taiwan 242, R.O.C.

ABSTRACT

A new method for measurement of Faraday rotation and linear birefringence in an optical fiber system was described. The birefringence of the system was changed by applying pressure on the fiber. A light beam passing through the fiber changes its state of polarization. The change contains information on the optical properties of the fiber. Mearsurements were performed both before and after the pressure was applied. The two sets of data were then used to calculate the birefringence and Faraday rotation. In current sensing, the method will not be limited by the birefringence effect. The influence of some environmental factors, which change the birefringence, is reduced. Experimental results showed that Faraday rotatation was approximately linear with respect to the electric current. The Verdet constant derived was 4.88×10^{-6}rad/A. On the other hand, the birefringence was nearly constant. The measured value was 133 ± 0.9^{0}. The results confirmed that the method was efficient and reliable for measurement of Faraday rotation and the birefringence.

Key Words: Faraday effect, birefringence, optical fiber.

Interval Picard-like Iteration Methods for Digital MOS Circuit Analysis

YING-WEN BAI
Department of Electronic Engineering
Fu-Jen University
Taipei, Taiwan 242, R.O.C.

ABSTRACT

Interval methods are a class of bounding approaches for providing interval solutions to systems of ordinary differential equations with uncertainty. VLSI circuits can be modeled and represented by systems of ordinary differential equations, and interval methods can be used to analyze them. These bounds are especially useful in providing circuit designers with worst case analysis. In the past, it has been shown that bounding is feasible for digital MOS circuits, due to their special properties, and that bounds for entire systems can be built from bounds for simple logic subcircuits. Only preliminary work has been done on bounds for typical MOS logic blocks, though. In this investigation, we explore more powerful interval approaches which can be used to analyze MOS subcircuits, thus helping to enable eventual implementation of a full bounding simulator. To improve the efficiency of obtaining interval solutions for subcircuits governed by general ODEs, the speeds of convergence of two approaches of interval Picard-like iteration method are compared.

Key Words: Interval Methods, Circuit Analysis, Restoring Property, Wrapping Effect, Contractive Mapping.

INTRODUCTION

Interval methods can be used to obtain an interval solution for analyzing digital

MOS circuits involving a bounded uncertainty. For instance, due to deviations in the fabrication processes, different chips may have different parameters. The range of parameters makes verification of the circuit operation difficult by traditional methods. One way to solve this problem is to apply interval methods to analyze the circuits, i. e., to consider the methods that can simultaneously handle entire sets of waveform intervals[1,2].

Interval iteration methods can be used to refine the interval solutions of ordinary differential equations. For the system of ODEs of a digital MOS circuit, under certain conditions, we apply interval iteration operators to previous interval solutions to generate new interval solutions. If the width of the new interval solutions less than the one of the previous interval solutions, then this iteration mapping is called contractive mapping. Usually, the more iterations we perform, the more CPU time we spend in refining the interval solutions. This relationship leads us to a trade-off between the CPU time and the accuracy of the solutions[3,4].

Many general interval iteration methods for ODEs have been derived in recent years[5,6,7]. Their performance is highly problematical and each method must face the *wrapping effect*[8,9], which is a tendency of the widths of the interval solutions to grow more rapidly than the widths of the optimal interval solution. Fortunately, digital MOS circuits have a signal restoring property whereby the *wrapping effect* can be reset numerically in the simulation. Besides, the monotonic property of digital MOS circuits makes them amenable to interval analysis. In the next section, we show the Picard-like interval operators which can be used in interval circuit analysis. In the third section, we show the way to obtain the behavior bound on digital MOS clusters. In the fourth section, we compare two possible approaches for analyzing each cluster. In section 5, we conclude with a general discussion of the topic of this paper.

INTERVAL ITERATION METHODS

Almost all interval iteration methods for solving ODEs have a few common characterisitics. First, theoretically, most of them allow us to compute the width of the interval solutions so as to approach the optimal interval solutions, which are limited by the uncertainty of the system and precision of floating point data. For example, the

time window size can be made very small in order to achieve a high accuracy. Second, all these methods provide users with a trade-off between the width of the interval solutions and computation efficiency. This trade-off can come from the size of the time window, higher order derivatives, or the number of iterations. Third, all these methods face the wrapping effect, which can produce an unwanted explosion of the computed error bounds[10,11].

For ODES $v'(t) = f(t, v(t))$,

$$t \in [0, b] = B \subset Real,\ v(0) = c \in C \subset I(R^m) \qquad (Eq.1)$$

$I(R^m)$ is a m dimensional interval real vector.

To obtain interval solution, we make an interval integration on both sides of (Eq.1) and then generate an interval iteration equation (Eq.2). In this equation, C represent the initial conditions. If F is inclusion monotonic, then the following operator P is inclusion monotonic in the interval iteration equation, because the interval integration can be a monotonic operation.

$$P(V(t)) = C(a, V(a)) + \int_a^{b(t)} F(s, V(s))ds \qquad (Eq.2)$$

Where

$v(t) \in V(t), f(t, v(t)) \in F(t, V(t))$.

$v(0)$: initial condition, $v(t)$ can be node voltages.

The operator P is an interval operation in which $P: V^{(k)} \to V^{(k+1)}$. The operator p is a real valued operator in which $p: v^{(k)} \to v^{(k+1)}$. Definition 1 and definition 2 define a class of the real valued operator p and interval operator P, which will be used in theorem 1.

Definition 1.

P is and interval majorant of p if $p(y) \in P(Y)$ for $y \in Y$.

Definition 2.

An interval operator P is inclusion monotonic if $X \subseteq Y$ implied $P(X) \subseteq P(Y)$.

Theorem 1.

If P is an inclusion monotonoc interval majorant of p, and if $P(V^{(0)}) \subseteq V^{(0)}$, then the sequence defined by $V^{k+1)} = P(V^{(k)})$, $k = 0, 1, 2, \cdots$

has the following properties:

(1) $V^{(k+1)} \subseteq V^k$, $k = 0,1,2\cdots$

(2) for every $a \leq t \leq b$, the limit

$$V(t) = \bigcap_{k=0}^{\infty} V^{(k)}(t)$$

exist as an interval $V(t) \subseteq V^{(k)}(t)$, $k=0, 1, 2, \cdots$

(3) any solution of ODE, which is in $V^{(0)}$ is also in $V^{(k)}$ for all k and in V as well; that is, if $v(t) \in V^{(k)}(t)$ for all $a \leq t \leq b$.

(4) if there is a real c, such that $0 \leq c \leq 1$, for which $X \subseteq V^{(0)}$, implies

$$\sup W(P(X(t)) \leq C \cdot \sup(W(X(t)), \quad a \leq t \leq b, c \in C$$

then the ODE. has the unique solution V (t) in $V^{(0)}$ given by (Eq.1), where sup is an abbreviation "supermum". Hence, the operator sup applies to the width to find the maximum width.

Traditionally, the interval Picard iteration method has been used as a proof of the existence of interval solutions of ODEs. The proof is presented in references[8,12]. although interval Picard iteration has a slow convergence speed, it can be a stable interval iteration operator. To have a higher rate of convergence, we can use a tighter contractive mapping operator; an interval Newton iteration operator. In this operator, more computations are needed to compute the second order derivative, but they can shrink the width of the interval solutions faster than the first order operator[8,12].

Besides developing high order interval iteration methods, we add a modification to the interval Picard iteration method. For each time point, once a contractive mapping operator is obtained, we can guess a narrower interval solution and then test if the mapping is contractive. This trial-and -error method can save some computation before the non-contractive mapping appears.

COMPUTING BOUNDS ON DIGITAL CLUSTERS

In this section we consider interval iteration methods to obtain the bounds on the responses of digital MOS logic blocks or clusters with interval input signals. An example of such a cluster is pictured in Fig. 1, along with its corresponding ODEs. Each node in this circuit has paths to ground and power supply and signals that are

alternately enabled to cause internal nodes to settle after each transition to one of the extreme voltages. The input in Fig. 1 is a ramp with a finite slope.

Basic observation shows that the voltages of the output nodes will approach a steady state gradually if there is a steady input. In addition, even if the input voltage is in a high steady interval, [4.5V, 5V], the output voltage will approach ground, because in that case the pull-down transistor will discharge all charge in C_1 and C_2, eventually. This relationship between input and output will push the upper and lower bound of the output to ground, if the input is held in the high state. In other words, the restoring property can reduce the width, i.e., the uncertainty, of the interval solution, in this restoring period.

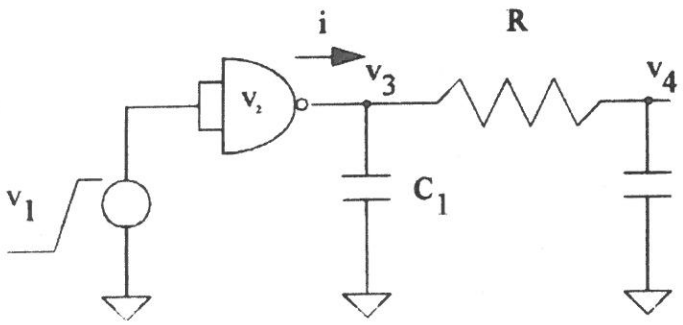

$$\frac{dv_3}{dt} = f_1(t, v_1, v_2, v_3, v_4) = \frac{1}{C_1}\left(i - \frac{v_3 - v_4}{R}\right) \quad (Eq.3a)$$

$$\frac{dv_4}{dt} = f_2(t, v_1, v_2, v_3, v_4) = \frac{1}{C_2}\left(\frac{v_3 - v_4}{R}\right) \quad (Eq.3b)$$

Fig. 1. Typical digital MOS cluster circuit

From Fig. 1, the circuit can be treated as an initial value problem in a first order system of ODEs as shown (Eq.1).

A common method, the interval Picard method, can be used to obtain the interval solution of (Eq.1). The definition and theorem of the interval Picard method can be seen in reference[8,12]. In this method there is an interval operator which includes interval integration and interval arithmetic operations to provide interval mapping.

In addition, the interval Picard-like method will be used in this paper to obtain the interval solutions of (Eq.1). the definition and theorem of the interval Picard-like method can be seen in reference[8,12]. In this method, besides interval integration and interval arithmetic operations, we need to compute the first order interval derivatives which can represent the first order characteristic of the ODEs.

Because of the differentiability of function F in (Eq.1), we can obtain an interval Picard-like iteration method to solve (Eq.1). The integrand of (Eq.4) is derived from the Taylor expansion of function F with respect to the middle solutions of the interval solutions[8,12].

$$V^{n+1}(t) = \left\{ C + \int_0^t f(s, middle(V^n(s)) + F_1(s)(V^n(s) - middle(V^n(s)))ds \right\} \cap V^n(t)$$

Where $\left[\frac{\partial}{\partial V_k} f_d(t,v)\right]_{d,k=1(1)m} \in F_1(t),\ \forall t \in B,\ v \in V$ (Eq.4)

middle $(V^n(s)) = [V^n_{max}(s) - V^n_{min}(s)]/2$

Our purpose is to obtain a contractive mapping which can refine the interval solutions by the iteration of (Eq.4). In other words, we will show $W(V^{n+1}) \leq W(V^n)$ under certain conditions, W representing the width of the interval solution and n the iteration index.

We must first define the maximum width of interval vectors.

$$W_m(X) \sup(e^{-\alpha t} W(X(t))),\ t \in B$$
$$\equiv \sup(e^{-\alpha t} \max W(X_k)),\ 1 \leq k \quad m, t \in B$$
$$\equiv \sup(e^{-\alpha t} \max(\tilde{X}_k(t) - \underset{\sim}{X}_k(t))),\ 1 \leq k \quad m, t \in B$$

Applying these difinitions to (Eq.4), we get:

$$W_m(V^{n+1}(t)) = \sup\left[e^{-\alpha t} \left\{ W(c) + \int_0^t W_m(F_1(s)(V^n - middle(V^n)))ds \right\} \right] \quad (Eq.5)$$

Simplifying the above equation, we obtain

$$W_m(V^{n+1}(t)) = \max\left[W(C), \frac{K_1}{\alpha} W_m(V^n(t)) \right],$$
$$K_1 = \underset{t \in B}{m} \cdot \max\left\{ \max\left[\underset{1 \leq d,k \leq m}{W} (F_{1,dk}(t) + |F_{1,dk}(t)|) \right] \right\} \quad (Eq.6)$$

From (Eq.6), if $K_1 \leq \alpha$, then $W_m(V^{n+1}(t)) \leq W_m(V^n(t))$, which means a tighter bound can be obtained by the interval Picard-like iteration method.

In the interval Picard-like iteration, for each finite time window, we integrate the

middle value of the solutions slope, and add the deviation of the slope over the whole waveform interval. If we choose a good initial interval solution for the time window size, we can obtain a contractive mapping in the integration over this time window. the existence of the contractive mapping also guarantees that the exact solution lies within the interval solution. In addition, the operation of the intersection in (Eq.4) will guarantee that the iteration never produces looser bounds than the bounds before iteration[8,12].

In Fig. 1, if the input is held in the high state, V_L^3 and V_L^4 : approach ground level, and V_U^3 and V_U^4 will be decreased also when the pulldown current is larger than the pullup current. In other words, the width of the interval solutions can be reduced in this period.

If the length of the restoring period is so short that the uncertainty can not be reduced to the amount of the threshold value of logic level, then the uncertainty will grow at the next stage until it reaches the range of the full power supply. If this occurs, the interval methods can only give us a loose bound, since the restoring period is so short that it can not remove the uncertainly generated during the switching period.

(Eq.7) is an interval iteration equation for the circuit in Fig. 1.

$$\begin{bmatrix} V_3^{n+1} \\ V_4^{n+1} \end{bmatrix} = \left\{ \begin{bmatrix} c_1 \\ c_1 \end{bmatrix} + \int_0^t \begin{bmatrix} f_1(s, middle(V_m)) \\ f_2(s, middle(V_m)) \end{bmatrix} + \begin{bmatrix} \frac{\partial f_1}{\partial v_3} & \frac{\partial f_1}{\partial v_4} \\ \frac{\partial f_2}{\partial v_3} & \frac{\partial f_2}{\partial v_4} \end{bmatrix} \begin{bmatrix} V_3^n - middle(V_3) \\ V_4^n - middle(V_4) \end{bmatrix} ds \right\} \cap \begin{bmatrix} V_3^n \\ V_4^n \end{bmatrix}$$

$$\text{Where} \cdot \frac{\partial f_1}{\partial v_3} = INT\left[\left(\frac{1}{C_1}\right)\left(\frac{\partial i}{\partial v_3} - \frac{1}{R}\right)\right], \frac{\partial f_1}{\partial v_4} = INT\left[\frac{1}{RC_1}\right]$$

$$\frac{\partial f_2}{\partial v_3} = INT\left[\frac{1}{RC_2}\right], \text{and } \frac{\partial f_2}{\partial v_4} = INT\left[-\frac{1}{RC_2}\right] \qquad (Eq.7)$$

For the general case, the partial derivative terms in (Eq.7) are intervals if the values of the components are intervals. The computation of (Eq.7) is a combination of an interval matrix multiplication and an interval matrix addition.

To solve the interval iteration equations, we treat the upper and lower bounds separately. We must avoid a situation whereby we are computing an upper bound on

the voltage derivative by assuming that the node voltage is at its lower bound and vice-versa, or the distance between the bounds will always grow.

COMPARISONS BETWEEN TWO APPROACHES OF SOLVING ODES

There are many ways to compare convergence speed for different interval methods used to analyze digital MOS circuits. first, for each time step size, one can look at the convergence speed for each iteration. Second, for each time window, one can examine the convergence speed for each relaxation. Third, for the different partition of the circuits, one can observe the convergence speed for each iteration and relaxation[6,12].

In this section, two approaches of interval Picard-like iteration method will be compared. The first approach was discussed in the previous section, involving an MOS gate with an RC load. The second approach considers the two parts of the circuit, the MOS gate and the RC load separately.

The interval iteration equations are shown in (Eq.8) and (Eq.9), which are slightly different from (Eq.7) in approach 1. In approach 2, we obtain the new interval solution for each node voltage by (Eq.8) and (Eq.9) and use the latest intervals as the input to the next integration equation. The relaxation in approach 2 solves the circuit equation for node 3 to node 4 back and forward, and the relaxation in approach 1 calculated node 3 voltages and node 4 voltages simultaneously.

$$V_3^{n+1}(t) = \left\{ c_1 + \int_0^t f_1(s, middle(V_m)) + \left[\frac{\partial f_1}{\partial v_3}\right](V_3^n - middle(V_3 - middle(V_3)ds \right\} \cap V_3^n \qquad (Eq.8)$$

$$V_4^{n+1}(t) = \left\{ c_2 + \int_0^t f_2(s, middle(V_m)) + \left[\frac{\partial f_2}{\partial v_4}\right](V_4^n - middle(V_4 - middle(V_4)ds \right\} \cap V_4^n \qquad (Eq.9)$$

where $\frac{\partial f_1}{\partial v_3} = INT\left(\left(\frac{1}{C_1}\right)\left(\frac{\partial i}{\partial v_3} - \frac{1}{R}\right)\right)$ and $\frac{\partial f_2}{\partial v_4} = INT\left[-\frac{1}{RC_2}\right]$

Fig. 2 shows the width of an interval solution of (Eq.7) in approach 1. In part I, since the input is kept at a constant low level, the output voltage will rise to the level of the power supply. When the upper bound of the output voltage is equal to the power

supply voltage, the lower bound will still continue to be pulled up because the pull up current is greater than the pull down current. In this period, the difference between the upper bound voltage and the lower bound voltage decreases.

In part Ⅱ of Fig. 2, since the input is increasing, the pulldown current increases and the pullup current decreases, thereby causing the output voltage to decrease. The transition creates uncertainty between the upper bound and the lower bound, so the uncertainty increases until the input voltages reach a steady high voltage.

In part Ⅲ of Fig. 2, since the input voltage is kept at a high level, the output voltage will eventually be pulled down. In this part, because the lower bound already reaches the ground level and the upper bound is still decreasing, the difference between the upper bounds and lower bounds decreases. In other words, the width of the interval solution can be restored.

Fig. 3 shows the width of an interval solution of (Eq.8) and (Eq.9) in approach 2. Comparing the results of approach 1 with the results of approach 2, approach 1 can provide a narrower maximum width for the interval solution. This meets the theoretical argument that the partition of the circuit can lead to extra width because of neglect of the coupling between subcircuits. In this example, the time window size is 1 ns and the number of the iterations is 4. The input waveform is shown in Fig. 1.

The RC load in the Fig. 1 does not have the restoring property which a typical CMOS gate has. The uncertainty at the input of the RC load can not be restored at the output, but the width of the interval solution at the output can follow the input and it will be dependent on the limit of the uncertainty at the input[13].

The operators in approach 1 and approach 2 are monotonic, because these operators are a kind of interval integration which is a monotonic operator. If there are two intervals and one is greater than the other, the monotonic operators are applied to both intervals. Therefore the output intervals will keep the same relation that the input intervals have[2]. Fig. 4 shows the interval integration which is a monotonic operator. The shaded area in Fig. 4a is larger than the shaded area in the Fig. 4b, where the interval integration of the larger interval will have a larger width.

Fig. 5 plots the maximum width of the interval solutions against the number of iterations for approaches 1 and 2. Approach 1 always has a smaller maximum width

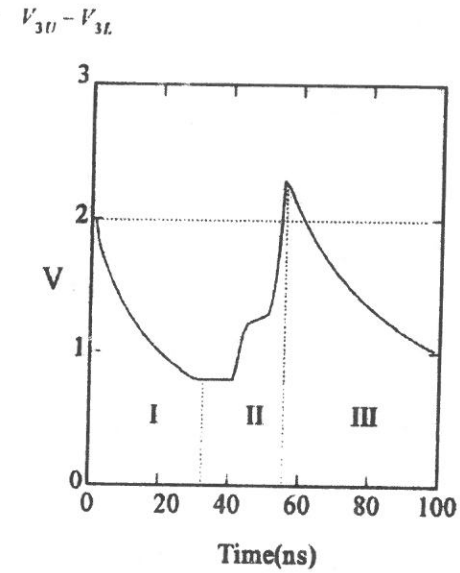

Fig. 2. The width of an interval solution of approach 1.

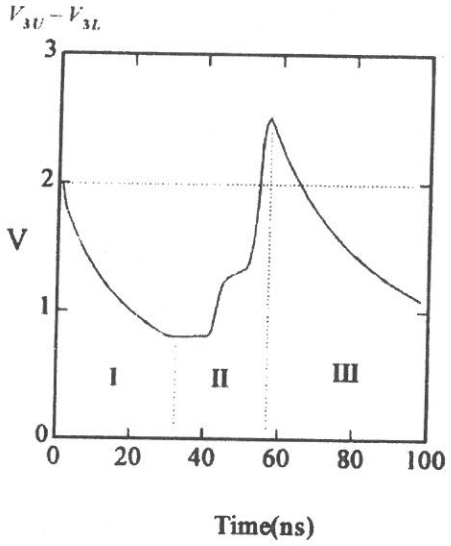

Fig. 3. The width of an interval solution of approach 2.

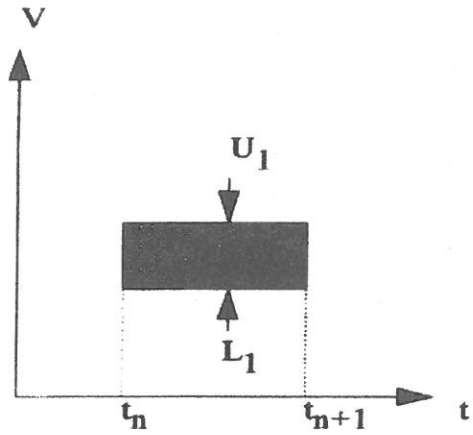

Fig. 4 (a). The width of the interval integration of the interval in approach 2.

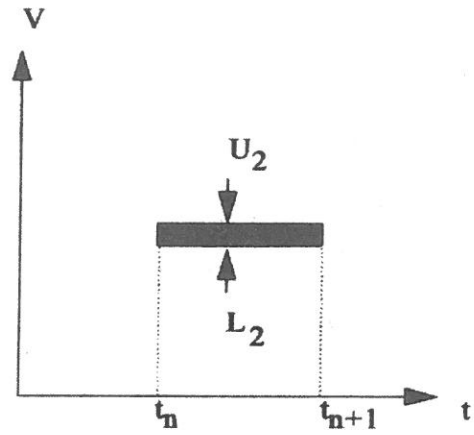

Fig. 4 (b). The width of the interval integration of the interval in approach 1.

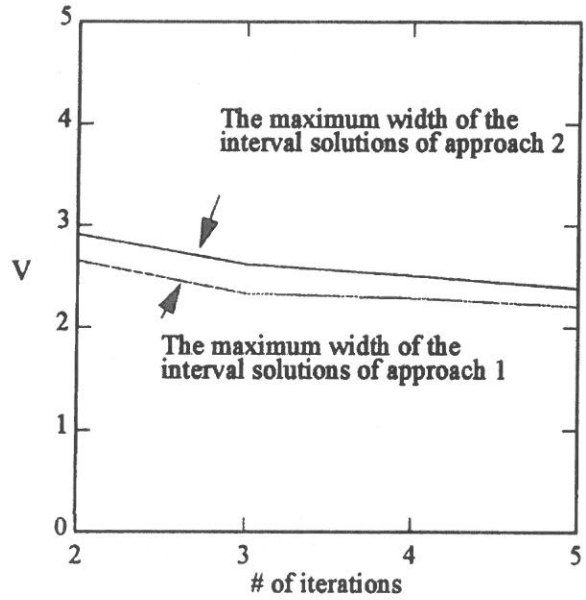

Fig. 5. Comparison of the maximum width of the interval solutions in approach 1 and approach 2.

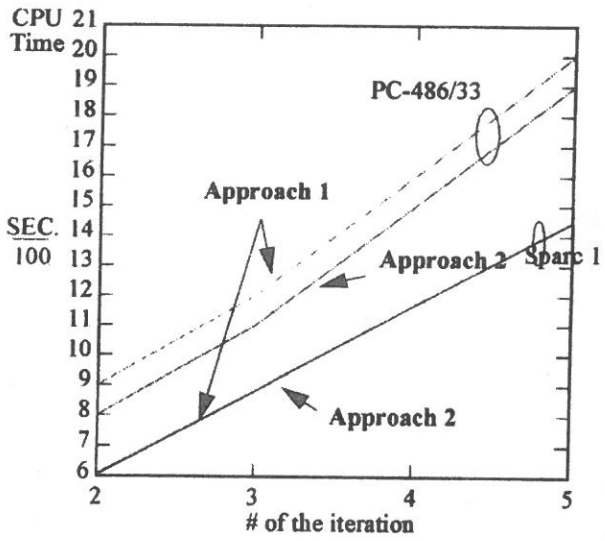

Fig. 6. Comparison the CPU time of approach 1 and approach 2.

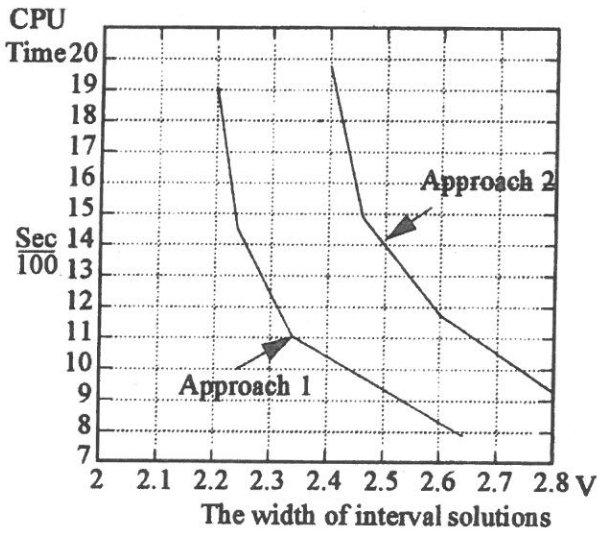

Fig. 7. The relationship of the CPU time and accuracy in approach 1 and approach 2.

than approach 2. This numerical result matches the theoretical result we discussed earlier.

Fig. 6 shows the CPU time with respect to the number of iterations. With the same number of iterations, approach 1 needs more CPU time than does approach 2. This result can be seen by comparing (Eq.7), (Eq.8) and (Eq.9). For each iteration, (Eq.7) of approach 1 needs more computation than does (Eq.8) and (Eq.9) of approach 2.

Fig. 7 shows the relationship between the CPU time and accuracy in both approach 1 and approach 2. Within each approach, the required CPU time increases with the desired accuracy, but overall approach 2 needs more CPU time to reach a given level of accuracy than approach 1.

CONCLUSION

Simple interval Picard-like methods can be effectively applied to the interval analysis of general digital MOS subcircuits, as long as the restoring period is long enough to restore the width of the interval solutions. In other words, the interval Picard－like methods provide a certain pattern of interval solutions for each subcircuit. This pattern of interval solutions includes increasing width during the transition period of the subcircuits, and then decreasing width during the settle period of the subcircuits.

In the interval iteration process, within a certain time subwindow, if the contractive mapping exists, then the interval solutions can be refined by continuing the iteration process. From the comparison of two approaches, we learn the iteration process provides users with a trade-off between accuracy of the interval solutions and computation time.

Large circuits can be partitioned into subcircuits, and then the interval analysis can be done for each of them. Although a partition can introduce extra width, because coupling between subcircuits is ignored, it can provide interval solutions with less computation because of the smaller circuit matrices required to analyze the subcircuits.

ACKNOWLEDGEMENT

The author would like to express his gratitude to Fu Jen Catholic University SVD

section for the financial support to the work.

REFERENCES

(1) C. A. Zukowski, "*Interval Arithmetic Applied to Digital Signal Waveforms for Computationally Efficient VLSI Circuit Verification*" Proc. of 13 IMACS World Cong. on Comp. & Appl. Math, pp. 1667-1668 (1991).

(2) C. A. Zukowski and Y. W. Bai, "*Interval Methods for Solving O. D. Es Characteristic of Digital MOS Integrated Circuits*", International Seminar Nonlinear Circuits and Systems Proceedings Vol. 1 pp. 65-73 (1992).

(3) K. L. E. Nickel, "*Using Interval Methods for the Numerical Solution of ODE's*", Applied Mathematics and Mechanics, Vol. 66 pp. 33-56, No. 11 (1986).

(4) H. J. Stetter, "*Algorithms for the inclusion of solutions of ordinary initial value problems*", in Equadiff 6: Proceedings of International Conference on Differential Equations and their Applications (Brno, 1985), edited by Jaramir Vormansky and Milos Zlamai, Lecture Notes in Mathematics No. 1192, Springer, Berlin, pp. 85-94 (1986).

(5) G. F. Cordiss, "*Survey of Interval Algorithm for Ordinary Differential Equations*" Applied Mathematics and Computation, Vol. 31, pp. 112-120 (1989).

(6) G. F. Corliss, "*Industrial Applications of Interval Techniques*", Computer Arithmetic and Self-Validating Numerical Methods, Academic Press, K, Ulrich, pp. 91-113 (1990).

(7) R. J. Lohner, "*Enclosing the Solutions of Ordinary Initial and Boundary value problems*", in Computer Arithmetic: Scientific Computation and Programming Languages, edited by Edgar W. Kaucher, Ulrich W. Kulisch, and Christian, Wliey-Teubner Series in Computer Science, Stuuragt 255-286 (1987)

(8) R. E. Moore, *Methods and Applications of Interval Analysis*, SIAM, Philadelphia (1979).

(9) R E. Moore, "*Survey of Interval Methods for Differential Equations*", in

proceedings of the 23rd IEEE Conference on Decision & Control, pp. 19529-1535 (1984).

(10) J. P. Aubin and A. Cellina, *Differential Inclusions*, Springer-Verlag (1984).

(11) D. M. Leenaerts, "*Application of Interval Analysis for Circuit Design*", IEEE Transaction on Circuits and Systems, Vol. 37, No. 6, pp. 803-807 (1990).

(12) H. Bauch, Dresden, "*On the Iterative Inclusion of Solutions in Initial-Value Problems for Ordinary Differential Equuations*", Computing 22, pp. 339-354, (1979).

(13) R. E. Bryant, "*A Switch-Level Model and Simulator for MOS Digital Systems*", IEEE Transactions on Computers, Vol. c-33, No. 2, pp. 160-170 (1984).

(14) P. K. Chan and M. D. F. Schlag, "*Bounds on Signal Delay in RC Mesh Networks*", IEEE Transactions on Computer-Aided Design. Vol. 8, No. 6, pp. 581-589 (1989).

(15) G. F. Corliss and L. R Rall, "*Adaptive, Self-validating Numerical Quadrature*", SIAM J. Sci. Stat. Comput. Vol. 8 No. 5 (1987).

(16) G. D. Hachtel and A. L. Sangiovanni-Vincentelli, "*A Survey of Third-Generation Simulation Techniques*", Proceeding of the IEEE, Vol. 69, No. 10, pp. 1264-1280 (1981).

85年10月28日 收稿
85年11月19日 修正
85年12月 4日 接受

區間類皮卡疊代方法在數位金氧半電路分析之研究

白英文
輔仁大學電子工程系

摘　要

區間方法可以提供具不確定參數之系統常微分方程式之區間解答。而在分析過程中超大型積體電路經常以系統常微分方程式來代表，所以區間方法可以提供超大型積體電路行爲的上下限，尤其適用在最壞情形之分析。過去針對特定的數位金氧半電路已經存在有特定的界限方法，用以求出其行爲的上下界限，而本研究則在於採用區間方法對一般性的數位金氧半電路進行分析，形成一個完整行爲界限之模擬模組雛型。除此之外，爲了提升分析效率，我們也經由分析不同的電路分割方式，用以提供計算效率與收斂速度之取捨。

關鍵詞： 區間方法，電路分析，復原性質，繞捲效應，收縮對映。

鄰苯二甲酸酯薄膜分析技術之研究

王彥雄　　史慶瑜
輔仁大學化學研究所

摘　要

鄰苯二甲酸酯類化合物（phthalate esters）之化學性質穩定，在各種橡膠、漆類或塑膠中當可塑劑（plasticizer）使用。近年來，由於塑膠製品應用範圍激增，國內石化塑膠業發達，爲了有效防止其污染，對於此等可塑劑之監測與檢驗更顯出其重要性。有機溶劑消耗最小量之薄膜萃取分析技術，爲近年萃取分析技術之突破，本研究擬報導以薄膜執行水中鄰苯二甲酸酯污染物分析時之條件及其萃取效率，待測物之偵測則以 GC-FID 完成之。

自行配製包括一個碳的甲基（methyl）到九個碳的壬基（nonyl）等不同碳鏈長度之鄰苯二甲酸酯共十一種標準品混合溶液，以此作爲評估方法開發及最佳條件的基礎，亦即以計算標準品添加後回收率，顯示不同執行條件對萃取之影響。探討條件依序爲（1）薄膜萃取前之預調適；（2）薄膜萃取後流析待測物溶劑之選擇；（3）執行流析前，溶劑之預浸透；（4）水樣加入助溶劑之效應。經回收率之比較，使用包括正己烷等四種不同流析溶劑，發現氯甲烷之平均回收率較二氯甲烷高兩倍，且氯甲烷對鄰苯二甲酸酯之流析效率可因於水樣中添加 0.5% 之甲醇而增高。其它一併探討條件諸如：（5）水樣流速；（6）待測物在薄膜上之穩定性；（7）薄膜之容量；（8）薄膜重覆使用性等。數據顯示萃取效率與水樣通過薄膜之流速無關，本實驗所採用之最短萃取時間爲 5 分鐘萃取 1 公升水樣。因此，水樣可以現場處理無須再攜回實驗室。

關鍵詞： 鄰苯二甲酸酯、薄膜分析技術、有機溶劑最小使用量、氣相層析儀、現場萃取。

一、引　　言

鄰苯二甲酸酯類化合物具低揮發性，且不易被氧化及水解，一般用作穩定之可塑劑。鄰苯二甲酸酯的基本結構是由鄰苯二甲酸（phthalic acid）與不同的醇（alcohols）經脫水反應共價鍵結而成。在室溫時此類化合物呈液態，但隨著分子中醇類部份烷基碳數之增加，黏稠狀或油狀物逐漸增加[7]。鄰苯二甲酸酯之熔點一般都不高，許多都低於0℃，其蒸氣壓都很低，因此，鄰苯二甲酸酯具有高沸點之特性。此外，鄰苯二甲酸酯屬親油性（lipophilic）化合物，在非極性溶劑中之溶解度隨烷基碳數增加而增加。

鄰苯二甲酸酯之親油性有利於該等分子對細胞之穿透。鄰苯二甲酸酯不易被酵素分解之穩定性質[2]，造成生物累積（bioaccumlation）現象發生於食物鏈之頂端，因此生物體發生突變（mutagenecity）、畸形（teratogenecity）及癌症（carcinogenecity）[3]。

鄰苯二甲酸酯可能污染之途徑有下列四種：（a）鄰苯二甲酸酯製程經廢水釋出；（b）塑膠等產品在添加製程中經空氣或水釋出；（c）產品使用期間滲漏進入空氣或水中；（d）產品拋棄時不當掩埋或焚化。

分析結果之準確度受樣品萃取、前處理、分析儀器之正確功能等相關因素之影響，其中以樣品萃取及前處理爲首要。當樣品基質複雜時，高回收率通常應伴隨待測物之有效萃取及干擾物之有效去除。液-液萃取法爲了達成高回收率，除了要使用大量不利於環境之有機溶劑外，更需耗時、耗勞。

薄膜分析萃取技術省時、省力、方便[4]。薄膜之大小厚度類似一般濾紙，但其中含60埃孔徑交聯填充物，其比表面積爲500m^2/g。此種表面積大、粒子小、且大小一致之特性，可有效萃取待測物，取代有機溶劑，若可短時間內分析處理大量體積之水樣，則可達成極低偵測極限之目的。

薄膜中的粒子化學鍵結不同的靜相。選擇適當靜相可以專一的將待測物自水樣中分離。適用於鄰苯二甲酸酯類萃取之靜相計有碳十八基（Octadecyl，C18）、碳八基（Octyl，C8）、環己基（Cyclohexyl，C6）及酚基與氰基，依Zief之研究[4]，鄰苯二甲酸酯類分子有苯環及烷基，故以碳18或酚基爲靜相所得效果最佳。考慮鄰苯二甲酸酯之非極性特質以及長度可達九個碳之烷基，本研究僅以碳十八薄膜作爲方法開發之研究。

二、材料與方法

(一) 儀器設備、條件

1. 氣相層析儀（Gas Chromatograph）：屬 CP－9001 型，係由 CHROMPACK 公司所製造。偵測器：火燄離子化偵測器（Flame Ionization Detector）
   積分器：採用 Spectra－Physics 公司所製造，型號爲 SP4290。
2. 層析分離管柱：採用 DB-5，靜相厚度爲 0.25mm 之熔融矽毛細管柱，其長度及內徑爲 30m×0.32mm ID。係由 J&W 公司所生產。
3. 氣體：氮氣，氫氣，壓縮空氣，純度均爲 0.9999 以上。
4. 淨水裝置：Millipore 公司製造，經過 R.O. 及離子交換處理。
5. 微量天秤：Presica 公司生產，型號 100M-300C（小數點 4 位）。
6. 超音波振盪器：Branson 公司生產，型號爲 3200。
7. 微量定量管：Kimble 公司生產，型號 71900，容積 100mL。
8. 氮氣吹乾濃縮器：Organmation Association 公司製造，型號 N-EVAP3。
9. 水流抽氣機：EYELA Aspirator 公司製造，型號 A-3s。

(二) 過濾紙及薄膜

1. 過濾紙：Whatman 5 號用以去除大型顆粒，並再以購自美國 Millipore 公司型號 HVLP 01300，其材質爲尼龍，孔徑大小爲 0.45μm 之濾紙來過濾水樣中之小型粒狀物。
2. 薄膜：註冊商標爲 Empore 由 3M 公司出品，其規格如下。
   厚度（thickness）爲 0.5mm；填充粒子粒徑爲 8μm；填充物比表面積（specific surface area）爲 500 m^2/gm；薄膜直徑（ID）爲 47mm；鍵結靜相（Bond phase）爲碳十八基（Octadecyl，C18）。

(三) 標準品與試劑

1. 所有待測之鄰苯二甲酸酯類標準品購自 Chem Service 公司，其名稱如下：鄰苯二甲酸甲酯（di-methyl phthalate，DMP）；鄰苯二甲酸乙酯（di-ethyl phthalate，DEP）；鄰苯二甲酸正丙酯（di-n-propyl phthalate，DPP）；鄰苯

二甲酸正丁酯（di-n-butyl phthalate，DBP）；鄰苯二甲酸戊酯（diamyl phthalate，DAP）；鄰苯二甲酸異辛酯（butyl benzyl phthalate，BBP）；鄰苯二甲酸-（2-乙基）-己酯（2-ethylhexyl phthalate，DEHP）；鄰苯二甲酸環己酯（dicyclohexyl phthalate，DCP）；鄰苯二甲酸正辛酯（di-n-octyl phthalate，DOP）；鄰苯二甲酸正壬酯（di-n-nonyl phthalate，DNP）；鄰苯二甲酸苯酯（diphenyl phthalate，DPhP）

2. 本實驗所用試劑有：
氰甲烷（Acetonitrile）；丙酮（Acetone）；甲醇（Methyl Alcohol）；硫酸鈉（Sodium Sulfate）。

（四） 實驗方法

1. 標準品配製

（1）儲備標準溶液（standard stock solution）之配製
以標準品原廠所附之純度證明計算並配製濃度爲 20000ppm 所需標準品重量及正己烷溶液體積。

（2）混合標準溶液（standard mixture solution，1000ppm）之配製
各取上述十一種儲備標準品溶液 0.2mL 於 4mL 定量瓶中混合，再以正己烷將混合液稀釋至 4mL 標記，密封冷藏備用。

2. 氣相層析條件

以 50ppm 之鄰苯二甲酸酯混合標準溶液 1μL，注入氣相層析儀，視滯留時間（Retention Time，RT）及峰寬計算解析度（Resolution，Rs）爲層析分離效率之參考依據。如此而定之層析儀控制條件如下：

氮氣流速爲 2mL/min；氫氣流速爲 30mL/min；空氣流速爲 300mL/min；補償氣體流速爲氮氣，30mL/min。其他條件如：

注射量爲 1μL；進樣口溫度爲 275℃；採用分流/非分流式注射，分流比爲 10:1；偵測器爲 FID；其溫度爲 300℃。管柱溫度程式爲：起始 170 ℃ 恆溫 5min，以 10℃/min 升至終溫 280℃，並於該溫保持 8min。

3. 檢量線製備

將標準品混合溶液（1000ppm）連續稀釋，配製成一系列五種濃度，由低濃度至

高濃度分別注入氣相層析儀中。其中當作起點之最低濃度，應稍高於本方法之偵測極限，最高濃度應接近但不得大於線性範圍。檢量線座標點，來自每一濃度與其積分面積；如此所得之五點以統計之最小平方法（least square method）作直線圖，並計算線性相關係數值（R^2）以評估其線性關係。

4. 校正因子及回收率計算

當五濃度點呈一直線關係時，該直線之斜率即爲校正因子（Calibration Factor，CF），任一濃度點 CF 之計算如下：

$$CF = \frac{\text{標準品波峰面積}}{\text{標準品濃度}}$$

由五個濃度點所得之五個不同 CF 值，其相對標準偏差百分率（Percent Relative Standard Deviation，%RSD）代表 CF 值間變異程度，其計算方法如下：

$$\%RSD = \frac{\text{CF 之標準偏差}}{\text{CF 之平均值}} \times 100$$

水樣基質回收率之計算如下：

$$\text{回收率，\%} = \frac{\text{添加水樣測得量} - \text{水樣原量}}{\text{添加量}} \times 100$$

5. 品質管制措施

(1) 儀器空白

以待測物經前處理步驟後所在溶劑注入氣相層析儀，以檢測儀器系統之干擾。

(2) 方法空白

以不含標準品添加之去離子水一公升，經過與樣品相同之前處理。即經薄膜萃取與濃縮步驟並注入氣相層析儀，以檢測本方法所潛在之系統干擾。

(3) 儀器偵測極限

將火燄離子化偵測器調至最靈敏，再將系列標準混合溶液，依高濃度往低濃度分別注入氣相層析儀。當低濃度標準品之訊號爲雜訊之 5 倍時，定爲儀器偵測極限。

(4) 方法偵測極限

方法偵測極限之求得，不同於儀器偵測極限之直接量測，而爲在 99% 可信度時待測物濃度大於零之統計值。故方法偵測極限值將所有分析步驟列入考慮。以標準品添加去離子水之方式製備水樣，歷經萃取、濃縮等步驟，得 10 倍於儀器偵測極限濃度之濃縮萃取液，分別注入氣相層析儀七次，計算七次重複分析所得濃度之標準偏差值，取該標準偏差值之三倍，爲本檢測之方法偵測極限[6]。

6. 干擾之預防

微量分析工作尤其需要避免干擾。報導曾指出，實驗室之地板、油漆、橡膠管等設備，均會緩慢釋放干擾物質因而影響分析結果，此等干擾可能污染標準品、溶劑[5]、玻璃製品、濾紙[6]及儀器用氣體[7]。本研究發現干擾時則以蒸餾（distillation）去除溶劑干擾，其他器材如鋁箔、玻璃器皿則以高溫烘烤 14 小時以去除干擾。

7. 水樣之薄膜分析

(1) 於組裝薄膜前，用 5mL 氯甲烷清洗樣品槽（sample reservior）等玻璃器材上之干擾物。

(2) 薄膜裝妥後，先加入 5mL 甲醇，使停留 3 分鐘做薄膜預調適（precondition）。之後抽掉一些甲醇，但仍保留 3-5mm 之甲醇於薄膜表面上，使薄膜不至變乾。

(3) 繼以 5mL 的試劑水，使其通過薄膜，但仍保留 3-5 mm 之試劑於薄膜表面之上。

(4) 於水樣中加入 0.5% 之甲醇當作助溶劑，開始水樣之薄膜萃取。

(5) 將水樣抽取至乾後移去收集錐形瓶，置換試管（20mL）於漏斗下以收集薄膜流析液（elution solvent）。

(6) 待測物之完全萃取有賴以 5mL 氯甲烷，清洗裝盛水樣之空瓶，並將清洗液倒入薄膜裝置之樣品槽。

(7) 重覆步驟（6）兩次。

(8) 收集氯甲烷流析液使其通過無水硫酸鈉管柱以去水。硫酸鈉管柱仍需做兩次之 5mL 氯甲烷流析。

(9) 上述所有去水流析液全數收集於圓底燒瓶內，並以旋轉減壓濃縮器濃縮至 3-

5mL，再以氮氣吹乾濃縮器濃縮至 1mL。

⑽ 取 1μL 注入氣相層析儀。

8. 水樣之採集

水樣採集後，須密封並貼妥封籤於採樣瓶上。封籤上應註明採樣者姓名、樣品型態、採樣時間、分析項目及採樣地點。水樣採集完畢後，立即以 pH 試紙（pH1-14）量測，以濃鹽酸溶液降低 pH 至～2，以防止水樣發生化學及生物反應，並冷藏於 4℃ 採樣箱保存。

水樣帶回實驗室後，先以 Whatman 5 號濾紙先行過濾大型顆粒，再將此濾液以 0.45μm 尼龍濾紙進行第二次過濾。如此前處理後之濾液於收集後應立即進行薄膜分析，未能馬上進行薄膜分析之濾液則密封置於 4℃ 之冰箱內。

三、結果與討論

(一) 鄰苯二甲酸酯類標準品之氣相層析分析

1. 方法偵測極限

添加相當於每一標準品絕對量 10μg 之標準品混合溶液至 1L 水樣中，此時水樣之濃度相當於每一標準品 10ppb。如此添加之水樣七個分別經薄膜分析萃取並濃縮至 1mL。以此濃縮液進行七次獨立之氣相層析注射，所得濃度標準偏差值之 3 倍即爲本研究之方法偵測極限，相關數據如表一所示。其中以鄰苯二甲酸正壬酯之方法偵測極限值最高，但仍小於 5ppm。圖 1 爲 50ppm 標準品混合液之氣相層析圖。

2. 標準品檢量線校正表

十一種鄰苯二甲酸酯標準品混合溶液，經配製成 5 種不同濃度後，以氣相層析儀決定其檢量線線性方程式、線性範圍、線性迴歸係數以及相對標準偏差百分率。鄰苯二甲酸酯類之線性迴歸係數 R^2 值至少在 0.99 以上，因此在計算未知濃度時，即可採用平均校正因子（CF）直接計算。校正因子間之 %RSD 值皆小於 14%，如表二所示。

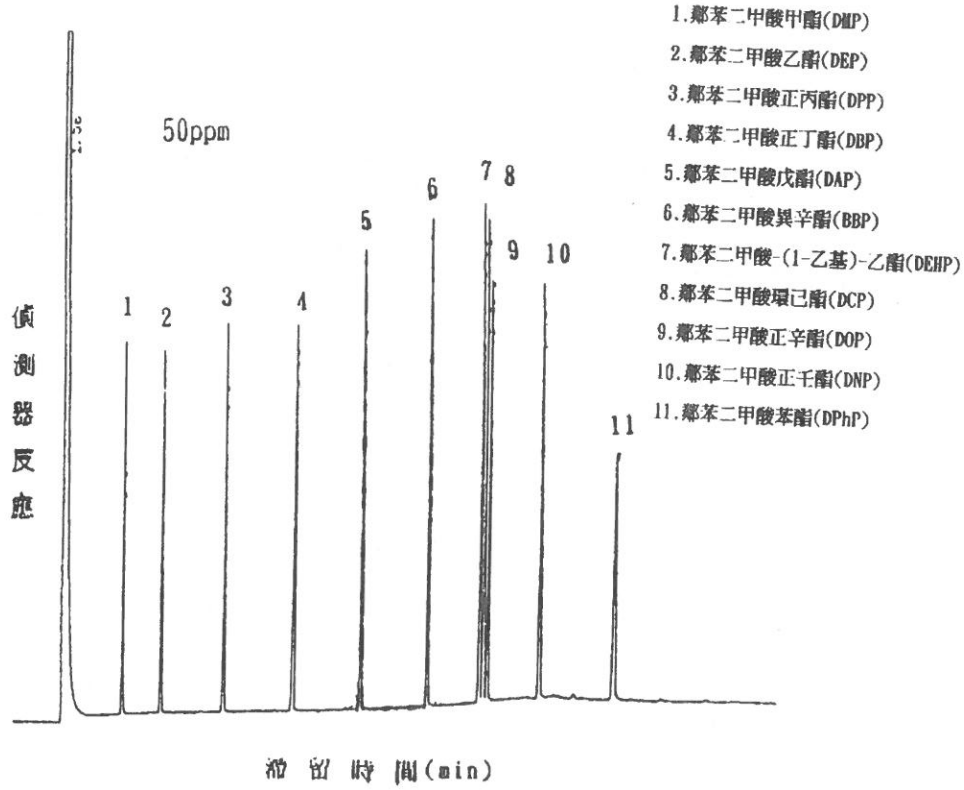

圖 1　爲 50ppm 標準品混合液之氣相層析圖。

表一　鄰苯二甲酸酯各個標準品之方法偵測極限

待測物	水樣（1L）濃度 (ppb)	濃縮液（1mL 正己烷）濃度（ppm）							平均濃度 (ppm)	SD (ppm)	RSD %	方法偵測極限（MDL） (ppm)
		1	2	3	4	5	6	7				
DMP	10	6.20	7.50	8.02	7.43	7.50	8.50	7.50	7.52	0.70	9.34	2.10
DEP	10	9.10	9.80	8.86	7.80	7.70	9.20	7.20	8.52	0.96	11.22	2.88
DPP	10	9.60	8.50	8.43	8.20	7.90	8.90	7.40	8.42	0.71	8.38	2.13
DBP	10	10.40	9.67	10.50	9.40	8.70	10.60	7.90	9.60	1.02	10.59	3.06
DAP	10	10.50	9.60	9.90	8.87	7.90	10.50	8.00	9.32	1.09	11.72	3.27
BBP	10	10.70	9.60	10.10	9.00	8.10	11.00	8.20	9.53	1.15	12.08	3.45
DEHP	10	10.90	9.80	10.20	8.86	8.40	10.90	8.20	9.61	1.13	11.81	3.39
DCP	10	9.60	9.10	5.60	6.70	8.10	9.70	8.20	8.14	1.53	18.77	4.59
DOP	10	10.80	9.90	9.90	9.00	8.10	11.00	8.10	9.54	1.18	12.41	3.54
DNP	10	9.10	8.70	6.20	5.50	7.90	9.70	8.00	7.87	1.53	19.30	4.59
DPhP	10	9.20	7.50	6.00	6.10	7.80	9.50	8.00	7.73	1.36	17.58	4.08

表二 標準品五濃度檢量線表

待測物	CF 值					檢量線方程式	R^2	CF 平均值	CF 標準差	%RSD
	5ppm	10ppm	25ppm	50ppm	75ppm					
DMP	711	774	849	816	831	Y = 835X − 425	0.9995	796.26	54.86	6.90
DEP	1226	1246	1073	976	931	Y = 900X + 3080	0.9982	1090.23	142.56	13.00
DPP	888	1005	1123	994	1030	Y = 1023X + 140	0.9974	1008.12	84.20	8.30
DBP	895	1077	1166	983	1041	Y = 1022X + 570	0.9951	1032.29	101.39	9.80
DAP	977	1229	1356	1109	1181	Y = 1157X + 820	0.9931	1170.70	140.93	12.00
BBP	1039	1360	1513	1199	13211	Y = 1288X + 604	0.9910	1286.39	176.01	13.60
DEHP	11210	1562	1726	1262	1488	Y = 1447X-1874	0.9903	1369.60	149.90	10.90
DCP	1306	1650	1709	1293	1454	Y = 1284X + 3087	0.9932	1435.88	174.01	12.10
DOP	1053	1324	1407	1060	1219	Y = 1194X + 374	0.9961	1203.74	110.90	9.20
DNP	1270	1699	1771	1381	1597	Y = 1534X + 772	0.9926	1568.70	176.07	11.20
DPhP	1153	1500	1588	1390	1429	Y = 1416X + 684	0.9969	1412.04	163.25	11.56

鄰苯二甲酸酯之定性分析評估，是以氣相層析儀所示之滯留時間視窗爲主要依據。表三爲個別標準品之滯留視窗，標準偏差（SD）來自五天獨立注射所得之滯留時間計算而出，由極高之精密度表示儀器穩定性高。

表三 標準品混合物之氣相層析滯留時間視窗（Retention Time Window）

待測物	滯	留	時	間	(min)			RT WINDOWS	
	RT1	RT2	RT3	RT4	RT5	RT 平均值	SD	FROM	TO
DMP	3.500	3.500	3.510	3.500	3.500	3.502	0.004	3.488	3.515
DEP	4.950	4.950	4.950	4.950	4.950	4.950	0.000	4.950	4.950
DDP	7.380	7.420	7.420	7.410	7.410	7.410	0.012	7.373	7.447
DBP	9.870	9.870	9.870	9.870	9.870	9.870	0.000	9.870	9.870
DAΓ	12.051	2.051	2.051	2.051	2.051	2.05	0.000	12.05	12.050
BBP	14.09	14.08	14.08	14.08	14.08	14.082	0.004	14.068	14.095
DEHP	15.66	15.66	15.65	15.66	15.65	15.658	0.004	15.644	15.671
DCP	15.78	15.78	15.77	15.78	15.78	15.782	0.004	15.768	15.795
DOP	15.90	15.90	15.89	15.90	15.90	15.902	0.004	15.888	15.915
DNP	17.510	17.510	17.510	17.510	17.510	17.510	0.000	17.510	17.510
DPhP	19.840	19.840	19.840	19.840	19.840	19.840	0.000	19.840	19.840

RT windows = RT 平均值 ± 3S.D.（標準偏差）

3. 流析溶劑之選擇

在薄膜萃取過程中，影響萃取效率重要因素之一是流析溶劑之選擇。薄膜粒子靜相對待測物抓取能力不成問題後，流析溶劑強度（solvent strength）必需高於靜相與待測物始能有效的流析，以提升萃取結果。

本研究所測試之四種溶劑分別爲正己烷、二氯甲烷、甲醇、及氰甲烷。爲減少實驗之變因，將待測物標準品濃度爲 500ppm 之混合液直接以 100μL 均勻點播於薄膜上，待蔭乾後分別以上述四種溶劑進行流析，濃縮至 1mL 後注入氣相層析儀。如表四可看出甲醇與氰甲烷回收率較高。但氰甲烷之平均回收率又較甲醇爲高，尤以分子較小之鄰苯二甲酸甲酯在氰甲烷之回收率較甲醇爲好。

表四　流析溶劑之選擇對回收率之影響

待測物	回收率，% (n = 2)			
	正己烷	二氯甲烷	甲醇	氰甲烷
DMP	29	51	79	95
DEP	44	50	88	95
DPP	69	51	96	97
DBP	80	50	99	98
DAP	82	48	99	96
BBP	63	46	95	95
DEHP	65	45	95	95
DCP	82	44	98	96
DOP	59	44	85	94
DNP	80	43	96	93
DPhP	82	45	95	94

4. 預調適測試

碳十八薄膜屬疏水性，薄膜使用前以甲醇預調適以活化靜相上官能基之必要性，在本實驗中再一次測試。

先以 5mL 之甲醇預調適與另一組未經調適之薄膜作爲對照組。實驗步驟仍將 500ppm 待測物標準品混合液 100μL 加入 1L 水樣中（50ppb），待完成所有薄膜萃取

步驟後，流析液濃縮至 1mL，取 1μL 注入氣相層析儀中，其結果如表五所示。發現預調適與否二者並無顯著差異，此結果似乎與一般薄膜文獻不同，可能由於鄰苯二甲酸酯類化合物與靜相間之相容性甚高的緣故。

表五　薄膜之預調適與回收率之關係

待測物	回收率，% (n = 2)	
	甲醇	對照組
DMP	75	81
DEP	88	88
DPP	95	91
DBP	98	92
DAP	97	91
BBP	98	91
DEHP	97	92
DCP	98	96
DOP	97	91
DNP	93	91
DPhP	91	90

經過預調適處理的一組實驗發現，凡未經調適之薄膜對水樣之阻力甚大，不易通過，需時爲預調適的 3-5 倍。其原因可能由於水之表面張力大，配合薄膜之微孔，發生相當之阻隔作用，當薄膜以甲醇預調適後，除能溼潤薄膜並有效降低覆於薄膜粒子上水之表面張力。

5. 水樣之助溶劑測試

本實驗以不加助溶劑爲對照組，添加組則分別於 1L 水樣中加入 5mL 之甲醇、丙酮、異丙醇，水樣之製備如同上述，亦即水樣中各待測物之濃度爲 50ppb。表六之結果可以看出，水樣中添加甲醇之回收率較不添加甲醇好，特別是鄰苯二甲酸甲酯在助溶劑加入的情況下可提升 8% 之回收率。反觀丙酮及異丙醇之添加，分子較小之鄰苯二甲酸酯回收率顯著降低。

表六 助溶劑之添加對回收率之影響

待測物	回收率，%			
	不加[1]	甲醇[2]	丙酮[1]	異丙醇[1]
DMP	75	83	36	22
DEP	88	93	94	80
DPP	95	97	96	89
DBP	98	98	96	95
DAP	97	97	95	97
BBP	98	96	96	99
DEHP	97	97	94	99
DCP	98	97	94	97
DOP	97	97	97	99
DNP	93	96	93	94
DPhP	91	96	93	92

1.二次重覆實驗平均值。
2.四次重覆實驗平均值。

6. 流析前溶劑預浸透測試

如何更有效的將待測物自靜相流析出來？是否與溶劑於流析前預浸透時間有關？爲本項測試的原因。實際操作時以抽氣機持續開著定爲浸透時間爲零。水樣通過後，將抽氣機關閉，倒入流析溶劑，浸透三分鐘後，打開抽氣機之操作定爲浸透時間爲三分鐘。而流析方式除了例行之 5mL 分三次進行流析外亦增加了一次 15mL 之測試。由表七，我們可看出，在測試之四種情況中，回收率表現並無顯著差異，顯示溶劑浸透與否與溶劑添加方式對回收率並不具決定性的影響。

7. 水樣通過薄膜之流速

水樣流速之大小決定了水樣中待測物與靜相間平衡的時間。本實驗分別以流速爲每分鐘 200mL、40mL、20mL 三種情況來進行測試。其結果如表八所示。除了鄰苯二甲酸甲酯外，其他待測之鄰苯二甲酸酯回收率均在 90% 以上。鄰苯二甲酸甲酯之極性頗高，若快速通過碳十八之靜相，其平衡時間可能受到影響。

8. 薄膜之重覆使用

本測試之目的即在探討薄膜材質之穩定性及重覆使用性。同一張薄膜重覆使用

表七　溶劑之預浸透測試與回收率之關係表

待測物	回收率, %			
	0Min[1]	0Min[1]	3Min[1]	3Min[2]
	15mL	5mL×3	15mL	5mL×3
DMP	78	81	80	83
DEP	86	89	88	93
DPP	89	94	91	97
DBP	92	96	93	98
DAP	94	97	93	97
BBP	98	98	95	96
DEHP	99	98	94	97
DCP	101	100	95	97
DOP	100	99	98	97
DNP	98	96	89	96
DPhP	96	99	90	96

1.二次重覆實驗平均值。
2.三次重覆實驗平均值。

表八　不同水樣流速對回收率之影響

待測物	回收率, %		
	200mL/min	40mL/min	20mL/min
DMP	78	83	90
DEP	85	93	97
DPP	90	97	98
DBP	95	98	97
DAP	96	97	96
BBP	97	96	96
DEHP	96	97	96
DCP	97	97	95
DOP	97	97	97
DNP	93	96	92
DPhP	92	96	91

於五個獨立樣品之萃取，並將其回收率作一比較。其結果如表九所示。薄膜之萃取效率在第四次使用時仍能維持相當之功能，但第五次使用時，其平均回收率開始顯著下降。

表九　薄膜重覆使用測試

待測物	回收率, %				
	第一次	第二次	第三次	第四次	第五次
DMP	78 (84)	78 (81)	80 (74)	82 (81)	31 (75)
DEP	89 (90)	85 (85)	88 (82)	87 (84)	59 (81)
DPP	95 (95)	90 (90)	91 (91)	90 (83)	79 (85)
DBP	98 (99)	95 (94)	93 (95)	91 (81)	88 (88)
DAP	99 (99)	96 (95)	93 (94)	95 (81)	82 (88)
BBP	99 (97)	97 (96)	95 (92)	93 (84)	91 (90)
DEHP	98 (94)	96 (95)	94 (92)	91 (86)	86 (90)
DCP	96 (94)	97 (94)	95 (92)	96 (84)	88 (86)
DOP	99 (94)	97 (96)	98 (91)	89 (86)	92 (89)
DNP	91 (91)	93 (94)	89 (90)	83 (85)	43 (85)
DPhP	86 (97)	92 (94)	90 (88)	89 (84)	45 (83)

註：括號內數據爲第二片薄膜（第二次實驗，n＝2）所作之重覆實驗。

9. 薄膜容量測試

將十一種標準品混合溶液由低濃度往高濃度分別以薄膜進行萃取，亦即本實驗水樣溶液之濃度定爲 10μg/L、50μg/L、250μg/L、1250μg/L 分別測試，其回收率結果如表十。

在濃度爲 1250 mg/L 之測試濃度時，待測物平均回收率較低濃度水樣溶液約下降 7-10%，此濃度可能爲薄膜發生穿透（breakthrough）之濃度。

10. 待測物穩定性測試

水樣萃取完成後薄膜分別以鋁箔包好，置入 4℃ 乾燥皿中或置於 4℃ 之採樣箱中，靜置七天，始進行流析步驟，其結果列於表十一。由表我們可以看出，乾式保存法較溼式保存法，其平均回收率爲高，若能減少靜置時間，乾式保存法應最具有取代傳統攜回水樣之潛力，亦即水樣於現場經薄膜處理後即可棄置。

表十　薄膜容量測試與回收率之比較

待測物	回收率, %			
	10μg/L	50μg/L	250μg/L	1250μg/L
DMP	79	83	86	60
DEP	94	94	93	85
DPP	91	96	94	89
DBP	93	98	96	90
DAP	93	98	96	89
BBP	94	97	95	86
DEHP	94	97	95	85
DCP	91	97	95	85
DOP	97	97	92	86
DNP	78	96	93	83
DPhP	75	96	91	82

表十一　分析物之保存與回收率之影響

待測物	回收率, %	
	保存於乾燥皿[1]	保存於採樣箱[2]
DMP	77	81
DEP	83	83
DPP	88	84
DBP	90	80
DAP	85	67
BBP	91	78
DEHP	88	72
DCP	74	54
DOP	91	81
DNP	67	52
DPhP	65	53

1.保存七天。
2.保存七天，維持 4℃。

四、結　　論

含十一種鄰苯二甲酸酯類化合物之水樣一公升，可在五分鐘內無需有機溶劑完成萃取，再以氣相層析配備火燄離子化偵測器，可在二十分鐘內完成所有待測物之分離，其最低偵測極限可達 2ppm 左右。

傳統溶劑萃取，所需採用之前處理與淨化，可由薄膜完全取代，且只需少量之有機溶劑用於薄膜之流析。薄膜萃取條件之最佳化，可由：（一）流析溶劑之選擇。（二）助溶劑之添加得以控制。以甲醇調適與否雖無明顯差異，但經調適之薄膜有助於水樣之通過，因而影響操作所需時間。另外，在實驗過程中，一些預期可能對回收率造成影響之變因，如水樣流速、預浸透時間等，其影響層面並不明顯。顯示薄膜萃取控制條件之耐用性（robustness）及簡易性，有利控制量測結果之準確。由薄膜有效使用次數及負載能力實驗結果顯示，本方法所使用之溶劑正確，並無發生批次間相互污染。重覆回收薄膜之可行性，可以大大的降低採樣成本。

水樣中之懸浮微粒往往阻礙水樣之通過薄膜，甚至於完全阻塞，因此水樣之前處理，例如以 0.45μm 濾紙過濾極爲重要。但如何有效改進更小粒子阻塞問題仍待探討。

薄膜萃取適用於有機待測物之萃取，除可取代淨化及預濃縮等功能外，待測物因靜相之特性達到從基質中檢選之目的。或許薄膜技術可利用於自複雜生物基質中進行特異性萃取。

五、謝　　誌

感謝聖言會與行政院環境檢驗所對本研究的補助。

參 考 文 獻

(1) Woodward, K. N. ed. Phthalate esters: Toxicity and Metabobism Vol. 1 CRC Press Boca Raton, Fla., (1988).

(2) Karnra, A. H. and W. L. Hayton, Aquatic Toxicol ., **15**, 27-36 (1989).

(3) Peakall, D. B. Residue Rev., **54**, 1-41 (1975).

(4) Application Note, EMPORE Extraction Disks with Bakerbond Bonded Phases J. T. Barker Chemical Co., Phillipsburg, NJ (1991).

(5) Vessman, J. and G. Rietz, J. Chromatogr., **100**, 153-156 (1974).

(6) 簡弘亮 土壤中鄰苯二甲酸酯超臨界流體萃取方法之建立，輔仁大學碩士論文，(1995).

(7) Ogata, J. N.; Okun, J. D.; Hylin, J. W. and A. Bevenue, J. Chromatogr., **189**, 425-427 (1980).

(8) Kratochvil, B. J. and K. Taylor, Anal. Chem., **53**, 924A-938A (1981).

85年10月17日 收稿
85年11月20日 修正
85年12月 4日 接受

The Analysis of Phathalate Esters Using Membrane Technology

Y. S. WANG AND C. Y. SHIH
Department of Chemistry
Fu-Jen University
Taipei, Taiwan 242, R.O.C.

ABSTRACT

Phthalate esters are known for their chemical stability. They are used as plasticizers in the products of polymers, paints, and plastics. Recently, increasing number of goods is made of plastics, and petroleum refinery is one of the fast growing industry in this country, prevention of plasticizers from our living environment and necessity of a clean and sensitive method for their detection become important ever. Membrane technology with minimum use of organic solvent has been a major breakthrough in analytical chemistry. In this study, thin membrane was used to extract phthalate esters from water. Subsequent chromatographic separation and quantitation were done by GC/FID.

Standard mixture solutions of eleven phthalate esters ranging from one carbon methyl to nine carbon nonyl on the alcohol moiety were prepared. The optimum membrane extraction procedures were evaluated by spiking water samples with known amount of standard mixture. The spiked water was carried through membrane, followed by a small amount of solvent elution, the percentage of recoveries of each analyte were then calaulated. The membrane parameters toward a better recovery were manipulated including (1) membrane preconditioning; (2) elution solvent selection; (3)membrane permeation before elution; (4)addition of modifier solvent into water sample. Recovery data from four different elution solvents including hexane showed that acetonitrile was 2 folds better than dichloromethane. And the acetonitrile recovery was further increased by addition of 5% methanol in water sample. Other effects on membrane were also tested such as(5)rate of passage for the water sample; (6)stability

of the analytes on membrane; (7) membrane capacity; (8) membrane reusability. We found flow rate of water sample was independent of extraction efficiency. Membrane technology is advantageous to enable the extraction in situ without bringing water samples back to the laboratory.

Key Words: phathalate esters; membrane analysis; minimum use of organic solvent; gas chromatography; in situ extraction

A Result on Nonlinear Filters

WEN-LIN CHIOU[1]
Department of Mathematics
Fu-Jen University
Taipei, Taiwan 242, R.O.C.

ABSTRACT

In this paper we consider the Duncan-Mortensen-Zakai equation for the Yau filtering system. We show that this equation can be solved explicitly with arbitrary initial condition by means of solving a system of ordinary differential equations and a Kolmogorov type equation.

Key Words: Duncan-Mortensen-Zakai equation, Kolmogorov equation, Recursive filters.

INTRODUCTION

In [10], Mitter pointed out that the innovation approach to nonlinear filtering theory is not, in general, explicitly computable. The idea of using estimation algebras to construct finite dimensional nonlinear filters was first proposed in Brockett and Clark [3], Brockett [2] and Mitter [10]. The method is to use Lie algebra to solve Duncan-Mortensen-Zakai (DMZ) equation, which is a stochastic partial differential equation. By working on the robust form of DMZ equation, we can reduce the problem to that of solving a time variant partial diffendntial equation.

The recent works Mitter[10], Tam-Wong-Yau[11], Dong-Tam-Wong-Yau[9], Yau[12], Chiou-Yau[7], Chen-Leung-Yau[4][5], Chiou[6], in which they used Lie algebraic method, has given us a deeper understanding of the DMZ equation which is essential for progress in nonlinear filtering as well as in stochastic control. However, it

---

[1] E-mail:math 1014@fujens.fju.edu.tw.funded by NSC grant NSC-85-2121-M-030-004

is extremely desirable to solve the DMZ equation or the corresponding time variant partial differential equation directly. S.-T. Yau and S. S.-T. Yau have studied this problem, and have obtained some remarkable results. In [13], an explicit colsed form solution of Kolmogorov equation was constructed, that is, the DMZ equation was completely solved in case of that all the $h_i(x)$ are constant (cf. the following system equation (2.0)). In [14], The DMZ equation was solved explicitly with arbitrary initial condition for the Kalman-Bucy filtering system and Benes filtering system, respectively. In this paper, I studied the Yau filtering system, which is a class of nonlinear filtering systems including both Kalman-Bucy and Benes filtering systems as special cases. The advantage of our approach is that one can write down the solution of DMZ equation in terms of the solution of Kolmogorov equation and the initial condition can be arbitrary, hence the recursive universal filters was derived. Notice that the recursive filter for Yau filtering system was previously derived only for maximal rank case and the state space dimension less than or equal to four. The novelty in this paper is that we no longer need maximal rank condition in our derivation and the state space dimension is arbitrary finite-dimensional.

THE FILTERING PROBLEM CONSIDERED, AND THE BASIC CONCEPT.

The filtering problem considered here is based on the following signal observation model:

$$\begin{cases} dx(t) = f(x(t))dt + g(x(t))dv(t), & x(0) = x_0 \\ dy(t) = h(x(t))dt + dw(t), & y(0) = 0 \end{cases} \tag{2.0}$$

in which x, v, y and w are respectively R^n, R^p, R^m and R^m -valued processes, and v and w have components which are independent, standard Brownian processes. We further assume that $n = p$, f, h are C^∞ smooth functions, and that g is an n by n C^∞ smooth matrix. we will refer to $x(t)$ as the state of the system at time t and to $y(t)$ as the observation at time t .

Let $\rho(t,x)$ denote the conditional probability density of the state given the observation $\{y(s):0 \leq s \leq t\}$. It is well known (see Davis [8], for example) that $\rho(t,x)$ is given by normalizing a function $\sigma(t,x)$, which satisfies the following

Duncan-Mortensen-Zakai equation (see Zakai [15], for example):

$$d\sigma(t,x) = L_0\sigma(t,x)dt + \sum_{i=1}^{m} L_i\sigma(t,x)dy_i(t),\ \sigma(0,x) = \sigma_0, \tag{2.1}$$

where

$$L_0 = \frac{1}{2}\sum_{i,j=1}^{n}\frac{\partial^2}{\partial x_i\partial x_j}(gg')_{ij} - \sum_{i=1}^{n}\frac{\partial}{\partial x_i}f_i - \frac{1}{2}\sum_{i=1}^{m}h_i^2.$$

and for $i = 1, \cdots\cdots, m$, L_i is the zero degree difference operaror of multiplication by h_i. σ_0 is the probability density of the initial point x_0. In this paper, we will assume σ_0 is a C^∞ function.

Equation (2.1) is a stochastic partial differential equation. In real applications, we are interesred in constructing state estimators from observed sample paths with some property of robustness, Davis in [8] studied this problem and proposed some robust algorithms.

In our case, his basic idea reduce to defining a new unnormalized density

$$u(t,x) = \exp(-\sum_{i=1}^{m}h_i(x)y_i(t))\sigma(t,x).$$

It is easy to show that $u(t,x)$ satisfies the following time varying partial differential equation

$$\begin{cases}\dfrac{\partial u}{\partial t}(t,x) = L_0\xi(t,x) + \sum_{i=1}^{m}y_i(t)[L_0,L_i]\xi(t,x) \\ \qquad\qquad + \dfrac{1}{2}\sum_{i,j=1}^{m}y_i(t)y_j(t)[[L_0,L_i],L_j]\xi(t,x), \\ \sigma(0,x) = \sigma_0,\end{cases} \tag{2.2}$$

where $[\cdot,\cdot]$ is the Lie bracket.

If $h_i(x) = c_i = constant$ for $1 \leq i \leq m$, then (2.2) reduces to the Kolmogorov equation

$$\begin{aligned}\frac{\partial u}{\partial t}(t,x) &= L_0\,u(t,x) \\ &= \left(\frac{1}{2}\sum_{i=1}^{n}\frac{\partial^2}{\partial x_i^2} - \sum_{i=1}^{n}f_i(x)\frac{\partial}{\partial x_i} - \sum_{i=1}^{n}\frac{\partial f_i}{\partial x_i}(x) - \frac{1}{2}\sum_{i=1}^{n}c_i^2\right)u(t,x).\end{aligned} \tag{2.3}$$

The following theorem was proven by S.-T. Yau and S. S.-T. Yau [13].

Theorem 1.

Kolmogorov equation (2.3) can be solved explicitly in a closed form. In fact if $\Sigma_{i=1}^{n} c_i^2$ is replaced by a bounded function, (2.3) can also be solved explicitly in a closed form.

It is shown in [13] that (2.2) is equivalent to

$$\begin{aligned}\frac{\partial u}{\partial t}(t,x) = {} & \frac{1}{2}\sum_{i=1}^{n}\frac{\partial^2 u}{\partial x_i^2}(t,x) + \sum_{i=1}^{n}\left(-f_i(x) + \sum_{j=1}^{m} y_i(t)\frac{\partial h_j}{\partial x_i}(x)\right)\frac{\partial u}{\partial x_i}(t,x) \\ & - \sum_{i=1}^{n}\frac{\partial f_i}{\partial x_i}u(t,x) - \frac{1}{2}\sum_{i=1}^{m} h_i^2(x)u(t,x) + \frac{1}{2}\sum_{i=1}^{m} y_i(t)\Delta h_i(x)u(t,x) \\ & - \sum_{i=1}^{m}\sum_{j=1}^{n} y_i(t)f_j(x)\frac{\partial h_i}{\partial x_k}(x)u(t,x) \\ & + \frac{1}{2}\sum_{i=1}^{m}\sum_{j=1}^{m} y_i(t)y_j(t)\sum_{k=1}^{n}\frac{\partial h_i}{\partial x_k}(x)\frac{\partial h_j}{\partial x_k}(x)u(t,x). \end{aligned} \tag{2.4}$$

The following theorem concerning about DMZ equation for Kalman-Bucy filtering systems with arbitrary initial condition was proved by S.-T. Yau and S. S.-T. Yau [14].

Theorem 2.

Consider the Kalman-Bucy filtering system with

$$h_i(x) = \sum_{j=1}^{n} c_{ij}x_j + c_i,\ 1 \le i \le m,\ \text{where } c_{ij} \text{ and } c_i \text{ are constants,} \tag{2.5}$$

$$f_i(x) = \sum_{j=1}^{n} d_{ij}x_j + d_i,\ 1 \le i \le m,\ \text{where } d_{ij} \text{and } d_i \text{ are constants,} \tag{2.6}$$

Choose a homogeneous quadratic $F(x) = \frac{1}{2}\sum_{i,j=1}^{n} e_{ij}x_ix_j$ with $e_{ij} = e_{ji}$ such that

$$(E + D)^T(E + D) = C^TC + D^TD \tag{2.7}$$

Hence $E = (e_{ij})$, $D = (d_{ij})$ are $n \times n$ matrix and $C = (c_{ij})$ is $m \times n$ matrix. Then the solution $u(t,x)$ for the Duncan-Mortensen-Zakai equation (2.4) is reduced to the solution $\tilde{u}(t,x)$ for the Kolmogorov equation

$$\frac{\partial \tilde{u}}{\partial t}(t,x) = \frac{1}{2}\Delta \tilde{u}(t,x) - \sum_{i=1}^{n}\left(f_i(x) + \frac{\partial F}{\partial x_i}\right)\frac{\partial \tilde{u}}{\partial x_i}(t,x)$$
$$= -\sum_{i=1}^{n}\left(\frac{\partial f_i}{\partial x_i}(x) + \frac{\partial^2 F}{\partial x_i^2}(x)\right)\tilde{u}(t,x), \tag{2.8}$$

where

$$\tilde{u}(t,x) = e^{F(x)+\sum_{i=1}^{n}a_i(t)x_i+c(t)}u(t,x+b(t)), \tag{2.9}$$

and $a_i(t), b_i(t)$ and $c(t)$ satisfy the following system of O.D.E.

$$a'_i(t) + \sum_{j=1}^{n} d_j a_i(t) - \sum_{l=1}^{m}\sum_{j=1}^{n} c_{lj}b_j(t)c_{li} - \sum_{j=1}^{m}\sum_{k=1}^{n} y_j(t)d_k c_{jk}$$
$$+ \sum_{j=1}^{n} d_j e_{ji} - \sum_{j=1}^{m} c_j c_{ji} = 0, \quad 1 \le i \le n. \tag{2.10}$$

$$\sum_{i=1}^{n} d_i a_i(t) + c'(t) - \frac{1}{2}\sum_{i=1}^{n} a_i^2(t) - \frac{1}{2}\sum_{i=1}^{m}\left(\sum_{j=1}^{n} c_{ij}b_j(t)\right)^2 - \sum_{i=1}^{m} c_i \sum_{j=1}^{n} c_{ij}b_j(t)$$
$$- \sum_{j=1}^{m}\sum_{i=1}^{n} y_j(t)c_{ji}\left(\sum_{k=1}^{n} d_{ik}b_k(t) + d_i\right) + \frac{1}{2}\sum_{i=1}^{m}\sum_{j=1}^{m} y_i(t)c_{ik}c_{jk}$$
$$+ \frac{1}{2}\sum_{k=1}^{n} e_{kk} - \frac{1}{2}\sum_{i=1}^{m} c_i^2 = 0, \tag{2.11}$$

$$b'(t) - a_i(t) + \sum_{j=1}^{m} c_{ji}y_j(t) - \sum_{j=1}^{n} d_j b_j(t) = 0 \quad 1 \le i \le n. \tag{2.12}$$

The following Theorem concerning about DMZ equation for Benes filtering systems with arbitrary initial condition was proved by S.-T. Yau and S. S.-T. Yau [14].

Theorem 3.

Consider the Benes filtering system with

$$h_i(x) = \sum_{j=1}^{n} c_{ij}x_j + c_i, 1 \le i \le m, \text{ where } c_{ij} \text{ and } c_i \text{ are constants,} \tag{2.13}$$

$$f_i(x) = -\frac{\partial F}{\partial x_i}, 1 \le i \le n, \text{ where } F \text{ is a } C^\infty \text{ function,} \tag{2.14a}$$

and

$$\Delta F(x) - |\nabla F(x)|^2(x) - \sum_{i=1}^{m} h_i^2(x) = \sum_{i,j=1}^{n} e_{ij}x_i x_j + \sum_{i=1}^{n} e_i x_i + e. \tag{2.14b}$$

Choose a C^∞ function $G(x)$ such that

$$\Delta G(x) + \frac{1}{2} \mid \nabla G \mid^2(x) + \sum_{i,j=1}^{n} e_{ij}x_i x_j + \sum_{i=1}^{n} e_i x_i + e = \text{constant} = 2d. \tag{2.15}$$

Then the solution $u(t,x)$ for the Duncan-Mortensen-Zakai (2.4) is reduced to the solution $\tilde{u}(t,x)$ for the Kolmogorov equation.

$$\frac{\partial \tilde{u}}{\partial t}(t,x) = \frac{1}{2}\Delta \tilde{u}(t,x) - \sum_{i=1}^{n} \frac{\partial G}{\partial x_i}(x) \frac{\partial \tilde{u}}{\partial x_i}(t,x) - \sum_{i=1}^{n} \frac{\partial^2 G}{\partial x_i^2}(x)\, \tilde{u}(t,x) + d\, \tilde{u}(t,x) \tag{2.16}$$

where

$$\tilde{u}(t,x) = e^{F(x+b(t))+G(x)+\sum_{i=1}^{n} a_i(t)x_i + c(t)} u(t, x + b(t)) \tag{2.17}$$

and $a_i(t), b_i(t)$ and $c(t)$ satisfy the following system of O.D.E.

$$b'_i(t) - a_i(t) + \sum_{j=1}^{m} c_{ji} y_j(t) = 0, \quad 1 \leq i \leq n, \tag{2.18}$$

$$c'(t) - \frac{1}{2}\sum_{i=1}^{n} a_i^2(t) + \frac{1}{2}\sum_{i=1}^{m}\sum_{j=1}^{m} c_{ik}c_{jk} y_i(t) y_j(t) + \sum_{i=1}^{n} e b_i(t) + \frac{1}{2}\sum_{i,j=1}^{n} e_i b_i(t) b_j(t) = 0, \tag{2.19}$$

$$a'_i(t) + \sum_{j=1}^{m} (e_{ij} + e_{ji}) b_j(t) = 0, \quad 1 \leq i \leq n. \tag{2.20}$$

DMZ EQUATION FOR YAU FILTERING SYSTEMS WITH ARBITRARY INITIAL CONDITION.

Main Theorem.

Consider the Yau filtering system with

$$h_i(x) = \sum_{j=1}^{n} c_{ij}x_j + c_i,\ 1 \leq i \leq m, \text{ where } c_{ij} \text{ and } c_i \text{ are constants,} \tag{3.1}$$

$$l_i(x) = \sum_{j=1}^{n} d_{ij}x_j + d_i,\ 1 \leq i \leq n, \text{ where } d_{ij} \text{ and } d_i \text{ are constants,} \tag{3.2a}$$

$$f_i(x) = l_i(x) + \frac{\partial \phi(x)}{\partial x_i},\ 1 \leq i \leq n, \text{ where } \phi(x) \text{ is a } C^\infty \text{ function,} \tag{3.2b}$$

$$F(x) = -\phi(x), \tag{3.2c}$$

and

$$\sum_{i=1}^{n}\frac{\partial f_i(x)}{\partial x_i}-\sum_{i=1}^{n}f_i^2(x)-\sum_{i=1}^{m}h_i^2(x)=2[\sum_{i,j=1}^{n}e_{ij}x_ix_j+\sum_{i=1}^{n}e_ix_i+e]. \tag{3.2d}$$

Choose a C^∞ function $G(x)$ such that

$$\sum_{i=1}^{n}\left(\frac{\partial^2 G(x)}{\partial x_i^2}+\frac{\partial l_i(x)}{\partial x_i}\right)+\sum_{i=1}^{n}\left(\frac{\partial G}{\partial x_i}(x)+l_i(x)\right)^2+2[\sum_{i,j=1}^{n}e_{ij}x_ix_j+\sum_{i=1}^{n}e_ix_i+e]=$$
$$\text{constant}=2d. \tag{3.3}$$

Then the solution $u(t,x)$ for the Duncan-Mortensen-Zakai (2.4) is reduced to the solution $\tilde{u}(t,x)$ for the Kolmogorov equation:

$$\frac{\partial \tilde{u}}{\partial t}(t,x)=\frac{1}{2}\Delta\tilde{u}(t,x)-\sum_{i=1}^{n}\left(\frac{\partial G}{\partial x_i}(x)+l_i(x)\right)\frac{\partial \tilde{u}}{\partial x_i}(t,x)$$
$$+\sum_{i=1}^{n}\left(\frac{\partial^2 G(x)}{\partial x_i^2}-\frac{\partial l_i(x)}{\partial x_i}\right)\tilde{u}(t,x)++d\,\tilde{u}(t,x) \tag{3.4}$$

where

$$\tilde{u}(t,x)=e^{F(x+b(t))+G(x)+\sum_{i=1}^{n}a_i(t)x_i+c(t)}u(t,x+b(t)) \tag{3.5}$$

and $a_i(t),b_i(t)$ and $c(t)$ satisfy the following system of O.D.E.

$$b'_i(t)-a_i(t)+\sum_{j=1}^{m}c_{ji}y_j(t)+\sum_{j=1}^{m}d_{ij}b_j(t)=0,\quad 1\le i\le n, \tag{3.6}$$

$$-\sum_{k=1}^{n}(\sum_{j=1}^{m}c_{jk}y_j(t))d_{ki}+\sum_{j=1}^{n}(e_{ij}+e_{ji})b_j(t)+a'_i(t)+\sum_{j=1}^{n}a_j(t)d_{ji} \tag{3.7}$$
$$+\sum_{i=1}^{n}\sum_{j,k=1}^{n}d_jd_{jk}b_k(t)=0,\quad 1\le i\le n,$$

$$-\sum_{i=1}^{n}\sum_{j=1}^{m}c_{ji}y_j(t)(\sum_{k=1}^{n}d_{ik}b_k(t)+d_i)+\sum_{i=1}^{n}e_ib_i(t)+\sum_{i,j=1}^{n}e_{ij}b_i(t)b_j(t)+c'(t)$$
$$-\frac{1}{2}\sum_{i=1}^{n}a_i^2(t) \tag{3.8}$$
$$+\frac{1}{2}\sum_{i,j=1}^{m}\sum_{k=1}^{n}c_{ik}c_{jk}y_i(t)y_j(t)+\sum_{i=1}^{n}d_ia_i(t)+\sum_{i=1}^{n}\sum_{j=1}^{n}d_id_{ij}b_j(t)$$
$$+\frac{1}{2}\sum_{i=1}^{n}[\sum_{j=1}^{n}d_{ij}b_j(t)]^2$$

$$= 0$$

Proof:

We only need to show that if $u\ (t,\ x)$ satisfies (2.4), then $\tilde{u}\ (t,\ x)$ given by (3.5) - (3.8) will satisfy Kolmogorov equation (2.3).

$$\begin{aligned}\frac{\partial \tilde{u}}{\partial t}(t,x) = e^{F(x+b(t))+G(x)+\sum_{i=1}^{n} a_i(t)x_i+c(t)}\Big\{&\Big[\sum_{i=1}^{n}\frac{\partial F}{\partial x_i}(x+b(t))b'(t)\\&+\sum_{i=1}^{n} a'_i(t)x_i + c'(t)\Big]u(t,x+b(t))\\&+\frac{\partial u}{\partial t}(t,x+b(t))+\sum_{i=1}^{n} b'_i(t)\frac{\partial u}{\partial x_i}(t,x+b(t))\Big\}\end{aligned}$$

$$\begin{aligned}\frac{\partial \tilde{u}}{\partial x_i}(t,x) = e^{F(x+b(t))+G(x)+\sum_{i=1}^{n} a_i(t)x_i+c(t)}\Big\{&\Big[\sum_{i=1}^{n}\frac{\partial F}{\partial x_i}(x+b(t))+\frac{\partial G}{\partial x_i}(x)\\&+a_i(t)\Big]u(t,x+b(t))+\frac{\partial u}{\partial x_i}(t,x+b(t))\Big\}\end{aligned}$$

$$\begin{aligned}\frac{\partial^2 \tilde{u}}{\partial x_i^2}(t,x) = e^{F(x+b(t))+G(x)+\sum_{i=1}^{n} a_i(t)x_i+c(t)}\Big\{&\Big(\frac{\partial F}{\partial x_i}(x+b(t))\\&+\frac{\partial G}{\partial x_i}(x)+a_i(t)\Big)^2 u(t,x+b(t))\\&+2\Big(\frac{\partial F}{\partial x_i}(x+b(t))+\frac{\partial G}{\partial x_i}(x)+a_i(t)\Big)\frac{\partial u}{\partial x_i}(t,x+b(t))\\&+\Big(\frac{\partial^2 F}{\partial x_i^2}(x+b(t))+\frac{\partial^2 G}{\partial x_i^2}(x)\Big)u(t,x+b(t))\\&+\frac{\partial^2 u}{\partial x_i^2}(t,x+b(t))\Big\}\end{aligned}$$

$$\begin{aligned}\frac{1}{2}\Delta\,\tilde{u}(t,x) = e^{F(x+b(t))+G(x)+\sum_{i=1}^{n} a_i(t)x_i+c(t)}\Big\{&\frac{1}{2}\sum_{i=1}^{n}\Big(\frac{\partial F}{\partial x_i}(x+b(t))\\&+\frac{\partial G}{\partial x_i}(x)+a_i(t)\Big)^2 u(t,x+b(t))\\&+\sum_{i=1}^{n}\Big(\frac{\partial F}{\partial x_i}(x+b(t))+\frac{\partial G}{\partial x_i}(x)+a_i(t)\Big)\frac{\partial u}{\partial x_i}(t,x+b(t))\\&+\Big(\frac{1}{2}\Delta F(x+b(t))+\frac{1}{2}\Delta G(x)\Big)u(t,x+b(t))\end{aligned}$$

$$+\frac{1}{2}\Delta u(t,x+b(t))\Big\}$$

$$\sum_{i=1}^{n} f_i(x)\frac{\partial \tilde{u}}{\partial x_i}(t,x) = e^{F(x+b(t))+G(x)+\sum_{i=1}^{n} a_i(t)x_i+c(t)}\Big\{\Big(\sum_{i=1}^{n} f_i(x)\frac{\partial F}{\partial x_i}(x+b(t))\Big)$$
$$+\sum_{i=1}^{n} f_i(x)\frac{\partial G}{\partial x_i}(x)+\sum_{i=1}^{n} f_i(x)a_i(t)\Big]u(t,x+b(t))$$
$$+f_i(x)\frac{\partial u}{\partial x_i}(t,x+b(t))\Big\}$$

$$\frac{\partial \tilde{u}}{\partial t}(t,x)-\frac{1}{2}\Delta\tilde{u}(t,x)+\sum_{i=1}^{n} f_i(x)\frac{\partial \tilde{u}}{\partial x_i}(t,x)$$
$$= e^{F(x+b(t))+G(x)+\sum_{i=1}^{n} a_i(t)x_i+c(t)}\Big\{\Big[\sum_{i=1}^{n}\frac{\partial F}{\partial x_i}(x+b(t))b'(t)$$
$$+\sum_{i=1}^{n} a'_i(t)x_i+c'(t)\Big]u(t,x+b(t))$$
$$+\frac{\partial u}{\partial t}(t,x+b(t))+\sum_{i=1}^{n} b'_i(t)\frac{\partial u}{\partial x_i}(t,x+b(t))$$
$$+\Big[\sum_{i=1}^{n} f_i(x)\frac{\partial F}{\partial x_i}(x+b(t))+\sum_{i=1}^{n} f_i(x)\frac{\partial G}{\partial x_i}(x)$$
$$+\sum_{i=1}^{n} f_i(x)a_i(t)\Big]u(t,x+b(t))+f_i(x)\frac{\partial u}{\partial x_i}(t,x+b(t))$$
$$-\frac{1}{2}\Big[\sum_{i=1}^{n}\Big(\frac{\partial F}{\partial x_i}(x+b(t))\Big)^2+\Big(\frac{\partial G}{\partial x_i}(x)\Big)^2+a_i^2(t)$$
$$+2\frac{\partial F}{\partial x_i}(x+b(t))\frac{\partial G}{\partial x_i}(x)+2a_i(t)\frac{\partial F}{\partial x_i}(x+b(t))$$
$$+2a_i(t)\frac{\partial G}{\partial x_i}(x)\Big]u(t,x+b(t))$$
$$-\sum_{i=1}^{n}\Big(\frac{\partial F}{\partial x_i}(x+b(t))+\frac{\partial G}{\partial x_i}(x)+a_i(t)\Big)\frac{\partial u}{\partial x_i}(t,x+b(t))$$
$$-\Big(\frac{1}{2}\Delta F(x+b(t))+\frac{1}{2}\Delta G(x)\Big)u(t,x+b(t))$$
$$-\frac{1}{2}\Delta u(t,x+b(t))\Big\}.$$

Observe that

$$\sum_{i=1}^{n}\frac{\partial G}{\partial x_i}(x)\,\frac{\partial\,\tilde{u}}{\partial x_i}(x,t)$$

$$= e^{F(x+b(t))+G(x)+\sum_{i=1}^{n}a_i(t)x_i+c(t)}\Bigg\{\Bigg[\sum_{i=1}^{n}\frac{\partial G}{\partial x_i}(x)\,\frac{\partial F}{\partial x_i}(x+b(t))$$

$$+\sum_{i=1}^{n}\left(\frac{\partial G}{\partial x_i}(x)\right)^2+\sum_{i=1}^{n}\frac{\partial G}{\partial x_i}(x)a_i(t)\Bigg]u(t,x+b(t))$$

$$+\sum_{i=1}^{n}\frac{\partial G}{\partial x_i}(x)\,\frac{\partial u}{\partial x_i}(t,x+b(t))\Bigg\}$$

Therefore

$$\frac{\partial\,\tilde{u}}{\partial t}(t,x)-\frac{1}{2}\Delta\,\tilde{u}(t,x)+\sum_{i=1}^{n}\frac{\partial G}{\partial x_i}(x)\,\frac{\partial\,\tilde{u}}{\partial x_i}(t,x)$$

$$= e^{F(x+b(t))+G(x)+\sum_{i=1}^{n}a_i(t)x_i+c(t)}\Bigg\{\Bigg[\sum_{i=1}^{n}\frac{\partial F}{\partial x_i}(x+b(t))b'(t)$$

$$+\sum_{i=1}^{n}a'_i(t)x_i+c'(t)\Bigg]u(t,x+b(t))$$

$$+\sum_{i=1}^{n}b'_i(t)\,\frac{\partial u}{\partial x_i}(t,x+b(t))-\frac{1}{2}\Bigg[\sum_{i=1}^{n}\left(\frac{\partial F}{\partial x_i}(x+b(t))\right)^2$$

$$+\left(\frac{\partial G}{\partial x_i}(x)\right)^2+a_i^2(t)$$

$$+2\frac{\partial F}{\partial x_i}(x+b(t))\frac{\partial G}{\partial x_i}(x)+2a_i(t)\frac{\partial F}{\partial x_i}(x+b(t))+2a_i(t)\frac{\partial G}{\partial x_i}(x)\Bigg]u(t,x+b(t))$$

$$-\sum_{i=1}^{n}\left(\frac{\partial F}{\partial x_i}(x+b(t))+a_i(t)\right)\frac{\partial u}{\partial x_i}(t,x+b(t))$$

$$+\left[\sum_{i=1}^{n}\frac{\partial G}{\partial x_i}(x)\,\frac{\partial F}{\partial x_i}(x+b(t))+\sum_{i=1}^{n}\left(\frac{\partial G}{\partial x_i}(x)\right)^2+\sum_{i=1}^{n}\frac{\partial G}{\partial x_i}(x)a_i(t)\right]u(t,x+b(t))$$

$$-\left(\frac{1}{2}\Delta F(x+b(t))+\frac{1}{2}\Delta G(x)\right)u(t,x+b(t))$$

$$+\sum_{i=1}^{n}\sum_{j=1}^{m}y_j(t)\,\frac{\partial h_j}{\partial x_i}(x+b(t))\,\frac{\partial u}{\partial x_i}(t,x+b(t))$$

$$-\sum_{i=1}^{n}\frac{\partial f_i}{\partial x_i}(x+b(t))u(t,x+b(t))-\frac{1}{2}\sum_{i=1}^{m}h_i^2(x+b(t))u(t,x+b(t))$$

$$+\frac{1}{2}\sum_{i=1}^{m}y_i(t)\Delta h_i(x+b(t))u(t,x+b(t))$$

$$-\sum_{i=1}^{m}\sum_{j=1}^{n}y_i(t)f_j(x+b(t))\,\frac{\partial h_i}{\partial x_j}(x+b(t))u(t,x+b(t))$$

$$+\frac{1}{2}\sum_{i=1}^{m}\sum_{j=1}^{m}y_i(t)y_j(t)\sum_{k=1}^{n}\frac{\partial h_i}{\partial x_k}(x+b(t))\frac{\partial h_i}{\partial x_k}(x+b(t))u(t,x+b(t))$$
$$-\sum_{i=1}^{n}f_i(x+b(t))\frac{\partial u}{\partial x_i}(t,x+b(t))\Big\}$$

Hence

$$\frac{\partial \tilde{u}}{\partial t}(t,x)-\frac{1}{2}\Delta\tilde{u}(t,x)$$
$$+\sum_{i=1}^{n}\frac{\partial G}{\partial x_i}(x)\frac{\partial \tilde{u}}{\partial x_i}(t,x)+\Delta G(x)\tilde{u}(t,x)$$
$$-\left(\frac{1}{2}\Delta G(x)+\frac{1}{2}\mid\nabla G\mid^2(x)\right)\tilde{u}(t,x)$$
$$=\frac{\partial \tilde{u}}{\partial t}(t,x)-\frac{1}{2}\Delta\tilde{u}(t,x)+\sum_{i=1}^{n}\frac{\partial G}{\partial x_i}(x)\frac{\partial \tilde{u}}{\partial x_i}(t,x)$$
$$+\left(\frac{1}{2}\Delta G(x)-\frac{1}{2}\mid\nabla G\mid^2(x)\right)\tilde{u}(t,x)$$
$$=e^{F(x+b(t))+G(x)+\sum_{i=1}^{n}a_i(t)x_i+c(t)}\Big\{\Big[\sum_{i=1}^{n}\frac{\partial F}{\partial x_i}(x+b(t))b'(t)$$
$$+\sum_{i=1}^{n}a'_i(t)x_i+c'(t)\Big]u(t,x+b(t))$$
$$+\sum_{i=1}^{n}b_i'(t)\frac{\partial u}{\partial x_i}(t,x+b(t))$$
$$-\frac{1}{2}\sum_{i=1}^{n}\Big[\left(\frac{\partial F}{\partial x_i}(x+b(t))\right)^2+a_i^2(t)+2a_i(t)\frac{\partial F}{\partial x_i}(x+b(t))$$
$$+2a_i(t)\frac{\partial G}{\partial x_i}(x)\Big]u(t,x+b(t))$$
$$-\sum_{i=1}^{n}\left(\frac{\partial F}{\partial x_i}(x+b(t))+a_i(t)\right)\frac{\partial u}{\partial x_i}(t,x+b(t))+\sum_{i=1}^{n}\frac{\partial G}{\partial x_i}(x)a_i(t)u(t,x+b(t))$$
$$-\frac{1}{2}\Delta F(x+b(t))u(t,x+b(t))+\sum_{i=1}^{n}\sum_{j=1}^{m}y_j(t)\frac{\partial h_j}{\partial x_i}(x+b(t))\frac{\partial u}{\partial x_i}(t,x+b(t))$$
$$-\sum_{i=1}^{n}\frac{\partial f_i}{\partial x_i}(x+b(t))u(t,x+b(t))-\frac{1}{2}\sum_{i=1}^{m}h_i^2(x+b(t))u(t,x+b(t))$$
$$+\frac{1}{2}\sum_{i=1}^{m}y_i(t)\Delta h_i(x+b(t))u(t,x+b(t))$$
$$-\sum_{i=1}^{m}\sum_{j=1}^{n}y_i(t)f_j(x+b(t))\frac{\partial h_i}{\partial x_j}(x+b(t))u(t,x+b(t))$$
$$+\frac{1}{2}\sum_{i=1}^{m}\sum_{j=1}^{m}y_i(t)y_j(t)\sum_{k=1}^{n}\frac{\partial h_i}{\partial x_k}(x+b(t))\frac{\partial h_i}{\partial x_k}(x+b(t))u(t,x+b(t))$$

$$
\begin{aligned}
&- \sum_{i=1}^{n} f_i(x + b(t)) \frac{\partial u}{\partial x_i}(t, x + b(t))\Big\} \\
&= e^{F(x+b(t))+G(x)+\sum_{i=1}^{n} a_i(t)x_i+c(t)} \Big\{ \Big[\sum_{i=1}^{n} \Big(b'_i(t) - a_i(t) + \sum_{j=1}^{m} y_j(t) \frac{\partial h_j}{\partial x_i}(x + b(t)) \Big) \\
&- \sum_{i=1}^{n} f_i(x + b(t)) + \sum_{i=1}^{n} \frac{\partial F}{\partial x_i}(x + b(t)) \Big] \frac{\partial u}{\partial x_i}(t, x + b(t)) \\
&+ \Big[\sum_{i=1}^{n} \frac{\partial F}{\partial x_i}(x + b(t)) b'_i(t) - \sum_{i=1}^{n} a_i(t) \frac{\partial F}{\partial x_i}(x + b(t)) \\
&- \sum_{i=1}^{m} \sum_{j=1}^{n} y_i(t) f_j(x + b(t)) \frac{\partial h_i}{\partial x_j}(x + b(t)) + \sum_{i=1}^{n} a'_i(t) x_i + c'(t) \\
&- \frac{1}{2} \sum_{i=1}^{n} \Big(\frac{\partial F}{\partial x_i}(x + b(t)) \Big)^2 - \frac{1}{2} \sum_{i=1}^{n} a_i^2(t) - \frac{1}{2} \Delta F(x + b(t)) \\
&- \sum_{i=1}^{n} \frac{\partial f_i}{\partial x_i}(x + b(t)) - \frac{1}{2} \sum_{i=1}^{m} h_i^2(x + b(t)) \\
&+ \frac{1}{2} \sum_{i=1}^{m} y_i(t) \Delta h_i(x + b(t)) \\
&+ \frac{1}{2} \sum_{i=1}^{m} \sum_{j=1}^{m} y_i(t) y_j(t) \sum_{k=1}^{n} \frac{\partial h_i}{\partial x_k} \frac{\partial h_j}{\partial x_k}(x + b(t)) \Big] u(t, x + b(t)) \Big\}.
\end{aligned}
$$

In view of (3.1), (3.2b), (3.2c), we have

$$
\begin{aligned}
&\frac{\partial \tilde{u}}{\partial t}(t, x) - \frac{1}{2} \Delta \tilde{u}(t, x) \\
&+ \sum_{i=1}^{n} \frac{\partial G}{\partial x_i}(x) \frac{\partial \tilde{u}}{\partial x_i}(t, x) + \Delta G(x) \tilde{u}(t, x) - \Big(\big(\frac{1}{2} \Delta G(x) + \frac{1}{2} \mid \nabla G \mid^2(x) \big) \Big) \tilde{u}(t, x) \\
&= e^{F(x+b(t))+G(x)+\sum_{i=1}^{n} a_i(t)x_i+c(t)} \Big\{ \sum_{i=1}^{n} \Big[(b'_i(t) - a_i(t) + \sum_{j=1}^{m} c_{ij} y_j(t) - l_i(x + b(t)) \Big] \frac{\partial u}{\partial x_i}(x + b(t)) \\
&+ \Big[\sum_{i=1}^{n} \frac{\partial F}{\partial x_i}(x + b(t)) b'_i(t) - \sum_{i=1}^{n} a_i(t) \frac{\partial F}{\partial x_i}(x + b(t)) + \sum_{i=1}^{m} \sum_{j=1}^{n} y_i(t) c_{ij} \frac{\partial F}{\partial x_j}(x + b(t)) \\
&- \sum_{i=1}^{m} \sum_{j=1}^{n} y_i(t) l_j(x + b(t)) c_{ij} + \sum_{i=1}^{n} a'_i(t) x_i + c'(t) - \frac{1}{2} \sum_{i=1}^{n} a_i^2(t) \\
&+ \frac{1}{2} \sum_{i=1}^{m} \sum_{j=1}^{m} \sum_{k=1}^{n} c_{ik} c_{jk} y_i(t) y_j(t) \\
&- \frac{1}{2} \Delta F(x + b(t)) - \frac{1}{2} \mid \nabla F \mid^2(x + b(t)) - \frac{1}{2} \sum_{i=1}^{m} h_i^2(x + b(t)) \Big] u(t, x + b(t)) \Big\}.
\end{aligned}
$$

Observe that

$$\begin{aligned}
&\sum_{i=1}^{n} l_i(x)\frac{\partial \tilde{u}}{\partial x_i}(x,t)\\
&= e^{F(x+b(t))+G(x)+\sum_{i=1}^{n} a_i(t)x_i+c(t)}\Bigg\{\Bigg[\sum_{i=1}^{n} l_i(x)\frac{\partial F}{\partial x_i}(x+b(t))\\
&\quad+\sum_{i=1}^{n} l_i(x)\frac{\partial G}{\partial x_i}(x)+\sum_{i=1}^{n} l_i(x)a_i(t)\Bigg]u(t,x+b(t))\\
&\quad+\sum_{i=1}^{n} l_i(x)\frac{\partial u}{\partial x_i}(t,x+b(t))\Bigg\},
\end{aligned}$$

and note that $\Sigma_{i=1}^{n}\frac{\partial l_i(x+b(t))}{\partial x_i}=\Sigma_{i=1}^{n}\frac{\partial l_i(x)}{\partial x_i}$, so we have

$$\begin{aligned}
&\frac{\partial \tilde{u}}{\partial t}(t,x)-\frac{1}{2}\Delta\tilde{u}(t,x)+\sum_{i=1}^{n}\left[\frac{\partial G}{\partial x_i}(x)+l_i(x)\right]\frac{\partial \tilde{u}}{\partial x_i}(t,x)\\
&+\sum_{i=1}^{n}\left[\frac{\partial^2 G(x)}{\partial x_i^2}+\frac{\partial l_i(x)}{\partial x_i}\right]\frac{\partial \tilde{u}}{\partial x_i}(t,x)\\
&-\frac{1}{2}\left[\sum_{i=1}^{n}\left(\frac{\partial^2 G(x)}{\partial x_i^2}+\frac{\partial l_i(x)}{\partial x_i}\right)+\sum_{i=1}^{n}\left(\frac{\partial G}{\partial x_i}(x)+l_i(x)\right)^2\right]\tilde{u}(t,x)\\
&=\frac{\partial \tilde{u}}{\partial t}-\frac{1}{2}\Delta\tilde{u}(t,x)+\sum_{i=1}^{n}\frac{\partial G}{\partial x_i}(x)\frac{\partial u}{\partial x_i}(t,x)+\left(\frac{1}{2}\Delta G(x)-\frac{1}{2}\mid\nabla G\mid^2(x)\right)\tilde{u}(t,x)\\
&+\sum_{i=1}^{n} l_i(x)\frac{\partial \tilde{u}}{\partial x_i}(t,x)+\left[\sum_{i=1}^{n}\frac{1}{2}\frac{\partial l_i}{\partial x_i}(x)-\sum_{i=1}^{n}\frac{\partial G}{\partial x_i}(x)l_i(x)-\frac{1}{2}\sum_{i=1}^{n} l_i(x)^2\right]\tilde{u}(t,x)\\
&=e^{F(x+b(t))+G(x)+\sum_{i=1}^{n} a_i(t)x_i+c(t)}\Bigg\{\sum_{i=1}^{n}\left[(b_i'(t)-a_i(t)+\sum_{j=1}^{m} c_{ji}y_j(t)-l_i(x+b(t))\right]\frac{\partial u}{\partial x_i}(x+b(t))\\
&+\Bigg[\sum_{i=1}^{n}\frac{\partial F}{\partial x_i}(x+b(t))b_i'(t)-\sum_{i=1}^{n} a_i(t)\frac{\partial F}{\partial x_i}(x+b(t))+\sum_{i=1}^{n}\sum_{j=1}^{m} y_j(t)c_{ji}\frac{\partial F}{\partial x_i}(x+b(t))\\
&-\sum_{i=1}^{n}\sum_{j=1}^{m} y_j(t)l_i(x+b(t))c_{ji}+\sum_{i=1}^{n} a_i'(t)x_i+c'(t)-\frac{1}{2}\sum_{i=1}^{n} a_i^2(t)\\
&+\frac{1}{2}\sum_{i=1}^{m}\sum_{j=1}^{m}\sum_{k=1}^{n} c_{ik}c_{jk}y_i(t)y_j(t)\\
&-\frac{1}{2}\Delta F(x+b(t))-\frac{1}{2}\mid\nabla F\mid^2(x+b(t))-\frac{1}{2}\sum_{i=1}^{m} h_i^2(x+b(t))\Bigg]u(t,x+b(t))\\
&+\left[\sum_{i=1}^{n} l_i(x)\frac{\partial F}{\partial x_i}(x+b(t))+\sum_{i=1}^{n} l_i(x)\frac{\partial G}{\partial x_i}(x)+\sum_{i=1}^{n} l_i(x)a_i(t)\right]u(t,x+b(t))
\end{aligned}$$

$$+\sum_{i=1}^{n} l_i(x)\frac{\partial u}{\partial x_i}(t,x+b(t))$$

$$+\left[\sum_{i=1}^{n}\frac{1}{2}\frac{\partial l_i}{\partial x_i}(x)-\sum_{i=1}^{n}\frac{\partial G}{\partial x_i}(x)l_i(x)-\frac{1}{2}\sum_{i=1}^{n} l_i(x)^2\right]u(t,x)\Bigg\}$$

$$=e^{F(x+b(t))+G(x)+\sum_{i=1}^{n}a_i(t)x_i+c(t)}\Bigg\{\sum_{i=1}^{n}\Bigg[(b'_i(t)-a_i(t)+\sum_{j=1}^{m}c_{ji}y_j(t)-l_i(x+b(t))$$

$$+l_i(x)\Bigg]\frac{\partial u}{\partial x_i}(t,x+b(t))$$

$$+\sum_{i=1}^{n}\left[b'_i(t)-a_i(t)+\sum_{j=1}^{m}c_{ji}y_j(t)-l_i(x+b(t))+l_i(x)\right]\frac{\partial F}{\partial x_i}(x+b(t))u(t,x+b(t))$$

$$+\Bigg[-\frac{1}{2}\sum_{i=1}^{n}\frac{\partial^2 F(x+b(t))}{\partial x_i^2}+\frac{1}{2}\sum_{i=1}^{n}\frac{\partial l_i(x+b(t))}{\partial x_i}-\frac{1}{2}\sum_{i=1}^{n}\left(\frac{\partial F(x+b(t))}{\partial x_i}\right)^2$$

$$+\sum_{i=1}^{n} l_i(x+b(t))\frac{\partial F(x+b(t))}{\partial x_i}-\frac{1}{2}\sum_{i=1}^{n} l_i(x+b(t))^2$$

$$-\frac{1}{2}\sum_{i=1}^{m} h_i^2(x+b(t))\Bigg]u(t,x+b(t))$$

$$+\Bigg[-\sum_{i=1}^{n}\sum_{j=1}^{m}y_j(t)l_i(x+b(t))c_{ji}+\sum_{i=1}^{n}a'_i(t)x_i+c'(t)-\frac{1}{2}\sum_{i=1}^{n}a_i^2(t)$$

$$+\frac{1}{2}\sum_{i=1}^{m}\sum_{j=1}^{m}\sum_{k=1}^{n}c_{ik}c_{jk}y_i(t)y_j(t)+\sum_{i=1}^{n} l_i(x)a_i(t)$$

$$-\frac{1}{2}\sum_{i=1}^{n} l_i(x)^2+\frac{1}{2}\sum_{i=1}^{n} l_i(x+b(t))^2\Bigg]u(t,x+b(t))\Bigg\}$$

In view of (3.2a), (3.2b), (3.2c) we have

$$\frac{\partial\tilde{u}}{\partial t}(t,x)-\frac{1}{2}\Delta\tilde{u}(t,x)+\sum_{i=1}^{n}\left[\frac{\partial G}{\partial x_i}(x)+l_i(x)\right]\frac{\partial\tilde{u}}{\partial x_i}(t,x)$$

$$+\sum_{i=1}^{n}\left[\frac{\partial^2 G(x)}{\partial x_i^2}+\frac{\partial l_i(x)}{\partial x_i}\right]\tilde{u}(t,x)$$

$$-\frac{1}{2}\left[\sum_{i=1}^{n}\left(\frac{\partial^2 G(x)}{\partial x_i^2}+\frac{\partial l_i(x)}{\partial x_i}\right)+\sum_{i=1}^{n}\left(\frac{\partial G}{\partial x_i}(x)+l_i(x)\right)^2\right]\tilde{u}(t,x)$$

$$=e^{F(x+b(t))+G(x)+\sum_{i=1}^{n}a_i(t)x_i+c(t)}\Bigg\{\sum_{i=1}^{n}\left[b'_i(t)-a_i(t)+\sum_{j=1}^{m}d_{ji}y_i(t)-\sum_{j=1}^{n}c_ib_j(t)\right]\frac{\partial u}{\partial x_i}(t,x+b(t))$$

$$+\sum_{i=1}^{n}\left[b'_i(t)-a_i(t)+\sum_{j=1}^{m}d_{ji}y_j(t)-\Sigma c_ib_j(t)\right]\frac{\partial F}{\partial x_i}(x+b(t))u(t,x+b(t))$$

$$
\begin{aligned}
&+\frac{1}{2}\Bigg[\sum_{i=1}^{n}\frac{\partial^2\phi(x+b(t))}{\partial x_i^2}+\sum_{i=1}^{n}\frac{\partial l_i(x+b(t))}{\partial x_i}\\
&-\sum_{i=1}^{n}\Big(\frac{\partial\phi}{\partial x_i}(x+b(t))+l_i\Big)^2-\sum_{i=1}^{m}h_i^2(x+b(t))\Bigg]u(t,x+b(t))\\
&+\Bigg[-\sum_{i=1}^{n}\sum_{j=1}^{m}y_j(t)\Big(\sum_{k=1}^{n}d_{ik}(x_k+b_k(t))+d_i\Big)c_{ji}+\sum_{i=1}^{n}a'_i(t)x_i+c'(t)-\frac{1}{2}\sum_{i=1}^{n}a_i^2(t)\\
&+\frac{1}{2}\sum_{i,j=1}^{m}\sum_{k=1}^{n}c_{ik}c_{jk}y_i(t)y_j(t)+\sum_{i=1}^{n}\Big(\sum_{j=1}^{n}d_{ij}x_j+d_i\Big)a_i(t)\\
&-\frac{1}{2}\sum_{i=1}^{n}\Big(\sum_{j=1}^{n}d_{ij}x_j+d_i\Big)^2+\frac{1}{2}\sum_{i=1}^{n}\Big(\sum_{j=1}^{n}d_{ij}(x_j+b_j(t))+d_i\Big)^2\Bigg]u(t,x+b(t))\Bigg\}\\
=\ &e^{F(x+b(t))+G(x)+\sum_{i=1}^{n}a_i(t)x_i+c(t)}\Bigg\{\sum_{i=1}^{n}\Big[b'_i(t)-a_i(t)+\sum_{j=1}^{m}d_{ji}y_i(t)-\sum_{j=1}^{n}c_jb_j(t)\Big]\frac{\partial\tilde{u}}{\partial x_i}(t,x+b(t))\\
&+\sum_{i=1}^{n}\Big[b'_i(t)-a_i(t)+\sum_{j=1}^{m}d_{ji}y_j(t)-\Sigma c_jb_j(t)\Big]\frac{\partial F}{\partial x_i}(x+b(t))u(t,x+b(t))\\
&+\frac{1}{2}\Bigg[\sum_{i=1}^{n}\frac{\partial f_i(x+b(t))}{\partial x_i}-\sum_{i=1}^{n}f_i(x+b(t))^2-\sum_{i=1}^{m}h_i^2(x+b(t))\Bigg]u(t,x+b(t))\\
&+\Bigg[-\sum_{i,k=1}^{n}\Big(\sum_{j=1}^{m}c_{ji}y_j(t)\Big)d_{ik}x_k-\sum_{i=1}^{n}\sum_{j=1}^{m}c_{ji}y_j(t)\Big(\sum_{k=1}^{n}d_{ik}b_k(t)+d_i\Big)\\
&+\sum_{i=1}^{n}a'_i(t)x_i+c'(t)-\frac{1}{2}\sum_{i=1}^{n}a_i^2(t)+\frac{1}{2}\sum_{i,j=1}^{m}\sum_{k=1}^{n}c_{ik}c_{jk}y_i(t)y_j(t)\\
&+\sum_{i=1}^{n}\Big(\sum_{j=1}^{n}d_{ij}x_j\Big)a_i(t)+\sum_{i=1}^{n}d_ia_i(t)\\
&+\sum_{i=1}^{n}\sum_{j,k=1}^{n}d_id_{ik}b_k(t)x_j+\sum_{i=1}^{n}\sum_{j=1}^{n}dd_{ij}b_j(t)+\frac{1}{2}\sum_{i=1}^{n}\Big[\sum_{j=1}^{n}d_jb_j(t)\Big]^2\Bigg]u(t,x+b(t))\Bigg\}.
\end{aligned}
$$

From (3.2d), we get

$$
\begin{aligned}
&\frac{1}{2}\Bigg[\sum_{i=1}^{n}\frac{\partial f_i(x+b(t))}{\partial x_i}-\sum_{i=1}^{n}f_i(x+b(t))^2-\sum_{i=1}^{m}h_i^2(x+b(t))\Bigg]\\
=\ &\sum_{i,j=1}^{n}e_{ij}(x_i+b_i(t))(x_j+b_j(t))+\sum_{i=1}^{n}e_i(x_i+b_i(t))+e\\
=\ &\sum_{i,j=1}^{n}e_{ij}x_ix_j+\sum_{i=1}^{n}e_ix_i+e+\sum_{i,j=1}^{n}e_{ij}x_jb_j(t)+\sum_{i,j=1}^{n}e_{ij}b_i(t)x_j\\
&+\sum_{i=1}^{n}e_ib_i(t)+\sum_{i,j=1}^{n}e_{ij}b_i(t)b_j(t)
\end{aligned}
$$

and hence

$$\frac{\partial \tilde{u}}{\partial t}(t,x) - \frac{1}{2}\Delta \tilde{u}(t,x) + \sum_{i=1}^{n}\left[\frac{\partial G}{\partial x_i}(x) + l_i(x)\right]\frac{\partial \tilde{u}}{\partial x_i}(t,x)$$
$$+ \sum_{i=1}^{n}\left[\frac{\partial^2 G(x)}{\partial x_i^2} + \frac{\partial l_i(x)}{\partial x_i}\right]\tilde{u}(t,x)$$
$$- \frac{1}{2}\left[\sum_{i=1}^{n}\left(\frac{\partial^2 G(x)}{\partial x_i^2} + \frac{\partial l_i(x)}{\partial x_i}\right) + \sum_{i=1}^{n}\left(\frac{\partial G}{\partial x_i} + l_i(x)\right)^2\right]\tilde{u}(t,x)$$
$$= e^{F(x+b(t))+G(x)+\sum_{i=1}^{n} a_i(t)x_i+c(t)}\left\{\sum_{i=1}^{n}\left[b'_i(t) - a_i(t) + \sum_{j=1}^{m} d_{ji}y_j(t) - \sum_{j=1}^{n} c_{ij}b_j(t)\right]\frac{\partial \tilde{u}}{\partial x_i}(t,x+b(t))\right.$$
$$+ \sum_{i=1}^{n}\left[b'_i(t) - a_i(t) + \sum_{j=1}^{m} d_{ji}y_j(t) - \sum_{j=1}^{n} c_{ij}b_j(t)\right]\frac{\partial F}{\partial x_i}(x+b(t))u(t,x+b(t))$$
$$+ \left[\sum_{i,j=1}^{n} e_{ij}x_ix_j + \sum_{i=1}^{n} e_ix_i + e + \sum_{i,j=1}^{n} e_{ij}x_jb_j(t) + \sum_{i,j=1}^{n} e_ib_i(t)x_j\right.$$
$$\left. + \sum_{i=1}^{n} e_ib_i(t) + \sum_{i,j=1}^{n} e_{ij}b_i(t)b_j(t)\right]u(t,x+b(t))$$
$$+ \left[-\sum_{i,k=1}^{n}\left(\sum_{j=1}^{m} c_{ji}y_j(t)\right)d_{ik}x_k - \sum_{i=1}^{n}\sum_{j=1}^{m} c_{ji}y_j(t)\left(\sum_{k=1}^{n} d_{ik}b_k(t) + d_i\right)\right.$$
$$+ \sum_{i=1}^{n} a'_i(t)x_i + c'(t) - \frac{1}{2}\sum_{i=1}^{n} a_i^2(t) + \frac{1}{2}\sum_{i,j=1}^{m}\sum_{k=1}^{n} c_{ik}c_{jk}y_i(t)y_j(t)$$
$$+ \sum_{i=1}^{n}\left(\sum_{j=1}^{n} d_{ij}x_j\right)a_i(t) + \sum_{i=1}^{n} d_i a_i(t)$$
$$\left. + \sum_{i=1}^{n}\sum_{j,k=1}^{n} d_id_{ik}b_k(t)x_j + \sum_{i=1}^{n}\sum_{j=1}^{n} d_id_{ij}b_j(t) + \frac{1}{2}\sum_{i=1}^{n}\left(\sum_{j=1}^{n} d_ib_j(t)\right)^2\right]u(t,x+b(t))\Bigg\}$$
$$= e^{F(x+b(t))+G(x)+\sum_{i=1}^{n} a_i(t)x_i+c(t)}\left\{\sum_{i=1}^{n}\left[b'_i(t) - a_i(t) + \sum_{j=1}^{m} d_{ji}y_j(t) - \sum_{j=1}^{n} c_{ij}b_j(t)\right]\frac{\partial \tilde{u}}{\partial x_i}(t,x+b(t))\right.$$
$$+ \sum_{i=1}^{n}\left[b'_i(t) - a_i(t) + \sum_{j=1}^{m} d_{ji}y_j(t) - \sum_{j=1}^{n} c_{ij}b_j(t)\right]\frac{\partial F}{\partial x_i}(x+b(t))u(t,x+b(t))$$
$$+ \left[\sum_{i,j=1}^{n} e_{ij}x_ix_j + \sum_{i=1}^{n} e_ix_i + e - \sum_{i=1}^{n}\sum_{k=1}^{n}\left(\sum_{j=1}^{m} c_{jk}y_j(t)\right)d_{ki}x_i\right.$$
$$+ \sum_{i=1}^{n}\sum_{j=1}^{n} e_{ij}b_j(t)x_i + \sum_{i=1}^{n}\sum_{j=1}^{n} e_jb_j(t)x_i + \sum_{i=1}^{n} a'_i(t)x_i$$
$$\left. + \sum_{i=1}^{n}\sum_{j=1}^{n} a_j(t)d_{ji}x_i + \sum_{i=1}^{n}\sum_{j,k=1}^{n} d_jd_{ji}b_k(t)x_i\right]u(t,x+b(t))$$
$$+ \left[-\sum_{i=1}^{n}\sum_{j=1}^{m} c_{ji}y_j(t)\left(\sum_{k=1}^{n} d_{ik}b_k(t) + d_i\right) + \sum_{i=1}^{n} e_ib_i(t) + \sum_{i,j=1}^{n} e_{ij}b_i(t)b_j(t) + c'(t)\right.$$
$$\left. - \frac{1}{2}\sum_{i=1}^{n} a_i^2(t) + \frac{1}{2}\sum_{i,j=1}^{m}\sum_{k=1}^{n} c_{ik}c_{jk}y_i(t)y_j(t) + \sum_{i=1}^{n} d_i a_i(t)\right.$$

$$+\sum_{i=1}^{n}\sum_{j=1}^{n} d_i d_j b_j(t) + \frac{1}{2}\sum_{i=1}^{n}\Big(\sum_{j=1}^{n} d_i b_j(t)\Big)^2\Big] u(t, x + b(t))\Big\}.$$

In view of (3.3), (3.6), (3.7) and (3.8), we have

$$\frac{\partial \tilde{u}}{\partial t}(t,x) - \frac{1}{2}\Delta \tilde{u}(t,x) + \sum_{i=1}^{n}\Big[\frac{\partial G}{\partial x_i}(x) + l_i(x)\Big]\frac{\partial \tilde{u}}{\partial x_i}(t,x)$$
$$+\sum_{i=1}^{n}\Big[\frac{\partial^2 G(x)}{\partial x_i^2} + \frac{\partial l_i(x)}{\partial x_i}\Big]\tilde{u}(t,x)$$
$$= e^{F(x+b(t))+G(x)+\sum_{i=1}^{n} a_i(t)x_i + c(t)} + \frac{1}{2}\Big[\sum_{i=1}^{n}\Big(\frac{\partial^2 G(x)}{\partial x_i^2} + \frac{\partial l_i(x)}{\partial x_i}\Big) + \sum_{i=1}^{n}\Big(\frac{\partial G}{\partial x_i}(x) + l_i(x)\Big)^2$$
$$+ 2\Big(\sum_{i,j=1}^{n} e_{ij}x_i x_j + \sum_{i=1}^{n} e_i x_i + e\Big)\Big] u(t,x),$$

or equally

$$\frac{\partial \tilde{u}}{\partial t}(t,x) = \frac{1}{2}\Delta \tilde{u}(t,x) - \sum_{i=1}^{n}\Big(\frac{\partial^2 G}{\partial x_i^2}(x) + l_i(x)\Big)\frac{\partial \tilde{u}}{\partial x_i}(t,x)$$
$$-\sum_{i=1}^{n}\Big(\frac{\partial^2 G(x)}{\partial x_i^2} + \frac{\partial l_i(x)}{\partial x_i}\Big)\tilde{u}(t,x) + d\,\tilde{u}(t,x)$$

which is a Kolmogorov equation.

REFERENCES

(1) Benes, V.: Exact finite dimensional filters for certain diffusions with nonlinear drift, *Stochastic*, 5: 65-72, 1981.

(2) Brockett, R. W.: Nonlinear systems and nonlinear estimation theory, in *The Mathematics of Filtering and Identification Applications*, M. Hazewinkel and J. S. Williems, eds., Reidel, Dordrecht, The Netherlands, 1981.

(3) Brockett R. W. and Clark, J. M. C.: The geometry of the conditional density functions, in *Analysis and Optimization of Stochastic Systems*, O. L. R. Jacobs, et. al. eds., Academic Press, New York, 1979.

(4) Chen, J., Leung C. -W. and Yau, S. S. -T.: Finite dimensional Filters with nonlinear drift VI: Classification of finite dimensional estimation algebras of maximal rank with state space dimension 3, *SIAM J. Control and Optimization*, to appear.

(5) Chen, J., Leung C. -W. and Yau, S. S. -T.: Finite dimensional Filters with nonlinear drift VIII: Classification of finite dimensional estimation algebras of maximal rank with state space dimension 4, (preprint), 1993.

(6) Chiou, W. -L.: Some results on estimation algebras on classification of finite - dimensional estimation algebras, *Systems Control Letters*, Vol. 28: 55-63, 1996.

(7) Chiou, W. -L. and Yau, S. S. -T.: Finite dimensioonal filters with nonlinear drift II: Brockett's problem on classification of finite - dimensional estimation algebras, *SIAM J. Control and Optimization*, Vol. 32, No. 1: 297-310, January 1994.

(8) Davis, M. H. A.: On a Multiplicative functional transformation arising in nonlinear filtering theory, *Z. Wahrsch. Verw. Gebiete*, 54: 125-139, 1980

(9) Dong, R. T., Tam, L. F., Wong, W. S. and Yau, S. S. -T.: Structure and classification theorems of finite dimensional exact estimation algebras, *SIAM J. Control and Optimization*, Vol 29, No. 4: 866-877, 1991.

(10) Mitter, S. K.: On the analogy between mathematical problems of nonlinear filtering and quantum physics, *Richerche di Automatica*, 10 (2): 163-216,

1979.

(11) Tam, L. F., Wong, W. S. and Yau, S. S. -T.: On a necessary and and sufficient condition for finite dimensionality of estimation algebras, *SIAM J. Control and Optimization*, Vol. 28, No. 1: 173-185, 1990.

(12) Yau, S. S. -T.: Finite dimensional filters with nonlinear drift I: A class of filters including both Kalman - Bucy filters and Benes filters, *Journal of Mathematical Systems, Estimation, and Control*, Vol 4, No. 2: 181-203, 1994.

(13) Yau, S. -T. and Yau, S. S. -T.: Finite dimensional filters with nonlinear drift III: explicit solution to Kolmogorov equation in nonlinear filtering problem. (preprint)

(14) Yau, S. -T. and Yau, S. S. -T.: Finite dimensional filters with nonlinear drift V: Duncan - Mortensen - Zaikai equation with arbitrary initial condition for Kalman - Bucy filtering and Benes filtering system. (preprint)

(15) Zakai, M.: On the optimal filtering of diffusion processes, *Z. Wahrsch. Verw. Gibe.*, 11: 230-243, 1969.

85年 9月20日 收稿
86年11月18日 修正
86年12月 4日 接受

在非線性過濾理論上的一個結果

邱文齡
輔仁大學數學系

摘　要

在本篇論文中，我們考慮 Yau 的過濾系統，我們得到 Duncan-Mortensen-Zakai 等式直接的明顯解，其中其起始條件是任給的，而其狀態空間維度是任意有限維的。這個解的獲得是解一組常微分方程等式與解一 Kolmogorov 型等式。從 DMZ 等式可構造出有限維的遞迴過濾，這是有別於用用估計代數來求得有限維遞迴過濾。在 Yau 的過濾系統中，目前最一般的假設是在當狀態空間維度小於或等於 4 的情況下，若估計代數具有最大秩則可構造出有限維的遞迴過濾；而我們所考慮的 Yau 過濾系統，沒有最大秩的限制，而其狀態空間維度是任意有限維的，所以以目前爲止，我們所得的 Duncan-Mortensen-Zakai 等式解是最一般化的。

關鍵詞： Duncan-Mortensen-Zakai 等式，遞迴過濾，Kolmogorov 型等式。

ABSTRACTS OF PAPERS BY FACULTY MEMBERS OF THE COLLEGE OF SCIENCE AND ENGINEERING THAT APPEARED IN THE 1996 ACADEMIC YEAR

蘇菲亞·可巴雷斯卡亞的世界（上）（下）簡介

顏 一 清

第 76 卷；第 43-50 頁（1995） 第 77 卷；第 47-54 頁（1996）

蘇菲亞·可巴雷斯卡亞是一位十九世紀的俄羅斯女子。當時的蘇俄女子不能受高等教育，她以假結婚的方式出國赴德國求學來衝破這個限制。當柏林大學不收留她時，她便請求名數學家威爾斯特勒斯私下指導她，而終於獲得哥丁根大學的博士學位。但她得面對失業的打擊。過後因學長雷富勒的多方奔走，她在斯特克赫爾姆（Stock-holm）大學取得教職。由於她的才調與努力後的優異表現，她被稱爲廿世紀前最傑出的女數學家。

A Note on Estimation Algebras on Nonlinear Filtering Theory

WEN-LIN CHIOU（邱文齡）

Systems Control Letters, **28**, 55-63 (1996)

The idea of using estimation algebras to construct finite dimensional nonlinear filters was first proposed by Brockett and Mitter independently. It turns out that the concept of estimation algebra plays a crucial role in the investigation of finite dimensional nonlinear filters. In his talk at the International Congress of Mathematicians in 1983. Brockett proposed to classify all finite dimensional estimation algebras. In this paper we consider some filtering systems. In a special filtering system: (1) We have some structure results. (2) For any arbitrary finite dimensional state space, under the condition that the drift term is a linear vector field plus a

gradient vector field, we classify all finite dimensional estimation algebras with maximal rank. (3) We classify all finite dimensional estimation algebras with maximal rank if the dimension of the state space is less than or equal to three. A more general filtering system is considered. The above three results can be 'used' locally. Therefore from the algebraic point of view, we have now understood generically some finite dimensional filters.

Thermal and Magnetic Studies of Nanocrystalline Ni

Y.D. YAO, Y.Y. CHEN, C.M. HSU, H.M. LIN, M. TAI, K.T. WU (吳坤東) AND C.T. SUO

NanoStructured Mater., **6**, 933 (1995)

Ultra-fine Ni particles with average particle sizes from 12 to 100 nm were prepared by the evaporation technique. The calorimetric effects of nanocrystalline Ni as well as the NiO and Ni bulk samples were measured between 300 and 800 K. Both an exothermal effect between 380 and 480 K and an endothermal peak near 560 K were observed for ultrafine Ni; only endothermal peak was observed for both NiO near 520 K and bulk Ni near 630 K. A shifted magnetic hysteresis loop and a slope change in saturation magnetization were observed below roughly 50 K for ultra-fine Ni particles with average particle sizes roughly below 50 nm. This is explained by the effect of exchange anisotropy interaction between the interfaces of the ferromagnetic region and the layers of antiferromagnetic NiO on the surface of the nanocrystalline Ni particles.

Optical and Magnetic Studies of SmCo and SmFe Films

K.T. WU (吳坤東), Y.D. YAO AND T.C. CHEN

J. Applied Physics, **79**, 6341 (1996)

Permanent magnetic materials based on iron, cobalt, and rare earths have been extensively studied during the past years. It is very interesting to study the physical

properties of film type permanent magnet materials. In this investigation, we report the optical and magnetic properties of SmCo, SmFe. Sm. Co, and Fe films as well as the comparison of the electrical resistivity and magnetization behaviors between these films. The optical transmittance and reflectance have been measured as functions of the wavelength and the thickness for all the films with thickness less than 2000 Å. The electrical resistivity and magnetization have been measured below room temperature. The slope of electrical resistivity is decreased with decreasing the thickness of the films. The films are transparent with thickness less than 800 Å for magnetic films. For films with thickness at 200 Å, the values of the transmittance are 50, 48, 38, 18, and 14 for Sm, SmCo, SmFe, Co, and Fe, respectively. This is explained due to the difference of the magnetic permeability of all the films. The oscillatory behaviors of reflection for all the films are qualitatively consistent with that of the theoretical predict for an absorbing surface. Up to now, the best magnetic properties for magnetic films at room temperature are with an intrinsic coercivity of 1450 Oe and an energy product of 4.5 MGOe.

Study of the optical properties of $In_{0.52}$ $(Al_xGa_{1-x})_{0.48}As$ by variable angle spectroscopic ellipsometry

J.-W. PAN, J.-L. SHIEH, J.-H. GAU, J.-I. CHYI, J.-C. LEE AND K.-J. LING (凌國基)

J. Appl. Phys. **78**, (1), 1 July 1995

The optical properties of $In_{0.52}$ $(Al_xGa_{1-x})_{0.48}As$ epilayers with various x values were systematically studied using variable angle spectroscopic ellipsometry in the wavelength range of 310-1700 nm. The refractive indexes were determined and could be given as $n(x) = 0.12x^2 - 0.51x + 3.6$ at the wavelength of 1.55 μm. The measured thickness of the epilayers agrees within 5.2% of the nominal thickness. The energies and broadening parameters of the E_1 and $E_1 + \Delta_1$ transitions as a function of Al composition were also examined based on the second-derivative spectra of the dielectric function. The comparison between the results and the reportted data is presented. ◎ 1995 American Institute of Physics.

Study of The Degree of Disorder in Optical Glasses

CHEN-KE SHU, CHIEN-CHIH KAO AND LUU-GEN HWA (華魯根)

Proceeding of Annual conference of the chinese Society for Material Science,
VoL. I, P. 547、548. Oct 1996

The degree of disorder in glassy materials was investigated by low frequency inelastic light scatterings. The characteristic length scale (structural correlation length) was determined with the aid of Martin-Brenig model from the position of the low frequency Raman peak and the sound velocity measurements. The value of the structural correlation length manifests itself as the measure of the degree of disorder in the glass structure. Some discrepancies of the Martin-Brenig model will be discussed in terms of our experimental results.

The Structural Investigation of a ZBLAN Glass by Vibrational Spectroscopy

LUU-GEN HWA (華魯根) AND CHEN-KE SHU

Chinese Journal of Physics, VoL. 34, No. 5 (1996)

The heavy metal fluoride glasses exhibit high transparency over the frequency range form the mid-IR to the near UV. They also possess low refractive index, low material dispersion, low linear scattering loss, and good chemical durability. These properties make them the promising candidate for a wide variety of applications ranging form laser windows to infrared fiber optics. The structural investigations of a typical heavy metal fluoride glass, ZBLAN, by vibrational spectroscopy (multi-phonon edge absorption, infrared reflectivity and polarized Raman scattering measurements) were performed. From our study, we are able to understand the fundamental vibrational characteristics of this glass and the primary mechanisms influencing its infrared transparency. The LOTO vibrational pair splitting was observed for this glass by IR reflectivity measurement at different incident angle. We believe that this type of crystal-like behavior is related to frozen in density and concentration fluctuations in the glass structure during the glass formation. The low

frequency Raman spectrum ($10 \sim 100\ cm^{-1}$) -the so called Boson Peak-was also studied for the same glass. The characteristic length scale (Structural Correlation Length) was calculated with the aid of Martin-Brenig model. The degree of disorder in the glass structure will be discussed in the light of the existing theory.

The Synthesis and Chemistry of 9-Chlorobicyclo [6.1.0] non-1 (9) -ene

GON-ANN LEE (李國安), JAY CHEN, CHAUR-SHENQ SHIAU AND CHIH-HWA CHERNG

Journal of the Chinese Chemical Sociery, **43**, 297-300 (1996)

9-Chlorobicyclo [6.1.0] non-1 (9) -ene (**4**), a 2-chlorinated 1, 3-fused cyclopropene, is synthesized and isolated from the dehalogenation of the 1-bromo-9, 9-dichlorobicyclo [6.1.0] nonane, itself derived from cyclooctene. Compound **4** undergoes ring opening reaction to generate cycloocteny chlorocarbene (**9**) which reacts with water via conjugate addition and ipso-addition to give (**E**) -2- (chloromethylene) cyclooctanol (**7**) and cyclooctene-1-carboxaldehyde (**8**), respectively. The conjugated addition of **9** with water is more favorable than the ipso-addition by 3: 1. Compound **4**, which is stable at-25℃ for weeks without any decomposition, reacts with oxygen to produce 2-chlorocyclonon-enone (**12**) via the ring-opening reaction adduct, vinyl alkylcarbene **10**.

Stereoselective synthesis and Diels-Alder Reaction of (*Z*) -and (*E*) -1, 2-Bis (phenylthio) -1, 3-butadiene

SHANG-SHING P. CHOU (周善行), DER-JEN SUN, AND HAI-PING TAI

Journal of the Chinese Chemical Society, **42**, 809-814 (1995)

Bromination of 3-phenylthio-2-sulfolene (**2**) with *N*-bromosuccinimide gave 2-bromo-3-phenylthio-2-sulfolene (**3**) which was converted mainly to 2, 3-bis (phenylthio) -2-sulfolene (**4**) by treatment with sodium phenylthiolate. Thermal

desulfonylation of **4** at different temperatures in the presence of a base (DBU) yielded stereoselectively the (*Z*) -and- (*E*) -1, 2-bis (phenylthio) -1, 3-butadiene (**6**). These two geometric isomers could be thermally interconverted. The Diels-Alder reactions of **6** were also investigated. Only the (*Z*) -diene **6a** could undergo the Diels-Alder reaction; the (*E*) -diene **6b** was *in situ* converted to the *Z* isomer before undergoing the Diels-Alder reaction. The reaction of **6a** with *N*-phenylmaleimide gave the cycloaddition product **7** with complete *endo* selectivity, but under daylight or during chromatography it readily underwent a thioallylic rearrangement to yield **8** with inversion of configuration. The cycloaddition of **6a** with methyl acrylate proceeded regiospecifically, but generating a mixture of *endo* and *exo* isomers. The *endo*/*exo* ratio could be increased by using $ZnCl_2$ as the catalyst.

Regio-and Stereocontrolled Synthesis and Diels-Alder Reactions of (Z) -2- (Phenylthio) -1- (trimethylsilyl) -1, 3-butadiene

SHANG-SHING P. CHOU (周善行) AND MAO-HSUN CHAO

Tetrahedron Letters, Vol. 36, No. 48, pp. 8825-8828 (1995)

The title compound was synthesized from its 3-sulfolene precursor 2- (trimethylsilyl) -3- (phenylthio) -3-sulfolene, and the Diels-Alder reactions of the diene were studied.

Synthesis and Applications of 3-Phenylthio-2-sulfolenes

SHANG-SHING P. CHOU (周善行) AND MAO-HSUN CHAO

Journal of the Chinese Chemical Society, **43**, 53-59 (1996)

Treatment of 3-phenylthio-2-sulfolene (**1**) with an equimolar proportion of butyllithium at-78℃ in THF followed by addition of an electrophile gave the 2-substituted 3-phenylthio-2-sulfolenes (**2**). The deprotonation was found to proceed only at the vinylic C-2 position. Some of the 2-sulfolenes **2** underwent desulfonylation

upon heating with base. Of particular interest was the conversion of 3-phenylthio-2-trimethylsilyl-2-sulfolene (**2h**) to its 3-sulfolene isomer **6** by sequential addition of butyllithium and salicylic acid at low temperatures. The 3-sulfolene **6** was desulfony lated by Kugelrohr distillation at 150℃ under vacuum to give (*Z*) -2-phenylthio-1-trimehtylsily-1, 3-butadiene (**8**). The regiochemistry of the Diels Alder reaction of this highly reactive diene **8** was found to be controlled by the phenylthio group, and the stereochemistry is *endo* addition. Diene **8** was oxidized to its sulfone derivative **12** which also underwent a stereospecific Diels-Alder reaction.

Electronic and Solvent Relaxation Dynamics of a Photoexcited Aqueous Halide

WEN-SHYAN SHEU (許文賢) AND PETER J. ROSSKY

Reprinted from The Journal of Physical Chemistry, 1996, 100, p1295

The details of the electronic and solvent relaxation dynamics following two-photon excitation of an aqueous halide ion are studied via nonadiabatic quantum molecular dynamics simulation. It is found that the branching ratio at very early times (<50 fs) between two channels, a minor channel involving direct electron detachment to a spatially separated solvent void and a dominant channel characterized by delayed adiabatic detachment following a cascade through excited electronic states of the ion, is determined by the effect of solvent dynamics on the values of the ionic and void electronic energies, as well as the relative small matrix elements for tunneling into void states. Solvent dynamics is also found to be important in controlling the rate of electron transfer whic leads to geminate recombination of proximal electron-halogen atom pairs. The sensitivity of this recombination rate to the relative energy levels of the unoccupied valence electron hole on the solvated halogen and that of the hydrated electron is indicated as the origin of the strong variation in the experimentally observed yield of diffusively free solvated electrons with halide species. In the case of delayed detachment, the symmetry characteristics of the one-electron state of the detaching electron are indicated as critical in facilitating the process; detachment is observed to

occur only once the predominantly s-like lowest charge transfer to solvent (CTTS) ionic excited state is reached, and then the onset of separation is essentially immediate. A favorable solvent fluctuation in the vicinity of the site of detachment also precedes the onset of separation. Further experiments are suggested to clarify remaining differences between these conclusions and published interpretations of experimentally observed very early time relaxation dynamics of the CTTS states.

P-C Bond Cleavage in Platinum Complexes Containing Bis(diphenylphosphino)methane Promoted with a Phase-transfer Catalyst

IVAN J. B. LIN (林志彪), H. I. SHEN, AND DA-FA FENG

Journal of the Chinese Chemical Society, **42**, 783-790 (1995)

With a phase-transfer catalyst, Pt-dppm (dppm = $Ph_2PCH_2PPh_2$) complexes undergo basic hydrolysis, in which a dppm ligand is hydrolyzed to produce PPh_2Me and PPh_2OH (or PPh_2O^-). The ease of this hydrolysis reaction depends partly on the molecular charges of the metal complexes. Hydrolysis of neutral [Pt(dppm)(L-L)](L-L = S_2CO^{2-}, $S_2P(O)(OEt)^{2-}$ and mnt = $S_2C_2(CN)_2^{2-}$) is slower than that of monocationic [Pt(dppm)(L'-L')] Cl (L'-L' = S_2CNEt_2, $(CH_2)_2S(O)Me$ and acetylacetonate) compounds. Among the neutral compounds, hydrolysis of [Pt(dppm)(mnt)] is more rapid than that of the other two. These results are rationalized according to the ease with whic partial positive charges are induced on the dppm phosphorus atoms. The steric effect due to ligands trans to dppm also influences the rate of hydrolysis of Pt-dppm compounds. When trans ligands are $Ph_2P(CH_2)_2PPh_2$, $Ph_2P(CH_2)_3PPh_2$ and $(Ph_2PO_2)H$, no hydrolysis of dppm occurs. Hydrolysis of Pt-dppm compounds depends further on the concentrations of both the phase-transfer catalyst and OH^- ions. All these results are consistent with nucleophilic attack of OH^- on dppm phosphorus atoms to release strain in the Pt-dppm ring.

Study of Au (I) -polypyrrole Interaction

JONG-RAU, JENG-CHENG LEE, AND SHOW-CHUEN CHEN (陳壽椿)

Synthetic Metals, **79**, 69-74 (1996)

Metal-deposited polypyrrole (Ppy) exhibiting traits of enhanced conductivities and catalysis has aroused interest in the investigation of metal-Ppy interaction. Recently, a Ppy-based NO_x-sensor was found to be interfered by metal ions such as Ag (I), Cu (II) and Pb (II), hinting at a strong interaction between cations and Ppy. Au (I) was chosen for study because of its possible stronger affinity to Ppy. Results from NMR, cyclic coltammetry (CV) and scanning electron microscopy (SEM) /energy-dispersive spectroscopy (EDS) study suggested the existence of the Au (I) -Ppy complex.

Synthesis and X-ray Studies of Noncentrosymmetric Merocyanine Dyes－A Series of Organic NLO Crystals

WIN-LONG CHIA (賈文隆), CHUN-NAN CHEN AND HUEY-JIUAN SHEU

Materials Research Bulletin, Vol. 30, No ll. pp. 1421-1430 (1995)

A series of 3-methyl-4- (p'-substituted styryl) pyridine methiodides were readily synthesized under mild condition with excellent yields. The 3-methyl group was expected to direct the molecular packing within the crystalline unit cell. X-ray diffraction analysis of 3-methyl-4-styrylpyridine methiodide crystal clearly showed that this compound was packed in a noncentrosymmetric way about 50 degrees with respect to the cvystal polar axis, and proved that the 3-methyl group on pyridine ring did change the molecular packing from centrosymmetric orientation to noncentrosymmetric orientation. However, all other compounds we investigated in this paper were found crystallized centrosymmetrically.

Styrene Maleimide Copolymer with Stable Second-Order Optical Nonlinearity

PO-HOU SUNG (宋博厚), CHUNG-YUNG CHEN, SHIN-YU WU AND JUNG Y. HUANG

J. Polym. Sci., Polym. Chem. Ed., **34**, 2189-2194 (1996)

Radical copolymerization of *N*- (azo dye) maleimide of *N*- (substituted phenyl) maleimide and styrene were carried out using 2, 2'-azobis-isobutyronitrile as an initiator in THF at 60℃. These copolymers exhibit high solubility in most of the organic solvents and excellent thermal stability up to 280℃ under nitrogen atmosphere. The copolymer films which were heated at 200-240℃ under high corona field exhibit d_{33}= 3-5 pm/V, in the Maker-fringe measurement. Experimental results also showed that the copolymer with azo dye as chromophore did not decay in second harmonic response even at 130℃.

Sol-Gel Process of Non-Linear Optical Silica Films with Organic Chromophore as Side Chain

PO-HOU SUNG (宋博厚), SHAO-LING WU AND, CHIEN-YANG LIN

J. Mater. Sci., **31**, 2443-2446 (1996)

A transparent silica film with organic chromophore, Disperse Red 1 (DR1), as side chain was prepared in this study by the sol-gel process. Next, the film was baked at 120℃ with corona discharge poling. The resulting films exhibited a second harmonic response, d_{33} = 46 pm/V. High poling stability was observed when the film was maintained at 60℃. The effects of HCl concentration on the molecular orientation and the thermal stability of the specimens were also investigated.

Improvement of Chemistry Courses for Non-Chemistry Major Undergraduates

SHANG-SHING P. CHOU (周善行) AND GON-ANN LEE (李國安)

中華民國八十五年第五十四卷第二期

This paper reports on the different chemistry courses offered to non-chemistry major undergraduates in our university. These courses include *general chemistry* for Department of Physics and Department of Biology, *organic chemistry* for Department of Biology and Department of Food Science and Nutrition, *analytical chemistry* for Department of Food Science and Nutrition, as well as *chemistry and life* (general education course) for college of Science and Engineering and College of Foreign Languages and Literatures. The aims and contents of these courses, teaching methods, and student performance are studied by interviewing with the department heads and teachers, and conducting questionaires with students who have undertaken or are taking these courses.

We found that most of the department heads do not have strong opinions about the exact course contents, but are very concerned about the reactions of the students to the course. The students are much interested in topics which are more related to the everyday life and to their own disciplines. The teachers feel in general that the credit hours are not enough, and the students are not very interested in these courses. The latter situation is especially serious for *general chemistry* which all students have learned in high school. We suggest that the teachers should emphasize more on the relationship of chemistry with daily life, and on subjects which the students may find greater difficulty. As to *organic chemistry* and *analytical chemistry*, the teachers should teach the most fundamental principles, and put emphasis on special topics which are more important for their future studies. The students who take the *chemistry and life* general education course have more diversed background and different motivation. The teachers should find their common interest and relate more to the impact of chemistry on the environment and society. For all these courses the teachers should continue to improve the teaching methodology and to motivate the student.

Molecular Actions of local Anesthetics in Pig Brain and Spinal Cord

S. F. CHIEN, F. S. YEN AND C. P. CHANG (張鎮平), AND C. T. LIN

J. Phys. Chem. **99**, 17442-17448 (1995)

Photophysical properties of dibucaine·HCl (DH^+, a representative local anesthetic drug) in different regions of pig brain and spinal cord were investigated by emission/excitation spectroscopy. At 77 K, the observed fluorescence band, maximum at 360 nm, and phosphorescence vibronic structures at 450, 485, and 520 nm indicate that the drug action species in the nervous system is a neutral dibucaine (D) located at an action site having a polar environment. The DH^+ anesthetic drug deprotonates at the plasma membrane surface, and then the resultant D species partitions into the interaction site of the nervous system. At room temperature, it was surprising to observe a strong intramolecular charge-transfer (ICT) band at 432 nm in addition to the normal fluorescence band at 390 nm. The ICT band originates from the N of the tertiary amine group to the quinoline analog of neutral dibucaine. When the selective sections of the drug-soaked spinal cord (i.e., central canal/gray matter, white matter, and surface plasma membrane) were examined separately, the neutral dibucaine species was identified to embed in a hydrophobic environment of the white and gray matter regions. These results could shed some light on the local anesthetic action mechanisms at the molecular level. The following possible local anesthetic drug actions in pig brain and spinal cord are discussed: (1) the drug transport mechanisms due to the dynamic processes of deprotonation-reprotonation (D/DH^+) in dibucaines, (2) the effects of the ICT nature of the drugs on the generation of electrical signaling in nerve cells and the adsorption and delivery of drugs across nerve membranes, and (3) the interference of releasing, receptor binding, and removal of neurotransmitters by the drug partition of D/DH^+ into the nervous system.

7-Azaindole-Assisted Lactam-Lactim Tautomerization via Excited-State Double Proton Transfer

PI-TAI CHOU, CHING-YEN WEI, CHEN-PIN CHANG (張鎮平) AND CHIENG-HWA CHIU

J. Am. Chem. Soc., **117**, 7259-7260 (1995)

The photophysics of 7-azaindole (7AI) have been studied extensively since Taylor et al. first reported the excited state double proton transfer (ESDPT) in the 7AI dimer. The current topic of ESDPT in a variety of 7AI hydrogen-bonded complexes has important applications for probing both solvation dynamics and biological systems. The ESDPT reaction in 7AI hydrogen-bonded systems can be classified into two categories. The acid, alcohol, and water assisted ESDPT in 7AI can be specified as a catalytic process since the molecular structure of the guest species (e. g., acetic acid in the acetic acid/7AI complex) remains unchanged (Figure la). On the other hand, adiabatic ESDPT in the 7AI dimer results in a $7AI^{T*}/7AI^{T}$ form (Figure lb) consisting of an excited and an unexcited proton-transfer tautomer (* represents the excited state). Since both host and guest molecules change their structures, the ESDPT is a noncatalytic process in which 7AI in the dimeric form acts not as a catalyst but rather as a reactant. The latter case is important from a chemistry perspective. In the acetic acid catalyzed ESDPT reaction, the $7AI^{*} \rightarrow 7AI^{T*}$ tautomerization has been estimated to be ~ 13 kcal/mol exothermic. Since the noncatalytic type of ESDPT requires simultaneous tautomerization for both 7AI and its guest molecule, this process, from the energy viewpoint, provides ~ 13 kcal/mol excess.

Structure and Thermodynamics of 7-Azaindole Hydrogen-Bonded Complexes

PI-TAI CHOU, CHING-YEN WEI, CHEN-PIN CHANG (張鎮平) AND KUO MENG-SHIN

J. Phys. Chem., **99**, 11994-12000 (1995)

The thermodynamics of a variety of 7-azaindole (7AI) hydrogen-bonded complexes in the ground state have been studied on the basis of absorption spectroscopy

in combination with *ab initio* calculations at 6-31G* level. The results indicate that the strength of hydrogen bonding significantly affects the ground-state electronic configuration of 7AI in both normal and tautomer forms. The enthalpy, $\triangle H$, of the association reactions was calculated to be -14.2, -11.3, and -9.2 kcal/mol for the 1:1 acetic acid/7AI complex, 7AI dimer, and methanol/7AI complex, respectively. These values are in fair agreement with the experimental results of -12.3, -9.5, and -6.3 kcal/mol. Calculations also show a stronger hydrogen-bonding effect in the tautomer complex forms than in their respective normal forms. Relative energy levels of excited-state double proton transfer are discussed on the basis of gorund-state thermodynamics in combination with the spectroscopic data.

Synthesis and Spectroscopic Studies of 4-Formyl-4'-*N*, *N*-Dimethylamino-1, 1'-Biphenyl: The Unusual Red Edge Effect and Efficient Laser Generation

PI-TAI CHOU, CHING-PIN CHANG (張鎮平) JOHN H. CLEMENTS, AND KUO MENG-SHIN

Journal of Fluorescence. Vol. 5. No. 4. (1995)

The synthesis and photohpysics of 4-formyl-4'-*N*,*N*-dimethylamino-1,1'-biphenyl are reported. The emission spectrum in various solvent polarities demonstrates solvatochromism, indicating that the fluorescence originates from an electonically excited species with a strong charge transfer character. The change in $\triangle\upsilon$ [υ_{max} (absorption) - υ_{max} (cinission)] varies from $\sim$ 1500 cm^{-1} in n-heptane to as much as $\sim$7500 cm^{-1} in acctonitule. In protic solvents, the unusual excitation energy-dependent steady-state emission (red edge effect), resulting from solvent dielectric relaxation, was observed in media with a low viscosity. The large Stokes-shifted and high-yield fluorescence led to the observation of the efficient lasing action. The frequency tunability of the laser output is strongly solvent dependent, generating a new charge transfer laser dye in the blue-green region

The Role of Lipid Peroxidation in Menadione-Mediated Toxicity in Cardiomyocytes

WOAN-FANG TZENG (曾婉芳), JIA-LUEN LEE AND TZEON-JYE CHIOU

J. Mol. Cell. Cardiol. **27**, 1999-2008 (1995)

The role of lipid peroxidation in menadione-mediated toxicity was studied in neonatal rat cardiomyocytes. Incubation of cardiomyocytes with menadione resulted in depleted cellular glutathione levels, increased intracellular Ca^{2+} and increased lipid peroxidation which all occurred prior to cell degeneration. Pre-treatment of cells with cysteine suppressed the menadione-induced cell degeneration and prevented changes in glutathione levels, intracellular Ca^{2+}, and lipid peroxidation. Pre-treatment of cells with fura-2 acetoxymethyl ester, a Ca^{2+} chelator, reduced menadione-induced cell degeneration and lipid peroxidation but it did not block cellular glutathione depletion. Pre-treatment of cells with deferoxamine mesylate, an iron chelator, also reduced both menadione-induced cell degeneration and lipid peroxidation; however, it did not prevent the menadione-induced increase in intracellular Ca^{2+}, nor the depletion of glutathione. Thus, the inhibition of menadione-induced lipid peroxidation by deferoxamine mesylate prevented cell degeneration even though intracellular Ca^{2+} remained elevated and glutathione remained depleted. The protective effects of deferoxamine mesylate and fura-2 AM on menadione's toxicity were inhibited by addition of $FeCl_3$ to cells. Ferric ions did not inhibit the protective effect of cysteine. These data suggest that menadione-induced cardiomyocyte degeneration is directly linked to iron-dependent lipid peroxidation and less tightly coupled to elevation in intracellular Ca^{2+} or depletion of glutathione.

Molecular Cloning and Expression of the Coat Protein Genes of Cf, a Filamentous Bacteriophage of *Xanthomonas Campestris* Pv. *Citri*

MEI-KWEI YANG (楊美桂), HUEI-MEI HUANG, YEN-CHUN YANG AND WEI-CHIH SU

Bot. Bull. Acad. Sin., **36**, 207-214 (1995)

Particles of the filamentous bacteriophage Cf contain a major coat protein, the B protein, with a molecular weight of approximately 6,000. In addition, a minor coat protein, the A protein, with a molecular weight of about 50,000, was also identified on sodium dodecyl sulfate-containing polyacrylamide gels. A 3.3 kbp *Hinc* II fragment derived from Cf genome was cloned into the expression plasmid pG308N, an *E. coli* plasmid which carries pL promoter. The recombinant plasmid pG33 and a series of deletion derivatives of pG33 were constructed and transformed into *E. coli* DG116 for expression of phage Cf genes. The genes coding for A and B proteins of Cf were found on the 2.0 kbp *Eco*RI-*Hinc* II fragment. The complete nucleotide sequences of the 2.0 kbp *Eco*RI-*Hinc* II insert were determined. The deduced amino acid sequence corresponds to a 62-amino acid-residue polypeptide that has a calculated Mr of 6070 was identified as the B protein by SDS/PAGE and immunoblotting. Another open reading frame (ORF419) downstream of the B protein gene (ORF62) was found, and was shown to code for a polypeptide of 419 amino acids with a calculated Mr of 44,676 that exhibits considerable identity to the A protein.

德基水庫集水區自然生態動植物種源調查計畫(四)
合歡山地區生態種源庫之調查

陳擎霞　李玲玲　李培芬

中華民國自然生態保育協會，第 1-61 頁（1996）

合歡山是中央山脈的分水嶺，位於德基水庫集水區之南，橫跨南投及花蓮二縣，屬於南投縣仁愛鄉及花蓮縣秀林縣行政範圍。由十四甲省道貫穿，南通昆陽、鳶峰、霧社、埔里、北抵大禹嶺，接八號省路即中橫公路，西往梨山，東達花蓮。本區原爲泰雅族原住民發祥地，是冬季冷峰迎風的坡面，也是亞熱帶的雪鄉。從畢祿山以南、合歡東峰、合歡主峰、合歡北峰與奇萊山遙遙相對，使合歡群峰護守著德基水庫集水區的南疆。合歡山區由於風景壯麗且交通方便，每逢假日必有大量遊客在各主要山頭及觀光據點活動，遊憩壓力頗大，極需調查並監測當地動植物相，以追蹤遊客活動的影響。畢祿山下之畢祿林道則因多處崩坍，除少數登山客外，較少人跡；荒廢的林道附近動植物的組成與分布亦值得調查。

調查結果顯示，合歡山地區及畢祿林道之植物至少有 300 種，分別隸屬 87 科 201 屬之內。其中蕨類植物有 11 科 15 屬 20 種；裸子植物有 3 科 11 屬 15 種；雙子葉植物有 64 科 152 屬 234 種；單子葉植物有 9 科 23 屬 31 種。合歡山地區及畢祿林道之野生動物至少有 84 種，分別隸屬 16 目 38 科 67 之內，包括哺乳類 6 目 9 科 15 屬 15 種，其中有 6 種特有種，2 種野生動物保育法所列保育類動物及新記錄種之亞洲寬耳蝠 1 種；鳥類 6 目 18 科 46 屬 52 種，其中有 11 種特有種及 18 種保育類動物；爬虫類有 1 目 3 科 4 屬 4 種，其中有 3 種特有種，2 種保育類動物；兩生類有 2 目 2 科 2 屬 2 種，其中山椒魚屬於特有種，亦屬於保育類；蝶類有 1 目 6 科 9 屬 11 種，其中曙鳳蝶屬於特有種，亦屬於保育類。

具有慣性負載之感應電動機轉軸扭轉振動分析

李 永 勳

1995 Procedling of the 16th Symposium on Electric Power Engineering, pp. 145-149, (1995)

本論文提出一個系統化方法來分析多重繞組電動機的扭轉振動特性，包括起動暫態下的電動機非線性磁化特性和驅動器與質量彈簧耦合系統間之元件交互作用對扭轉振動之影響。系統模擬和 FFT 分析結果顯示具有適當位移之複端逆轉換器驅動之具慣性負載的多重繞組感應電動機的扭轉振動振幅會減少，且動態特性亦獲得改善。同時，起動分析證明選用適當切換協調的起動方法能夠大爲減少起動暫態扭轉振盪轉矩。因此，超出動態扭轉應力設計極限的永久性元件損壞風險也大爲降低。

Tracking Control of Robot Manipulators with Parametric Uncertainty

KUO-KAI SHYU, KOU-CHENG HSU (徐國政) AND PENG-HSIEN CHU

15th IASTED International Conference on Modelling, Identification and Control, Innsbruck. Austria, pp. 39-42 (1996)

An adaptive variable-structure-like controller for robot manipulators with parametric uncertainty whose upper bound was unknown was derived in this work. It was shown by simulation, without knowing the bounds of the uncertainty, the

presented adaptive variable-structure-like controller can, not only stabilize the robot manipulators but also reduce the chattering phenomena. Moreover, the tracking errors of the robot manipulators can also be guaranteed to converge to zero, which prevents the divergence of the estimation law for the unknown uncertainty bound.

Decentralized Variable Structure Control Design for Uncertain Large-Scale Systems

KOU-CHENG HSU (徐國政), AND KUO-KAI SHYU

15th IASTED International Conference on Modelling, Identification and Control, Innsbruck, Austria, pp. 274-277 (1996)

In this paper, a new decentralized variable structure control for large scale interconnected systems is proposed. This new decentralized variable structure control ensures the global reaching condition of the sliding mode of the composite system. Furthermore, the convergence speed to the sliding mode can be assured at least with a given exponential speed by the proposed controller. Finally, a numerical example is included to illustrate the result.

Asymmetric Interpolation Lattice

JENQ-TAY YUAN (袁正泰)

IEEE Transactions on Signal Processing, Vol. 44, No. 5, pp. 1256-1261 (1996)

This paper presents a new lattice structure for linear interpolation. The interpolation lattice structure is *asymmetric* in the sense that the number of past and future values linearly weighted to estimate the current value does not have to be identical. The lattice structure provides a computationally efficient and structurally flexible realization for the interpolation lattice. It also leads to a generalization of the concepts of the well-known linear prediction lattice and symmetric interpolation lattice.

Separation of Cinese Characters From Graphics

JING-YUH WANG, LIANG-HUA CHEN (陳良華), KUO-CHIN FAN
AND HONG-YUAN MARK LIAO

Proceeding of International Conference on Document Analysis and Recognition,
Montreal, Canada, pp. 948-951 (1995)

In this paper, we propose a robust algorithm to separate Chinese characters form line drawings. This approach is based on the clustering of all feature points in the images. Using our algorithm, all Chinese characters can be completely separated from graphics without regard to the size, orientation and location of Chinese characters even if the characters touching or overlapping line problem occurs. Experiments chow that our algorithm can be applied to both geographical information systems and forms processing.